Membrane-Inlet Mass Spectrometry

Studies of Natural and Artificial Photosynthesis

vorgelegt von Diplom-Biologin

Katrin Beckmann

aus Gelsenkirchen

Von der Fakultät II - Mathematik und Naturwissenschaften
der Technischen Universität Berlin

zur Erlangung des akademischen Grades

Doktor der Naturwissenschaften
- Dr. rer. nat. –

Genehmigte Dissertation

Promotionsausschuss:

Vorsitzender: Prof. Dr. Thomas Friedrich

Berichter/Gutachter: Prof. Dr. rer. nat. Johannes Messinger

Berichter/Gutachter: Prof. Dr. rer. nat. Peter Hildebrandt

Berichter/Gutachter: Prof. Dr. rer. nat. Wolfgang Lubitz

Tag der wissenschaftlichen Aussprache: 11. März 2008

Berlin 2008
D 83

Für meine Eltern

Alles ist einfacher, als man denken kann, zugleich verschränkter als zu begreifen ist.

(Johann Wolfgang von Goethe)

CONTENTS

ABSTRACT

Beckmann, Katrin:

Membrane-Inlet Mass Spectrometry Studies of Natural and Artificial Photosynthesis

Oxygenic photosynthesis provides molecular oxygen and nearly all vital nutrients for heterotrophic organisms. The catalytic center for the generation of molecular oxygen from the photosynthetic oxidation of water is termed *oxygen evolving complex* (OEC). It is located on the luminal site of the protein-pigment complex Photosystem II (PSII). The OEC consists of an inorganic, x-oxygen bridging ($x \geq 5$) tetra-manganese-calcium (Mn_4O_xCa) complex and its specific protein surrounding. The protein matrix does not only bind the inorganic components but also regulates the proton coupled electron transfer, substrate supply and product release. The Mn_4O_xCa complex passes stepwise through five redox states. The redox intermediates are termed S*i* states with the index ($i = 0 - 4$) giving the number of stored oxidizing equivalents. The reaction is driven by light induced charge separation in the chlorophyll containing reaction center of PSII.

In the present work the photosynthetic water splitting reaction is studied in detail by time-resolved membrane-inlet mass spectrometry (MIMS) and isotopic labeling. MIMS enables a direct connection between reaction vessel and mass spectrometer (MS), because a gas permeable membrane separates the sample from the high vacuum of the MS.

Within the scope of this work diverse PSII-systems were constructed and the following results were obtained by MIMS:

1) Measurements of $H_2{}^{16}O/H_2{}^{18}O$-substrate water exchange kinetics of PSII samples, in which the natural cofactors Ca^{2+} and Cl^- have been substitute for Sr^{2+} and/or Br^-, showed that Ca^{2+}/Sr^{2+} as well as Cl^-/Br^- substitution accelerate the slow phase of substrate water exchange. For these experiments, thylakoids were isolated from the thermophilic cyanobacterium *Thermosynechoccus eleongatus*, which were grown either in medium containing $CaCl_2$, $CaBr_2$, $SrCl_2$ or $SrBr_2$.

2) Oxygen pressure of up to 20 bar has no detectable influence on the light induced oxygen evolving activity of thylakoids and PSII membrane fragments. Hereby, a product inhibition of PSII, which was described in the literature and shown by indirect UV absorption measurements, was proven wrong.

3) Hydrogen carbonate is not the substrate for the photosynthetic oxygen production in PSII. This result clears out last doubts, that water and not hydrogen carbonate is the direct substrate of the photosynthetic water splitting reaction.

4) Artificial solar water splitting is a promising approach towards the production of renewable energy carriers. In a study comparing water splitting activities of diverse synthetic Mn-compounds, a Mn-dimer was firstly found that generates O_2 in accordance with the $H_2{}^{18}O$-enriched water, closely resembling the theoretical values for true water oxidation upon addition of different chemical oxidants (oxone and lead tetraacetate). The oxygen evolution with lead tetraacetate was substoichiometric and also further addition of oxone changed the isotopic composition of the produced oxygen towards unlabelled oxone. Nevertheless, this could be a first step towards the development of artificial water splitting catalysts.

ZUSAMMENFASSUNG

Beckmann, Katrin:

Membrane-Inlet Mass Spectrometry Studies of Natural and Artificial Photosynthesis

Die oxygene Photosynthese ist die Lebensgrundlage der heterotrophen Organismen, da sie den lebensnotwendigen molekularen Sauerstoff und fast alle Nährstoffe liefert. Das katalytische Zentrum der photosynthetischen Wasserspaltungsreaktion wird als Sauerstoff-entwickelnder Komplex (OEC, englisch: oxygen evolving complex) bezeichnet und befindet sich an der luminalen Seite des Protein-Pigment-Komplexes Photosystem II (PSII). Der OEC besteht aus einem anorganischen, (x)-Sauerstoff-verbrücktem ($x \geq 5$) tetra-Mangan-Calcium (Mn_4O_xCa)-Komplex und einer speziefischen Proteinumgebung, die nicht nur die anorganischen Komponenten bindet, sondern auch den protonengekoppelten Elektronen-transport, die Substratzufuhr und auch den Produktausstoß reguliert. Im Mn_4O_xCa-Komplex werden, angetrieben von lichtinduzierten Ladungstrennungen im chlorophyll-haltigen Reaktionszentrum von PSII, fünf Redoxzustände schrittweise durchlaufen. Diese Redoxintermediate werden als S_i-Zustände bezeichnet, wobei der Index ($i = 0 - 4$) die Zahl der gespeicherten Oxidationsäquivalenten angibt.

In der vorliegenden Arbeit wird die photosynthetische Wasserspaltung mit Hilfe von zeitaufgelöster Membraneinlass-Massenspektrometer (MIMS, englisch: membrane-inlet mass spectrometry) und Isotopenmarkierung detailliert untersucht. MIMS erlaubt eine direkte Verbindung zwischen Reaktionsgefäß und Massenspektrometer (MS), wobei eine gasdurchlässige Membran die Probe vom Hochvakuum des MS trennt. Im Rahmen dieser Arbeit wurden unterschiedliche Membraneinlasssysteme konstruiert und damit folgende Ergebnissen erzielt:

1) Durch Messung der $H_2{}^{16}O/H_2{}^{18}O$-Substratwasseraustauschkinetiken von PSII-Proben, deren natürliche Kofaktoren Ca^{2+} und Cl^- durch Sr^{2+} und/oder Br^- ersetzt waren, wurde gezeigt, dass sowohl Ca^{2+}/Sr^{2+} als auch Cl^-/Br^- Austausch die langsame Phase des Substratwasseraustausches beschleunigt. Für diese Experimente wurden Thylakoide verwendet, die aus dem thermophilen Cyanobakterium *Thermosynechoccus eleongatus* isoliert wurden, dessen Anzuchtsmedien entweder $CaCl_2$, $CaBr_2$, $SrCl_2$ oder $SrBr_2$ enthielten.

2) Sauerstoffdrücke bis 20 bar haben keinen detektierbaren Einfluss auf die lichtinduzierte Sauerstoffbildungsaktivität von Thylakoiden und PSII-Membranfragmenten. Hiermit konnte eine in der Literatur beschriebene Produktinhibition von PSII, auf die aus indirekteren UV-Absorptionsmessungen geschlossen wurde, nicht bestätigt werden.

3) Hydrogencarbonat ist nicht das Substrat für die O_2-Bildung im PSII. Diese Ergebnisse räumen letzte mögliche Zweifel daran aus, dass tatsächlich Wasser, und nicht Hydrogencarbonat, das direkte Substrat der photosynthetischen Wasserspaltung ist.

4) In einer vergleichenden Studie der Wasserspaltungsaktivität von verschiedenen synthetischen Mn-Verbindungen wurde erstmals ein Mn-Dimer gefunden, das bei Zugabe von zwei unterschiedlichen chemischen Oxidationsmitteln (Oxone oder Bleitetraacetat) Sauerstoff mit der korrekten Isotopenmarkierung von $H_2{}^{18}O$-angereichertem Wasser produziert. Diese O_2-Freisetzung war allerdings substoichiometrisch, und bei weiteren Zugaben von Oxone veränderte sich die Isotopenzusammensetzung des freigeszten O_2 hin zu der des unmarkierten Oxones. Dennoch könnte dies ein erster Schritt hin zu der Entwicklung von artifiziellen Wasserspaltungskatalysatoren sein.

VERÖFFENTLICHUNGEN

Teile dieser Arbeit wurden bereits publiziert:

PEER-REVIEWED ARTICLES:

1. **Clausen J, Beckmann K, Junge W, Messinger J** (2005) Evidence that Exchangeable Bicarbonate is Not a Substrate for Photosynthetic Oxygen Evolution. *Plant Physioliol.* **139**: 1444–1450

2. **Beckmann K, Ishida N, Boussac A, Messinger J** (2008) Effects of Calcium/Bromide Substitution on Substrate Water Exchange Rates in Photosystem II. *In* Allen JF et al. (Eds.), *Photosynthesis. Energy from the Sun: 14th International Congress on Photosynthesis*, in press

3. **Styring S, Beckmann K, Berggren G, Uchtenhagen H, Anderlund M, Thapper A, Messinger J, Kurz P** (2008) Oxygen Evolving Reactions by Synthetic Manganese Complexes. *In* Allen JF et al. (Eds.), *Photosynthesis. Energy from the Sun: 14th International Congress on Photosynthesis*, in press

CONFERENCE CONTRIBUTIONS:

4. **Beckmann K, Messinger J** (2005) *Isotopes 2005*, No Direct Role for Bicarbonate in Photosynthetic Oxygen Evolution. Bath, UK, 27-1st July *(oral & poster presentation)*

5. **Beckmann K, Messinger J** (2006) *SOLAR-H Conference*, MIMS- an Ideal Tool for Studying Natural and Artificial Photosynthesis. Gelsenkirchen, Germany, 26-28th April *(poster presentation)*

6. **Beckmann K, Clausen J, Junge W, Messinger J** (2006) *International Meeting in Honour of Prof. Barber "Photosynthesis in the Post-genomic Era: Structure and Function of Photosynthesis"*. Water, Not Bicarbonate is the Direct Substrate in Photosynthetic Oxygen Evolution. Pushchino, Russia, 20-26th August *(oral & poster presentation)*

7. **Beckmann K, Messinger J** (2006) *15. Photosynthese-Workshop "Nord-West"*, Is the Photosynthetic Oxygen Deriving from Bicarbonate or from Water? Aachen, Germany, 7-8th September *(oral presentation)*

8. **Beckmann K, Ishida N, Boussac A, Messinger J** (2007) *14th International Congress of Photosynthesis,* Effects of the Calcium/Strontium and Chloride/Bromide Substitution on Substrate Water Exchange Rates in Photosystem II. Glasgow, Scotland, 23-27th July *(poster presentation)*

9. **Beckmann K, Ishida N, Boussac A, Messinger J** (2007) *16. Photosynthesis Workshop "Nord-West"*, Time-Resolved Membrane-Inlet Mass Spectrometry – an Ideal Tool for Studying Photosynthetic Oxygen Evolution. Mülheim an der Ruhr, Germany, 3-4th May *(poster presentation)*

ABBREVIATIONS

Catalase	H_2O_2 oxidoreductase
Chl	Chlorophyll
CI	Chemical ionization
Cyt b_6f	Cytochrome b_6f complex
DCBQ	2,5-Dichlorobenzoquinone
DCMU	3-(3,4-dichlorophenyl)-1,1-dimethylurea
EI	Electron impact ionization
ENDOR	Electron nuclear double resonance
EPR	Electron Paramagnetic resonance
ESI	Electro spray ionization
EXAFS	Extended x-ray absorption fine structure
FeCy	Ferricyanide $[Fe(CN)_6]^{3-}$
FIOP	Flash induced oxygen pattern
FWHM	Full width half maximum
m/z	Mass-to-charge ratio
MALDI	Matrix-assisted laser desorption ionization
Mes	2-(N-morpholino)ethanesulfonic acid
MIMS	Membrane-inlet mass spectrometry
MS	Mass spectrometry
MSP	Manganese stabilizing protein
OEC	Oxygen evolving complex
PC	Plastocyanine
Pmf	Proton motive force
PQ	Plastoquinone
PSI	Photosystem I
PSII	Photosystem II
PTFE	Teflon
Q_A	Primary quinone electron acceptor
Q_B	Secondary quinone electron acceptor
T. elongatus	*Thermosynechococcus elongatus*
TOF	Time-of-flight
XANES	X-ray absorption spectroscopy
XRD	X-ray diffraction
Y_D	Tyrosine D (D2-Tyr 160)
Y_Z	Tyrosine Z (D1-Tyr 161)

DANKSAGUNG

Den Doktortitel für eine Promotion erhält nur eine Person, tatsächlich aber sind viele, direkt und indirekt, an einer solchen Arbeit beteiligt. Im Folgenden möchte ich mich daher bei den Menschen bedanken, ohne die es die vorliegende Arbeit gar nicht gäbe.

Dr. Johannes Messinger hat mich während der gesamten Dauer meiner Arbeit optimal betreut und großartig unterstützt. Sein Vertrauen, die sehr guten Arbeitsbedingungen, Diskussionen sowie das sehr angenehme Arbeitsklima waren wichtige Grundlagen zum Gelingen meiner Arbeit. Darüber hinaus hat er fruchtbare Kooperationen mit externen Arbeitsgruppen sowie meine Teilnahme an verschiedenen Konferenzen, auf denen ich meine Arbeit vorstellen und weitere interessante Gedanken aufnehmen konnte, ermöglicht. Auch die Ermunterung und Unterstützung bei der Organisation eines Photosynthese-Workshops in Mülheim hat meine Forschungsergebnisse bereichert und meine persönliche Entwicklung vorangetrieben. Dafür bedanke ich mich herzlich.

In der Arbeitsgruppe „Messinger“ herrschte jederzeit eine sehr gute Arbeitsatmosphäre mit viel Spaß und gegenseitiger Unterstützung. Insbesondere mit **Dmitriy Shevela** habe ich viele ausführliche Gespräche über Photosynthese, das Leben und den ganzen Rest geführt. **Dr. Ji-Hu Su** hat mich nicht nur mit zahlreichen Anregungen, sondern auch mit exotischen Früchten versorgt. **Birgit Nöring** hat mir den Start am Max-Planck-Institut sehr erleichtert und war mir, insbesondere durch ihren schier unerschöpflichen Vorrat an Spinatpräparationen, während der gesamten Promotionszeit eine wertvolle Hilfe. **Ethel Hüttel** hat mich nicht nur bei der Laborarbeit, sondern auch mit ihrer Süßigkeitengrundversorgung großartig unterstützt. Ihnen allen danke ich herzlich.

Udo Klar hat durch hervorragende technische Unterstützung dafür gesorgt, dass die Versuchsaufbauten auch funktionierten wie geplant (oder besser). Ich bedanke mich auch besonders für die oftmals sehr schnelle Hilfe bei neuen und alten Versuchsaufbauten.

Für die hervoragende Zusammenarbeit bedanke ich mich ganz herzlich bei **Dr. Philipp Kurz**, **Hannes Uchtenhagen** und **Prof. Dr. Stenbjörn Styring**, **Naoko Ishida** und **Dr. Alain Boussac**, **Dr. Jürgen Clausen** und **Prof. Dr. Wolfgang Junge**. Ich möchte mich sowohl für die so verschiedenen wie interessanten Aufgaben und auch die sehr hilfreichen Diskussionen bedanken. Mit Dr. Jürgen Clausen, Naoko Ishida und Dr. Philipp Kurz habe ich spannende und lustige Stunden im Labor verbracht.

Jörg Rathke, meine Eltern, **Ilse und Nikolaus Beckmann**, meine Schwester **Ingrid Beckmann** und meine Großtante **Liselotte Dickoré** haben entscheidend dazu beigetragen, dass ich mich überhaupt für den Weg der Promotion entschieden habe. Durch

ihre Unterstützung, ihr Interesse an Inhalt und Fortgang der Arbeit(en), durch lehrreiche Gespräche und nicht zuletzt die Bewahrung eines Rückzuggebietes im familiären Nest, in dem ich wieder Kraft schöpfen konnte, konnte ich mich voll und ganz auf meine berufliche Aufgabe konzentrieren und habe mit ihrer Hilfe auch schwierige Phasen meistern können. Dafür danke ich von Herzen.

Durch ein offenes Ohr, einen guten Rat oder einfach unterhaltsame Ablenkung in schöpferischen Pausen waren mir **Vera Andrades Vazquez, Sonja Jurek, Fatma Kirchberg, Maren Männel, Andrea Schmitz** und drei Generationen der **Familie Ditters** eine großartige Hilfe. Mein Dank für die Begleitung seit dem Studium gilt **Dr. Steffanie Wawro, Dr. Jeanette Seidel, Dr. Oliver Dangel, Dr. Carsten Kötting und Dr. Christian Kandt.** Ihnen allen danke ich besonders.

Mit **Dr. Anke Mennenga** habe ich viele humorvolle Mittagszeiten verbracht. Darüber hinaus hat sie mit scharfem Blick meine Arbeit Korrektur gelesen. Dafür bedanke ich mich sehr.

Bei **Dmitriy Shevela, Malwina Szczepaniak** und **Chavdar Slavov** bedanke ich mich für die spannende, stressige, aber auch heitere Zeit bei der Organisation eines Photosynthese-Workshops.

Mein Dank gilt **Prof. Dr. Wolfgang Lubitz**, der mir als Direktor des Max-Planck-Institues in Mülheim/Ruhr die Arbeit unter hervorragenden Arbeitsbedingungen durch eine sehr gute Infrastruktur sowie optimale technische Einrichtungen ermöglicht hat. Er hat durch großzügige Unterstützung und anregende Rückfragen die Qualität der vorliegenden Arbeit gefördert.

Chapter 1

Introduction

1. INTRODUCTION

1.1. Photosynthesis

To sustain life, each organism uses energy stored in organic substances. The organic matter is acquired either autotrophically, by building up energy rich compounds out of inorganic resources gained from the environment (assimilation) or heterotrophically, by incorporating or decomposing other organisms. Photosynthesis is a photoautotrophic process to convert carbon dioxide and water into carbohydrates and other organic substances by employing sunlight. This process occurs in plants, algae and cyanobacteria.

The evolution of oxygenic photosynthesis started about three billion years ago in cyanobacteria (BUICK 2000; DISMUKES ET AL. 2001; XIONG AND BAUER 2002). It was a dramatic event for the earth's biosphere: it changed the atmosphere from being reducing to being oxidizing. The first photosynthetic organisms liberating oxygen had, in addition to increased efficiency, the great advantage of being able to poison competitors with molecular oxygen. Other organisms, as well as the photosynthetic once eventually adapted and developed sophisticated defensive radical scavenging mechanisms against the reactive singlet oxygen and started to take advantage of the aerobic atmosphere. Dioxygen allowed developing highly efficient respiration processes and increased the efficiency of the sugar exploitation by a factor of ~ 10 (RENGER 1997). The increasing dioxygen concentration in the atmosphere built, through photochemical chain reactions (photo-dissociation), the protective ozone layer in the stratosphere (15 km – 50 km above earth). This layer absorbs a large part of the highly damaging ultra violet (UV) radiation and thereby decreases the level of UV light which reaches the surface of the earth (OLSON AND BLANKENSHIP 2004).

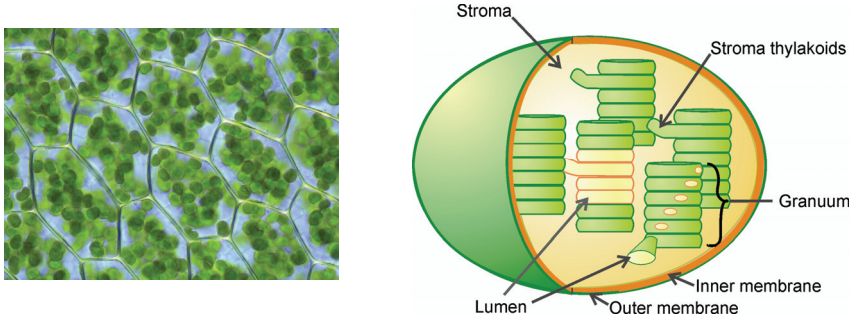

FIGURE 1:

Chloroplasts in lamina cells of *Plagiomnium affine* on the left and a schematic view of a chloroplast on the right.

The unit where oxygenic photosynthesis takes place, is the chloroplast, a typically 5 µm long organelle, with two outer membranes enclosing the stroma (Fig. 1).
The stroma comprises a closed membrane system, which is subdivided into helically stacked grana thylakoid and connecting stroma thylakoid regions. The stroma further contains soluble proteins as well as plasmid DNA, ribosomes and starch granular. Illumination of intact thylakoid membranes yields O_2, NADPH and ATP. The latter two products are consumed to provide energy for the reduction of CO_2 to carbohydrates inside the stroma (MARTIN ET AL. 2000).

According to the endosymbiontic theory, the origin of chloroplasts in eukaryotic cells was an endophagocytosis event, where engulfing of an autotrophic cyanobacterium had taken place. Symbiosis between the host and the cyanobacterium led to the evolution of the first chloroplast that was genetically dependent on the eukaryotic cell (encoded in the chloroplast genome are only ~ 5% of the proteins). Arguments supporting the endosymbiont theory are *(i)* chloroplasts contain circular DNA indicating an origin from cyanobacteria, *(ii)* the stroma contains prokaryotic ribosomes, *(iii)* two membranes surround the chloroplasts. The outer membrane is possibly the food vacuole, which had originally enclosed the cyanobacterium while the inner one is the original membrane of the prokaryot. Thylakoid membranes are predominately composed of galactolipids rather than of phospholipids like in the cell plasma membrane and other organelles (WEBB AND GREEN 1991). Triple and quadruple membranes might result from repeated endosymbiosis, *(iv)* living intermediates exist *e.g.* several coral and snail species permanently host algae in their cells. One example of *Acaryochloris marina* is *Didemnid ascidian* hosting cyanobacteria (MIYASHITA ET AL. 1996).

1.1.1. The Photosynthetic Electron Transport Chain

To perform the unique process of photosynthesis three large protein-pigment complexes are integrated into the thylakoid membrane of the chloroplast. Here, electrons are excited by light energy and transported via the photosynthetic electron transport chain. The chain is assembled of Photosystem II (PSII), the Cytochrome b_6f complex (Cyt b_6f) (BERRY ET AL. 2000) and Photosystem I (PSI) (GOLBECK 2006)

(Fig. 2). Two mobile electron carriers, Plastoquinone (PQ) and Plastocyanin (PC) link PSII with Cyt b_{559} and Cyt b_6f with PSI, respectively (HILL AND BENDALL 1960).

PSII is mainly located in the stacked grana membranes, while PSI is found in the stroma thylakoids. Membrane stacking is not required for electron transfer and photophosphorylation. Spatial separation of PSII and PSI is believed to prevent quenching of PSII by PSI. PSI would draw excitation energy from the PSII antenna system (see below), since *(i)* it absorbs at longer wavelengths (BUTLER AND STRASSER 1977) and *(ii)* PSI is three-times faster in exciton trapping than PSII (TRISSL AND WILHELM 1993).

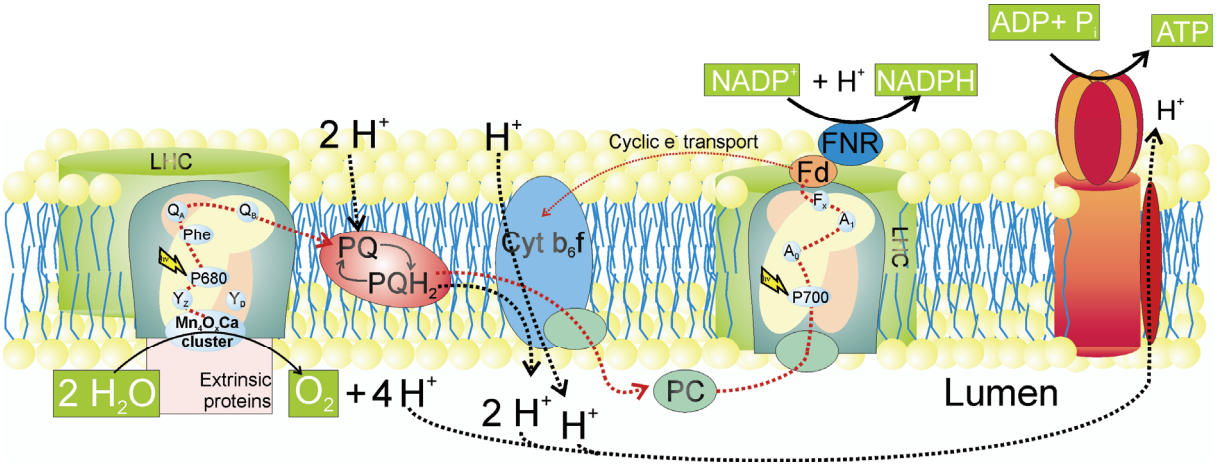

Figure 2:

Electron transport chain integrated in the thylakoid membrane. Electrons, extracted from water, are transferred via integral multi protein complexes and mobile electron carrier to reduce $NADP^+$ to NADPH. A proton gradient is established across the thylakoid membrane to drive ATP synthesis.

Associated with the two photosystems are integral membrane proteins termed *light-harvesting complexes*, which absorb light quanta in the visible region and transfer the excitation energy to PSII and PSI. Light-harvesting complexes (LHCII and LHCI) provide a large area for capturing radiation by binding a great number of pigments (chlorophylls (Chl) *a* and *b*, carotins). Photon absorption raises a pigment molecule to an excited singlet state. *Via* the Förster mechanism (ATKINS AND DE PAULA 2006) the energy hops to a nearby pigment (0.1 - 5 ps) and finally reaches the reaction center with high efficiency. More than 90% of the absorbed energy arrives at the reaction centre (NELSON AND YOCUM 2006).

In PSII, where the electron transport starts, the excitation energy is used to oxidize the primary electron donor, a chlorophyll moiety termed *P680* to give P680*. Charge separation is achieved by transporting the exited electron onto a pheophytin molecule ($Pheo_{D1}$). To stabilize the charge separation the electron is rapidly transferred onto

the tightly bound quinone Q_A. Electrons are passed to the plastoquinone Q_B site. The formed radical cation $P680^{\bullet+}$, with its strong oxidation potential of +1.2 V, is the driving force for the electron extraction from water at the oxygen evolving complex (OEC). To bridge the distance of approximately 10 Å between $P680^{\bullet+}$ and the site of water oxidation, the redox active Tyrosine Z (Y_Z at D1-161) functions as intermediate electron carrier. Finally, with $Q_A^{\bullet-}$ as reductant, plastoquinone is reduced to quinol with two electrons and under uptake of two protons. Plastohydroquinone (PQH_2) is released into the plastoquinone pool in the thylakoids membrane (PETROULEAS AND CROFTS 2005). The electrons are transferred *via* the Cyt b_6f complex and the mobile carrier PC to PSI.

Photosynthetic organisms use the light driven electron transport to build up the energy equivalent adenosine triphosphate (ATP) and nicotinamide adenine dinucleotide phosphate (NADPH). The energy carriers provide the energy for biosynthetic reactions of the calving cycle for the endergonic reduction of CO_2 to carbohydrates. In this way, the water oxidizing chemistry of PSII provides the electrons and, together with the PQ/PQH_2 cycle, the protons that form NADPH and ATP:

$$2\ H_2O + 4\ ADP + 2\ NADP^+ \xrightarrow{8h\nu} O_2 + 4\ ATP + 2\ NADPH \qquad \textbf{(1)}$$

ATP is synthesized by the large protein complex CF_0-CF_1 ATP synthase (MCCARTY ET AL. 2000; JUNGE AND NELSON, 2005) located in the thylakoid membrane. In a process termed *Photophosphorylation*, the proton motive force (pmf) is used to convert ADP and P_i to ATP. PSII establishes the pmf across the thylakoid membrane and the Cyt b_6f complex through release of protons from water oxidation and by the vectorial transport by plastoquinone (PQ)/plastoquinol (PQH_2). The synthesis of NADPH is more directly coupled to the electron transfer. After the absorption of another light quantum at PSI the electrons are transferred to the stromal side and reduce the soluble ferredoxin by PSI, which in turn reduces $NADP^+$ in the ferredoxin-$NADP^+$ reductase.

1.1.2. Photosystem II

PSII is a homodimeric protein-cofactor complex. Several crystal structures of cyanobacterial PSII have been published, (BIESIADKA ET AL. 2004; FERREIRA ET AL. 2004; KAMIYA AND SHEN 2003; LOLL ET AL. 2007; ZOUNI ET AL. 2001).

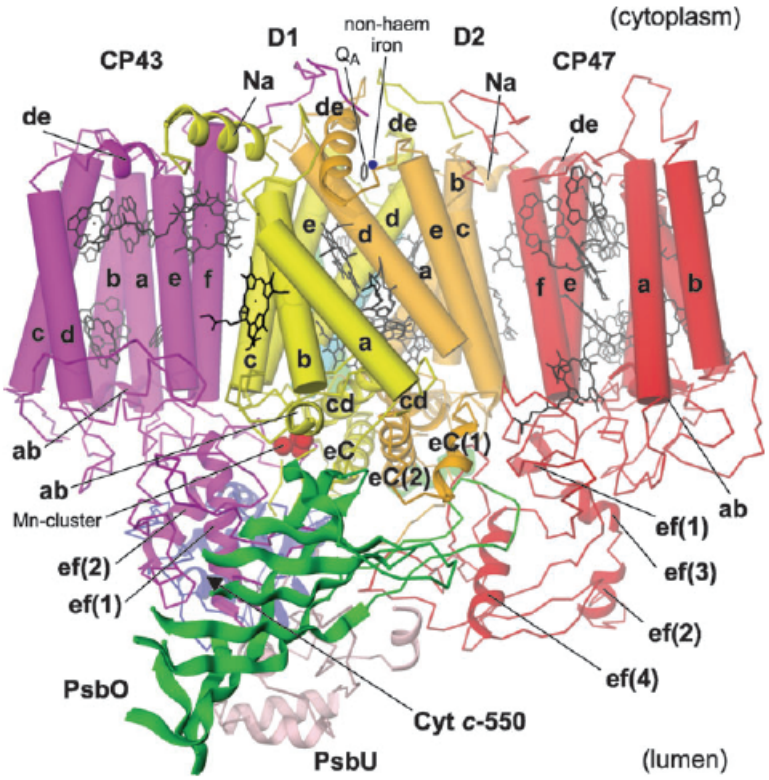

Figure 3:

X-ray crystal structure of the PSII monomer of *T. elongatus* (BIESIADKA ET AL., 2004) at a resolution of 3.2 Å. The major subunits D1 and D2 are in yellow and orange respectively. Subunits CP43 is displayed in magenta, CP 47 in red, while the membrane extrinsic subunits 33 (PsbO) and 23 (PsbU) are displayed in green and pink.

The six largest of the at least 16 membrane-intrinsic subunits of the monomer were identified at 3.0 Å resolution in the thermophilic cyanobacterium *Thermosynechococcus elongatus*. The main protein subunits are the reaction center proteins D1 and D2 (Fig. 3), ligating the redox active cofactors (NIXON ET AL. 2005). The inner antenna proteins CP47 (PsbB) binds 16 chlorophyll *a* (Chl *a*) molecules while CP43 (PsbC) is proposed to comprise 13 Chl *a* molecules (BRICKER AND FRANKEL 2002). Further identified were the α- and β-subunits of the heterodimeric cytochrome b_{559} complex (PsbE and PsbF), binding β-carotins, which provide protection against photo-induced damage (SHI AND SCHRÖDER 2004; STEWART AND BRUDVIG 1998). A number of low molecular weight proteins of unknown function could not be defined at the given resolution (BIESIADKA ET AL. 2004; LOLL ET AL., 2007). The membrane-extrinsic subunits PsbO (33 kDa), PsbP (23 kDa) and PsbQ (17 kDa) which stabilize the Mn_4O_xCa cluster had been assigned to the luminal side of PSII. In Cyanobacteria the latter two subunits are PsbV (17 kDa) and PsbU (12 kDa)

of cytochrome c_{550} (ROOSE ET AL. 2007; SEIDLER 1996),. The PsbO subunit is also referred to as *Manganese stabilizing protein* (MSP). PsbP and PsbQ were shown to be essential for the ligation of the cofactors Ca^{2+} and Cl^- (GREGOR ET AL. 2005; VAN GORKOM AND YOCUM 2005).

1.1.3. The oxygen evolving complex

The catalytic center of water oxidation, named *oxygen evolving complex* (OEC) is located on the luminal side of PSII. Three extrinsic proteins and the inner antenna proteins shield the OEC from the aqueous phase of the lumen. The OEC serves as storage unit for four oxidizing equivalents, thereby connecting the four-electron water oxidizing chemistry to the one electron demand of the primary charge separation in PSII.

The OEC comprises inorganic cofactors including manganese, calcium and bridging oxygen to form the Mn_4O_xCa cluster (x = number of μ-oxo-bridges) and possibly chloride. The redox-active intermediate electron carrier D1-Tyrosine 161 (Y_z) (DEBUS ET AL. 1988; DEBUS ET AL. 2005; METZ ET AL. 1989) is oxidized by $P680^{\bullet+}$ through long range electron transfer (~10 Å) yielding $Y_Z^{\bullet}$. It receives electrons from the Mn_4O_xCa cluster to drive the water oxidizing reaction. Yz is defined as part of the OEC (see Section 1.1.5). The OEC further provides the binding sites for substrate water. The amino acid ligands are vital for the water splitting reaction. The OEC is ligated by D1 and D2 (MICHEL AND DEISENHOFER 1988) as well as one amino acid of CP43 (Arg 357). The protein matrix seems to be of high importance. It controls the entry of substrate water as well as the exit of the produced oxygen and protons. It functions in positioning the essential cofactors and supports structural changes of the Mn_4O_xCa cluster during water oxidation (HILLIER AND MESSINGER 2005).

1.1.4. Structure of the Mn_4O_xCa cluster

The x-ray crystal structures of PSII provides only very limited information on the geometry and ligand environment of the Mn_4O_xCa cluster, because the x-ray dose applied for x-ray crystallography reduces most of the Mn^{III} and Mn^{IV}, present in the

dark-stable S_1 state of the Mn_4O_xCa cluster, to Mn^{II}. This leads to significant structural changes in the Mn_4O_xCa cluster, which was shown by recording Mn K edge *x-ray absorption near edge spectra* (XANES) and *extended x-ray absorption fine structure* (EXAFS) spectra (GRABOLLE ET AL. 2006; YANO ET AL. 2005). It is thus impossible to derive a defined structural model by *x-ray diffraction* (XRD) in the native assembly and indeed the position of the Mn ions in the published PSII structures varies significantly (Fig. 4).

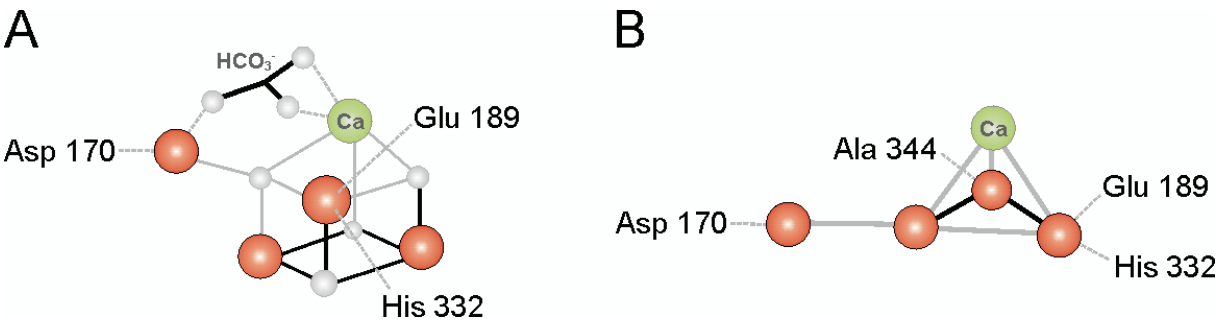

Figure 4:

Proposed models of the OEC on the basis of XRD measurements (MESSINGER AND RENGER 2008). The structures of the Mn_4O_xCa cluster vary greatly, because photoreduction destroys Mn-Mn distances and Mn-O-Mn bridges. A: (FERREIRA ET AL. 2004) at 3.5 Å, B: (LOLL ET AL. 2005) at 3.0 Å resolution.

With EXAFS it is possible to obtain spectra at 1000 fold lower radiation dose in comparison to the XRD measurements. Radiation damage by photoreduction (monitored with XANES) is further reduced by the ability to perform the experiments at 10 fold lower temperatures (10 K). Recently EXAFS experiments on PSII single crystals were obtained along the three PSII crystal axes. This enabled to limit the number of possible models for the structural arrangement of the Mn_4O_xCa cluster to four (YANO ET AL. 2006).

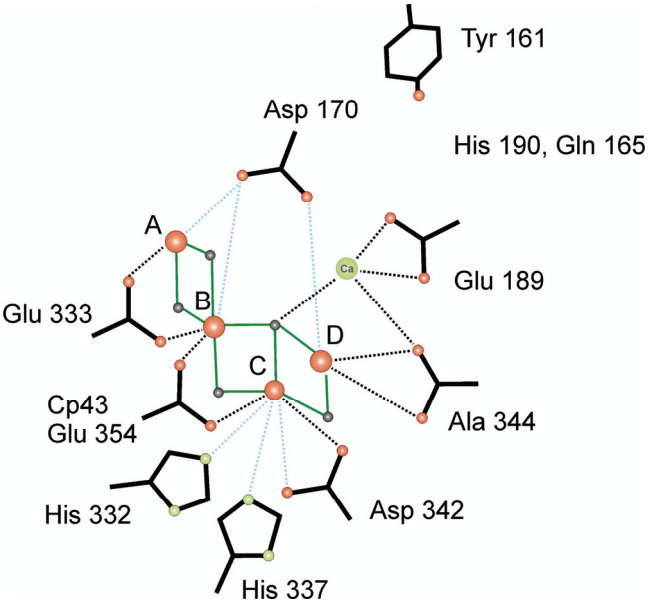

Figure 5:

Current model of the OEC in the S_1 state. The structure of the Mn_4O_xCa cluster derived by Mn EXAFS on PSII single crystals was placed into the PSII structure of Loll et al., 2005 to identify possible amino acid ligands. Spheres represent Mn (red), bridging oxygen atoms (grey) and Ca (green). Figure taken from Yano and co-workers (YANO ET AL. 2006). Three alternative models could be derived which deviate slightly in the position of Ca, the relative orientation of the bridges and/or the overall placement of the cluster into the protein matrix.

The obtained structural models were placed into the electron density map of the x-ray crystal structure analysis in order to combine the high resolution EXAFS- information on the structure of the Mn_4O_xCa cluster with the putative amino acid ligands (Fig. 5).

1.1.5. Kok Model

Many different studies have been published about the mechanism of photosynthetic water splitting. The basis for these studies was set out by experiments performed by Joliet and co-workers (JOLIOT ET AL. 1969) and Kok and co-workers (KOK ET AL. 1970) (Fig. 6). Joliot discovered in 1969 that illumination of dark-adapted algae and chloroplast suspensions gives rise to a specific O_2 release pattern with a periodicity of four. Illumination with a train of short single turnover flashes (FWHM ~ 5 µs) of photosynthetic samples, leads to the following characteristics: *(i)* no oxygen evolution after the first flash (the small oxygen consumption is due to the Mehler reaction, i.e. O_2 reduction by PSI). *(ii)* A small oxygen evolution after the second flash, *(iii)* a maximum oxygen yield after the third flash and *(iv)* from then on maxima of O_2 evolution are observed after each fourth flash, until each flash-illumination yields approximately the same amount of O_2 ("damping of the oscillation pattern").

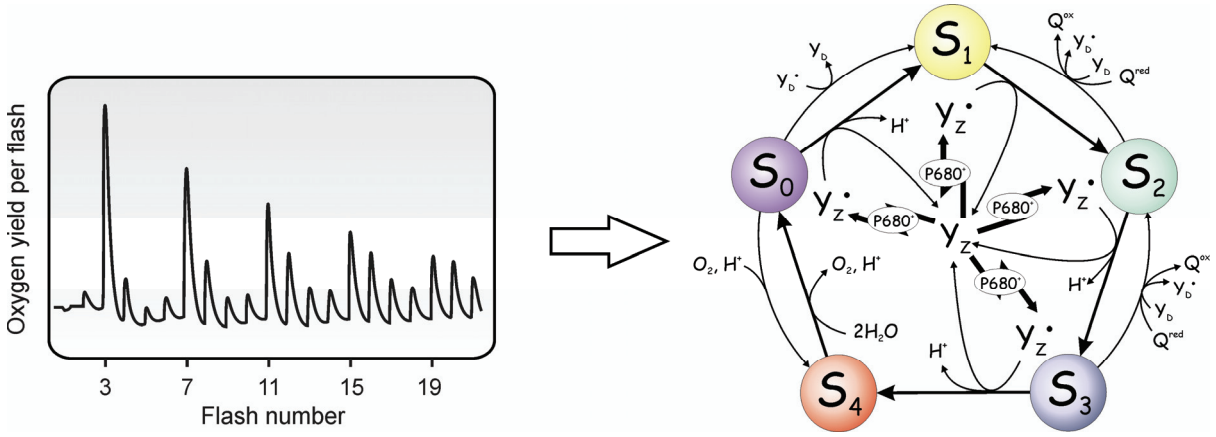

Figure 6:

Kok model. Kok and co-workers (KOK ET AL. 1970) postulated a scheme to explain flash-induced oxygen evolution patterns (FIOPs) of dark adapted chloroplast suspensions (JOLIOT ET AL. 1969). Such FIOPs (left side, 2 Hz frequency) are characterized by an oscillation pattern with a period of four and a first maximum O_2 yield after the 3rd flash. The Mn_4O_xCa cluster cycles through five different S states, S_i, with i = 0 – 4 (right side). The S_1 state is dark-stable, which explains that the first O_2 burst is detected after the 3rd flash. With each cycle 4 e^- are extracted from 2 H_2O and 1 O_2 molecule is produced. Y_z is oxidized by $P_{680}^{\bullet+}$ and receives one electron at a time from the OEC. Figure taken from (MESSINGER AND RENGER 2008).

Based on such flash patterns Kok and co-workers (KOK ET AL. 1970) were the first to propose a kinetic scheme with a cyclic reaction sequence through five intermediary states. The Mn_4O_xCa cluster, cycles through five different S_i states, where i represents the number of stored oxidizing equivalents (i = 0 – 4). The lowest redox state is S_0, formally referred to as the catalytic site with bound water, and the highest redox state is S_4, formally referred to as the catalytic site with bound O_2. The transition from S_3 to S_0 probably involves several reaction intermediates, which may not be resolved due to the short-lived nature of this transition. The S_1 state is dark-stable, which explains why the first O_2 burst occurs after three flashes. Kuhn and co-workers (KUHN ET AL. 2005) propose the physiological reason to be an avoidance of a possible back reaction of S_0 to S_4 at long dark times, which may liberate reactive H_2O_2.
With each cycle four electrons are extracted from two water molecules and one dioxygen molecule is formed at each Mn_4O_xCa cluster (Eq. 2):

$$2\ H_2O \xrightarrow{h\nu} O_2 + 4\ e^- + 4\ H^+ \qquad \textbf{(2)}$$

The Kok model was extended to include reduced S-states which are observable by addition of exogenous reductants like hydroxylamine and hydrazine (BECK AND BRUDVIG 1988; BOUGES 1971; KOK AND VELTHUYS 1976; MESSINGER AND RENGER 1990; MESSINGER ET AL. 1991; MESSINGER ET AL. 1997; MESSINGER ET AL. 2001A). Some authors include the redox-active Y_Z into the definition of the OEC, because it does not only transfer electrons between the Mn_4O_xCa cluster and $P680^{\bullet+}$ (BRITT 1996; HOGANSON AND BABCOCK 1997), but also acts as a strong proton acceptor (KRISHTALIK 1990), reviewed in (NUGENT ET AL. 2004). Y_Z may therefore be directly involved in the water splitting reaction of the Mn_4O_xCa cluster. However, Y_Z does not take part in long-term storage of oxidizing equivalents. Corresponding to Y_Z, D2 also contains a tyrosine known as Y_D (RENGER AND KUHN 2007); D2-Tyr 161 in spinach (DEBUS 1992) and D2-Tyr 160 in *Synechocystis sp.* (DEBUS ET AL. 1988; VERMAAS ET AL. 1988).

In the dark, the Mn_4O_xCa cluster is slowly oxidized from S_0 to S_1 by $Y_D^{\bullet}$ ($S_0 + Y_D^{\bullet} \rightarrow S_1\ Y_D$) (Fig. 6) (MESSINGER AND RENGER 1993; MESSINGER ET AL. 1993; STYRING AND RUTHERFORD 1987; VASS ET AL. 1990). Back-reactions from S_3 to S_2 and S_2 to S_1 are induced by Y_D and electrons stored at the acceptor side (Q_A^-, Q_B^-, Q_BH_2). The latter

reductions occur via P680 and Y_Z (DINER 1977; ISGANDAROVA ET AL. 2003; MESSINGER ET AL. 1993; NUGENT ET AL. 1987; RUTHERFORD AND INOUE 1984; VERMAAS ET AL. 1984).

Within the Kok model, miss (α) and double hit (β) probabilities explain a dephasing of the O_2 oscillation pattern with advancing flash number. The miss event leaves the Mn_4O_xCa cluster in the same state as before the flash excitation ($S_i \rightarrow S_i$). It occurs when a stable charge separation cannot be achieved (CHRISTEN AND RENGER 1999; DE WIJN AND VAN GORKOM 2002; MESSINGER AND RENGER 2008; RENGER ET AL. 1988; SHINKAREV AND WRAIGHT 1993). The miss parameter is pH dependent (BERNAT ET AL. 2002; CHRISTEN ET AL. 1999). It is assumed to be statistically distributed over all PSII centers within a flash train (HILLIER AND MESSINGER 2005; MESSINGER AND RENGER 2008).

The double hit parameter explains the small O_2-yield after the second flash and is due to the longer "tail" of Xe flashes, which induces a second S-state transition in approximately 2-3% of the PSII centers. The centre proceeds twice with one flash ($S_i \rightarrow S_{i+2}$). The use of ns-laser flashes circumvents double hits. (HILLIER AND MESSINGER 2005; MESSINGER ET AL. 1993; MESSINGER AND RENGER 2008; JURSINIC 1981).

1.1.6. Thermodynamics of the water splitting reaction

The antenna system absorbs light and transfers the excitation energy to the PSII reaction center (P680) (see Section 1.1.1). Its reduction potential has been estimated to ΔG° ($P680^{\bullet+}/P680$) = +1.25V (RAPPAPORT ET AL. 2002). The differences in standard Gibbs energy between the S-states cannot be determined directly by redox titration measurements, but is estimated. It has to be kept in mind that configurational energy rather than the Gibbs energy is essential for the individual reaction steps of the OEC (KRISHTALIK 1990; KRISHTALIK 1986). The protein matrix influence the redox potential greatly, e.g. it was shown that the midpoint potential of the bacterial reaction centre ($P870^{\bullet+}$) could be increased by electrostatic interactions of neighbouring ligands (ARTZ ET AL. 1997).

The energy of a 680 nm photon is 1.8 V, while the average energy necessary to extract one electron from water at pH = 7 is 0.82 V. Still, it is not possible to oxidize water to

molecular oxygen in solution with a light quantum of 680 nm, because the first electron extraction has an energy demand of 2.3 V. The OEC bypasses the first high-energy step by accumulating oxidizing equivalents in the Mn_4O_xCa cluster, before the chemistry takes place. For this the energy of one 680 nm photon is sufficient. The values for $\Delta G^{\circ'}$ (S_{i+1}/S_i) are S_0: 0.85 eV, S_1: 1.10 eV, S_2: 1.15 eV and S_3: 1.0 eV (Fig. 7) and clearly below the value of ΔG° ($P680^{\bullet+}/P680$). The $S_3 \rightarrow S_0$ transition is estimated to be $\Delta G^{\circ'}$ = -105 meV (RENGER 1997; RENGER 2001; MESSINGER AND RENGER 2008).

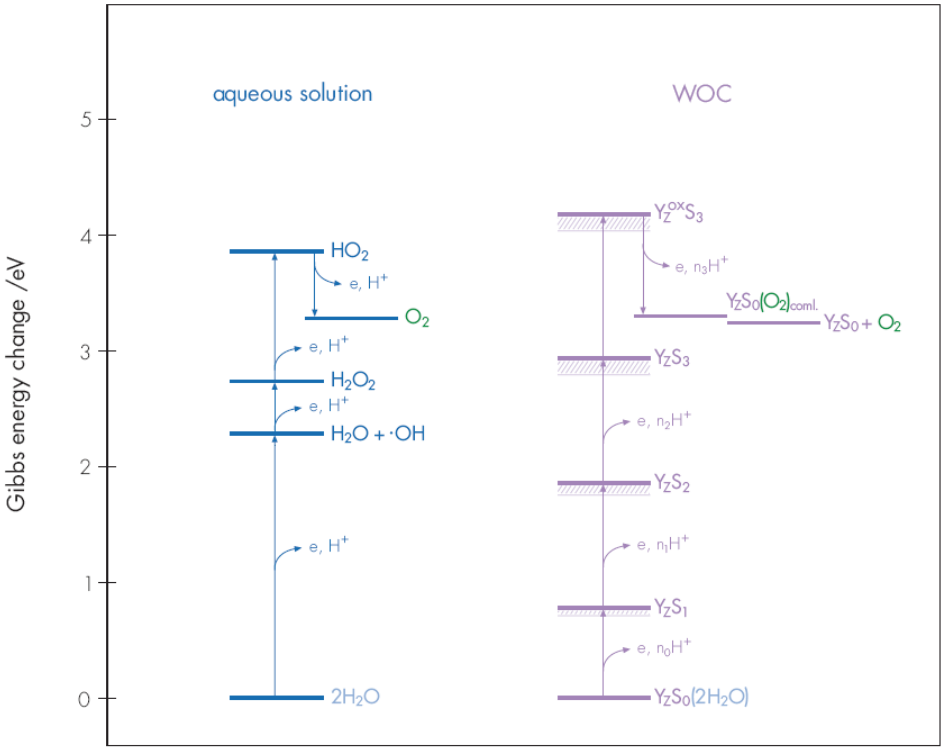

Figure 7:

Thermodynamics of the four-step water splitting reaction into molecular oxygen and four protons in solution and estimated steps for the OEC. Figure taken from (MESSINGER AND RENGER 2008).

By enabling a concerted water oxidizing reaction in one final step, the OEC bypasses the energetically disadvantageous hydroxyl radical and other high-energy intermediates with potentials greater than 1 V. Accumulation of oxidation equivalents requires to compensate for the increasing positive charge. Through successive deprotonation events charge accumulation is avoided, which would make further electron abstraction increasingly difficult. This is with the exception of the $S_1 \rightarrow S_2$ transition. Here, the OEC accumulates one positive charge in accordance to the proposed proton release pattern of 1:0:1:1, which is thought to trigger electrostatically

the major structural changes taking place in the $S_2 \rightarrow S_3$ transition (MESSINGER AND RENGER 2008).

1.1.7. Inorganic cofactors of the OEC

The OEC has been reported to depend on several inorganic cofactors. The redox-inert *calcium* has been shown to be an essential cofactor of the OEC. The stoichiometry of calcium in higher plants is 2 Ca^{2+} per PSII with one calcium ion tightly bound to the LHCII (CHEN AND CHENIAE 1995; HAN AND KATOH 1993; SHEN ET AL. 1988A). The second ion is less tightly bound and connected with the OEC function. One Ca^{2+} ion per OEC is sufficient for O_2 evolution (ÄNDELROTH ET AL. 1988; CAMMARATA AND CHENIAE 1987; KATOH ET AL. 1987; SHEN ET AL. 1988B). EXAFS measurements reveal very similar distances for Mn-Ca and Mn-Sr of 3.4 Å and 3.5 Å, respectively. This provides conclusive evidence that the active site of the OEC is a heteronuclear Mn-Ca cluster with calcium structurally linked (CINCO ET AL. 1998; CINCO ET AL. 2002; CINCO ET AL. 2004; LATIMER ET AL. 1998; MIQYASS ET AL. 2007; MIQYASS AND VAN GORKOM 2007; YACHANDRA 2005; YANO ET AL. 2005B).

Calcium depletion leads to full loss of oxygen evolving activity. After its removal, the S_2 state is still formed, but the normal S_3 state is not reached, giving rise to a characteristic EPR signal, termed *split signal* (TANG ET AL. 1996, UN ET AL. 2007). Strontium, with its only slightly larger ionic radius and similar pK value for water or hydroxide ligands, is the only ion that maintains the O_2 evolving activity at least partly, with a significant slow down in oxygen evolution rates (BOUSSAC ET AL. 2004; BOUSSAC AND RUTHERFORD 1988; ISHIDA ET AL. 2008; LEE AND BRUDVIG 2004).
To study the effect of calcium on the water oxidizing reaction, depletion procedures (*e.g.* low pH) are applied. As a harsh procedure might cause secondary effects, the results could be misleading. To avoid a possible destruction of the OEC, another attempt is to substitute the cofactor biosynthetically. It was shown that the growing of the thermophilic cyanobacterium *T. elongatus* in the presence of Sr^{2+} instead of Ca^{2+} results in an exchange of Ca^{2+} by Sr^{2+} (ISHIDA ET AL. 2008).

A functional role of calcium has been found recently (HENDRY AND WYDRZYNSKI 2003). Based on time-resolved membrane inlet mass spectrometry measurements (MIMS) of

substrate water exchange kinetics, calcium is proposed to bind one of the two substrate water molecules (Chapter 4).

Chloride is proposed to be an essential cofactor. The extend to which chloride depletion disturbs the function of water oxidation, seems to depend on the experimental procedure (WYDRYZINSKI ET AL. 1990). This contradiction is the cause for a lively and ongoing discussion. It is thus of highest interest to learn about the role of chloride in water oxidation.

Ishida and co-coworkers (2008) established a procedure to non-invasively exchange the proposed cofactor Cl^- against its functional surrogate Br^-. Just as in the case of Ca^{2+}/Sr^{2+} exchange, the growing of *T. elongatus* in the presence of Br^- instead of Cl^- results in an exchange of Cl^- by Br^- (ISHIDA ET AL. 2008). They thereby deliver the tool to study chloride's function and binding site without applying harsh chemical procedures.

Chloride might be of functional relevance in interaction with substrate water. It possibly is involved in substrate water binding, like in the case of calcium. It was also proposed to be part of the network to transport produced protons from the site of water oxidation to the lumen (OLSON AND ANDREASSON 2003). An established method to determine substrate water exchange kinetics by MIMS permits finding out whether chloride interacts with substrate water either directly or indirectly. It is most interesting, if a substitution of chloride by bromide would influence the substrate water exchange rates (see Chapter 4).

Hydrogen carbonate was revealed to bind at the non-heme iron and thereby affect the acceptor side reactions (VAN RENSEN ET AL. 1999). Interpretations of measured effects were complicated by the difficulty to distinguish between acceptor and donor site of PSII. Hence the binding of hydrogen carbonate to the electron donor side, possible to the Mn_4O_xCa cluster directly, was discussed. For summaries of this long-standing discussion on a functional or structural role of hydrogen carbonate on the donor side see (KLIMOV AND BARANOV 2001; VAN RENSEN 2002; VAN RENSEN AND KLIMOV 2005). In 2008 Shevela and co-workers were finally able to disprove a direct ligation of hydrogen carbonate to the Mn_4O_xCa cluster (SHEVELA ET AL. 2008). They showed that the measured effects were clearly induced by the essential cofactor hydrogen carbonate at the donor site of PSII by MIMS and EPR spectroscopy.

Hydrogen carbonate was not only discussed to be a ligand of the Mn_4O_xCa cluster, it was also proposed to be the direct electron donor for the photosynthetic electron transport (Eq. 3). A substrate is *per* definition loosely bound, and this discussion is therefore independent of the proof that hydrogen carbonate is not a ligand to the Mn_4O_xCa cluster by Shevela and co-workers. Most scientists believe water to be the direct electron donor, but in the case proposed by Metzner in 1979 (METZNER 1979), water would still be the source of oxygen production, because the liberated CO_2 would replenish the HCO_3^- pool by rapid re-hydration of carbon dioxide to hydrogen carbonate (Eq. 4).

$$2\ HCO_3^- + 2\ H^+ \xrightarrow{h\nu} O_2 + 2\ CO_2 + 4\ H^+ + 4\ e^- \qquad \textbf{(3)}$$

$$2\ CO_2 + 2\ H_2O \longleftrightarrow 2\ HCO_3^- + 2\ H^+ \qquad \textbf{(4)}$$

The latter reaction could be catalyzed by a PSII intrinsic carbonic anhydrase (STEMLER 2002). This proposal is analyzed in chapter 3 (see also (CLAUSEN ET AL. 2005; HILLIER ET AL. 2006)).

Hydrogen carbonate is further proposed to be essential for the process of photoactivation, which is the light driven reaction sequence that leads to the assembly of the Mn_4O_xCa cluster into apo-PSII through ligation of manganese and calcium. Two light reactions separated by an intermediate dark time are required to drive the endergonic process (ANANYEV AND DISMUKES 1996; BLUBAUGH AND CHENIAE 1992; CHENIAE 1980; CHENIAE AND MARTIN 1973; DEBUS 1992A; MESSINGER AND RENGER 2008; RADMER AND CHENIAE 1977; STRASSER AND SIRONVAL 1972; TAMURA ET AL. 1989; TAMURA AND CHENIAE 1987).

1.1.8. Future Directions of Photosynthesis Research

The expanding field of artificial photosynthesis is a direct application of the described progress made in understanding the complicated mechanism of oxygenic photosynthesis and in determining the structure of the Mn_4O_xCa cluster and its ligand environment. Oxygenic photosynthesis serves as blueprint for artificial photosynthesis with the goal to use the unlimited sources light energy and water to

produce H_2 as energy rich fuel and thus answering rising energy demands, while accounting for the necessity to supply "clean" energy (for details see Chapter 6). This intricate system, which developed approximately over the past 3 billion years, has not been successfully engineered so far.

1.2. Mass Spectrometry

Mass spectrometry (MS) is one of the most accurate methods for molar weight determination. The concept of mass spectrometry was developed by J.J. Thomson (1913), on the basis of work by Wilhelm Wien in 1898 (AUDI 2006). Since then, it has advanced to a versatile and important analytic tool in science and engineering for purposes ranging from analyzing single atoms and small molecules to studying organisms up to the cell level (KALTASHOV AND EYLES 2005).

The fundamental principle of mass spectrometry is that electric, magnetic or radio frequency fields can influence charged particles.

$$m\ddot{\mathbf{r}} = q(\vec{E} + [\dot{\mathbf{r}} \times \vec{B}]) \qquad \textbf{(5)}$$

As the trajectory of a particle ($\vec{r}$) depends on both mass (m) and charge (q) it is not possible to manipulate trajectories of neutral atoms in electromagnetic fields. Therefore, it is a prerequisite for the mass spectrometry to generate ions prior to separation. A mass spectrometer measures ion abundance as a function of ionic mass-to-charge ratio after ionizing (and vaporizing if necessary) the sample. Thus, the effectiveness of ionization/vaporization defines the sensitivity of the measurement. Effectiveness is the amount of neutral particles, converted to ions and conducted to the next segment of the instrument.

High vacuum is required for mass spectrometry to prevent collision of generated ions with atmospheric gas molecules in the mass analyzer. This would lead to disturbances of the ions' trajectory.

Each mass spectrometer consists of three parts shown as block diagram (Fig. 8):

(i) *Ion generation*

(ii) *Ion separation according to m/q ratio either in space or time*

(iii) *Ion detection.*

Figure 8:

Fundamental building blocks of mass spectrometers.

The building blocks are connected to an inlet system. A personal computer is used for data analysis.

1.2.1 Sample Ionization

Electron Impact Ionization (EI)

Electron Impact Ionization (SIUZDAK 1996) is the original and most widely used technique to ionize gases and small organic compounds that readily evaporate upon heating. The volatile sample enters the ionization chamber, where it is ionized. The chamber has an ion source, a heated filament on one side, emitting electrons, and an electron trap (gold surface) on the opposite side. Two magnets placed behind source and trap, constrain the electrons into an "electron beam". The molecular ions are created through electron/molecular interaction (collision) with the sample molecules according to (Eq. 6):

$$M + e^- \longrightarrow M^{\bullet +} + 2\ e^- \qquad \textbf{(6)}$$

An arrangement of computer-controlled slits covers the opening of the chamber through which the newly created ions are extracted and thus form the ion beam. For a limited range of substances in low abundance also negative radical-anions ($M^{\bullet -}$) may be created. But since only positive ions are generated significantly by EI, it is more accurate to use m/z (z = positive charge) instead of m/q (q = charge) (KALTASHOV AND EYLES 2005).

Ionization of the sample leads in many cases to dissociation of the analyte molecule into ions with smaller mass (fragmentation), depending on primary structure, electron energy and ion source temperature (Eq. 7):

$$M + e^- \longrightarrow M^{\bullet+} + 2\,e^- \longrightarrow A^+, B^+, \text{etc.} \qquad \textbf{(7)}$$

This is used for the identification of substances. The resulting fragmentation patterns ("cracking patterns") are highly specific for each molecule. This provides a "finger print". (Databases with fragmentation patterns of numerous molecules, including biopolymers are available at e.g. http://webbook.nist.gov/chemistry/mw-ser.html; MS companies sell the library software).

The relative molecular mass of a molecule is almost the same as the mass of the created molecular ion, because the mass of the ejected electron is very small in comparison to the total mass of the molecule. Since most ions produced by EI have a single, positive charge, the mass to charge ratio corresponds directly to the relative molecular mass of the molecule, thus if z = 1 (which is usually the case) then m/z = m.

It is possible to record a mass spectrum plotting the mass of each ion on the x-axis and the abundance of the ion at each mass on the y-axis, or to plot the abundance of the ion over time, with ion abundance as the number of individual ions. The signal response can be analyzed both quantitatively and qualitatively, because the peak heights or areas represent the ionized sample amount.

Further ionization techniques are e.g. the *Chemical Ionization* (CI), which is based on the EI technique (Eq. 8), but the protonated molecular ions do not fragment as easily as the ions formed by EI. A reagent is used to react with the analyte molecule to form ions by a proton transfer (Eq. 9). The reactive ions (CH_5^+) are produced by introducing large excess of methane (CH_4) into an EI ion source (Eq. 10).

$$CH_4 + e^- \longrightarrow CH_4^{\bullet+} + 2\,e^- \qquad \textbf{(8)}$$

$$CH_4^{\bullet+} + CH_4 \longrightarrow CH_5^+ + CH_3^{\bullet} \qquad \textbf{(9)}$$

$$CH_5^+ + M \longrightarrow CH_4 + MH^+ \qquad \textbf{(10)}$$

The two "classical" ionization methods EI and CI are both vital as analytic techniques, but do not allow analysis of biopolymers. The advance of *Electro Spray Ionization* (ESI) and *Matrix Assisted Laser Desorption Ionization* (MALDI) provided the possibility to study intact proteins with no apparent mass limitation. John Fenn was honored with the Nobel Prize in Chemistry (2002) for the discovery of ESI-MS. The aqueous analyte dissolved in an appropriate solvent enters a capillary tube, which has a high electrical potential to vaporize the sample at its tip. The analyte emerges as a spray of charged droplets. The solvent droplets evaporate and the residual multiple charged sample ions are pulled into the MS. While ESI produces macromolecular ions directly from the solution bulk, MALDI desorbs analyte molecules from solid surfaces. Focused, high-density monochromatic laser radiation, which is either pulsed or continuous, is directed onto a sample target to vaporize and ionize it. The yield may be increased by mixing or dissolving the sample in a matrix. Mostly, few fragment ions are produced. Laser desorption may be used for either depth or surface profiling (for reviews see (KALTASHOV AND EYLES 2005; KONERMANN ET AL. 2008)).

1.2.2 Mass Analyzer and Ion Detection

While *Time-of-Flight* (TOF) instruments use the time it takes for ions to fly across an evacuated tube, to separate ion of different weight, *magnetic/electric sector field instruments* use the specific deflection of ion trajectories in a magnetic/electric field for this. These instruments enable separation of ions according to their individual m/z ratio with very high accuracy (the resolution is measured as a few parts per million). The fact is used that ions are deflected in the magnetic field in proportion to their square root of their m/z value and by the potential through which they have been accelerated. A *quadrupole analyzer* consists of four parallel, equidistantly spaced rods (poles) operating with crossed electromagnetic fields to pass ions through the center of the assembly. Variable static (DC) or alternating (RF) electric fields are utilized with limited resolution to either fast scan the m/z range (wide band pass mode) or to select ions by any specific m/z value (narrow band pass mode, where ions of the other m/z values collide with the poles). Different mass analyzers exist. They may be combined as *hybrid mass spectrometers* to take advantage of the strengths of each individual system. Although the techniques are quite different, only a few examples are named, because ions are always directed towards a collector for recording the number of the arriving ions at each m/z value. The mass analyzer is also

referred to as “ion optics” (ion beams may be directed and focused in electric, magnetic and radio frequency fields as light beams by glass lenses), because it focuses the ions on the collector after separating the ions according to their m/z values.

The detection system is chosen to fit the mass analyzer. Quadrupoles allow the ions of different m/z value to pass sequentially. Thus a point ion collector, which collects ions sequentially, is needed. A magnetic sector field instrument separates ions according to their m/z value by deflecting them in space, so an array ion collector, which records the ions simultaneously along a plane, is advantageous. Still, by increasing or decreasing the magnetic field it is also possible to focus the ions sequentially on a point detector. E.g. TOF is used only in combination with point ion collectors. Examples for point ion collectors are Faraday cups and electron multipliers, which generate electrical currents proportional to the number of ions arriving. (For review, see (KALTASHOV AND EYLES 2005; KONERMANN ET AL. 2008)).

1.2.3 Membrane-Inlet Mass Spectrometry

To detect processes online in aqueous solutions, the liquid sample has to be transferred from the liquid to the gaseous phase and it has to enter the high vacuum space. If the sample is gaseous, an interface between gaseous phase and high vacuum is required. Such an interface can be created in many ways.

An elegant solution is to separate the liquid phase and gaseous phase from the high vacuum by a gas permeable membrane. This technique named *membrane-inlet mass spectrometry (MIMS)* was developed by Georg Hoch and Bessel Kok in 1963 (HOCH AND KOK 1963) (see details in Fig. 9).

A porous support, which does not present a diffusion barrier, stabilizes the membrane. To prevent liquid entering the mass spectrometer, in case of membrane tearing, a cryogenic trap is installed between membrane and ion source. It is a vessel filled with dry ice and ethanol, ~ 200 K, or liquid nitrogen, 77 K. The “cooling trap” also freezes out water vapor in the tubing leading to the ion source. Entering of water vapor should be prevented, because it causes a poor signal to noise ratio by destabilizing the high vacuum and thus the ionization. Both temperature and length of the cryogenic trap determine which gaseous compounds are trapped.

Three valves frame the tubing between inlet and ionization chamber (instrument). The first valve allows closing the tubing directly behind the inlet. The second valve opens into a vacuum pump and thus enables the creation of a pre-vacuum in the tubing. The third valve opens into the ionization chamber and the high vacuum created by the turbo pumps. The additional vacuum pumping system in the tubing outside the instrument removes any frozen liquids in the cooling loop.

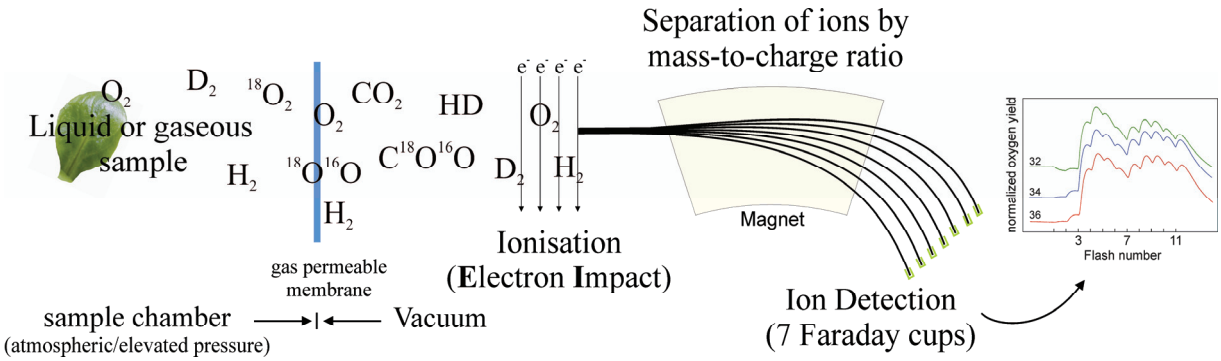

Figure 9:

A magnetic sector field mass spectrometer with electron impact ionization is equipped with a membrane-inlet. Gaseous molecules pervaporate the membrane and enter the ion source. The ions are then separated in the magnetic sector field in space. An array of Faraday cups allows simultaneous collection of seven masses according to their mass per charge ratio (m/z). Displayed is the set-up, which was used in this work.

To detect different isotopes simultaneously, an array of 7 Faraday cups was chosen as detection device for the present study. The deflected ions collide with a metal sheet and electrons released through the impact create an electrical current that is measured directly. Computer controlled positioning of the magnet allows selecting which gases are collected by the cups. One setting is the simultaneous detection of m/z = 32 (O_2), 34 ($^{18}O^{16}O$) 36 ($^{18}O_2$) and 40 (Ar), 44 ($^{12}CO_2$), 46 ($^{12}C^{18}O^{16}O$), 48 ($^{12}C^{18}O_2$). Another preset cup alignment is to detect either m/z = 2 (H_2) and 3 (DH), or 3 (DH) and 4 (D_2).

A trigger to initiate the reaction is required for kinetic analysis. The triggering process disrupts equilibrium conditions and allows measuring relaxation processes with a defined starting point. The triggering enables time-resolution and thus determining rate constants. For photochemical processes, e.g. photosynthesis an optical trigger is used. Further possibilities to start the reaction of interest are e.g. mixing of the reactants where the speed depends on the time scale of the reaction. It can be as short as a few microseconds (KNIGHT ET AL. 1998; SHASTRY ET AL. 1998). Or caged-

compounds which are photo-destroyed at a defined time can be used (ALLIN AND GERWERT 2001; KOTTING ET AL. 2007; SCHLICHTING ET AL. 1990).

Magnetic sector field mass spectrometry permits distinguishing between atoms and small molecules with different isotopic composition. Thereby this technique allows tracking the isotopic labelled reactants (*e.g.* the substrate) in the biochemical reactions.

Isotopes are defined as atoms with the same number of protons, but a different number of neutrons and thus different atomic weight. Most elements can exist in stable and unstable forms. The latter is radioactive (noble prize, Francis William Aston, 1922). There are 80 elements with at least one stable isotope.
The difference in weight might result in a separation between the light and heavy isotopes in the course of (bio)chemical reactions termed *isotope fractionation*. This becomes relevant, for example, in the case of carbon fixation, where ^{12}C is preferred over ^{13}C leading to an enrichment of the heavier atom in the atmosphere. Stable isotopes of molecules ubiquitous in biology ($^{12}C/^{13}C$, $^{1}H/^{2}H$ (D), $^{14}N/^{15}N$, $^{16}O/^{17}O/^{18}O$ and $^{31}P/^{32}P$) usually do not exceed 1%. The numerical values vary depending on the uncertainties of the absolute isotope abundance measurements (COPLEN ET AL. 2002).

Table 1:

Accurate mass and natural abundance of oxygen isotopes (AUDI AND WAPSTRA 1993; COPLEN ET AL., 2002).

ISOTOPE	ACCURATE MASS, U (STD, *μu*)	NATURAL ABUNDANCE
^{16}O	15.994 914 622 3 (0.0025)	0.997 6206 (5)
^{17}O	16.999 131 50 (0.22)	0.000 3790 (9)
^{18}O	17.999 160 4 (0.9)	0.002 0004 (5)

For reactions with water as proposed substrate, e.g. oxygenic photosynthesis and artificial compounds producing dioxygen, it is apparent to introduce isotopic labelled water ($H_2{}^{18}O$) and to detect produced labelled oxygen species in response to the $H_2{}^{18}O$ incubation time (Table 1, Fig. 14).

1.3. Thesis goal

The aim of this work was to study diverse problems concerning the natural and artificial photosynthetic oxygen evolution by employing isotopic labelling and isotopic ratio membrane-inlet mass spectrometry (MIMS).

An important part of the work was to develop and test specifically designed inlet systems for MIMS. The new inlet-systems were then used to obtain information about (*i*) the identity of the substrate in photosynthetic oxygen evolution, (*ii*) the involvement of the proposed cofactors chloride and calcium in substrate water binding and (*iii*) a possible product inhibition of Photosystem II at elevated oxygen pressure.

Another goal was to establish a general method, which can be used to characterize the water-splitting efficiency of artificial compounds.

Chapter 2

Materials & Methods

2. MATERIALS & METHODS

2.1. Membrane-Inlet Mass Spectrometry

Membrane-inlet mass spectrometry employs a specific inlet design that allows online detection of (dissolved) gasses. The interface between the gaseous or liquid sample and the high vacuum of the instrument is a semi-permeable membrane. The limitations to the reaction cell design are membrane stability and inlet size to maintain a stable vacuum within the instrument. In this work different cell designs are introduced, spanning cells to measure gaseous and liquid samples to a cell allowing measurements of liquid samples at elevated pressure of up to 20 bar.

The isotopic ratio magnetic sector field mass spectrometer (Thermo Finnigan, Delta ^{plus}XP) is equipped with an electron impact ion source and seven Faraday cups to simultaneously detect $^{16}O_2$ (m/z = 32), $^{16}O^{18}O$ (m/z = 34), $^{18}O_2$ (m/z = 36) and $^{12}C^{16}O_2$ (m/z = 44), $^{12}C\ ^{16}O^{18}O$ (m/z = 46), $^{12}C^{18}O_2$ (m/z = 48). At m/z = 36 two different species are detected, $^{18}O_2$ and an isotope of Argon, ^{36}Ar. At m/z = 40 the main Argon peak is simultaneously detected online. In accordance with the different abundance of the isotopes, the faraday cups have different amplification factors. Cup 1 and 5 detect the most abundant, unlabeled oxygen and carbon dioxide species (m/z = 32 and 44 respectively). Amplification is comparatively low ($1 \cdot 10^9$). Single labeled species are collected with cups 2 and 6, respectively (m/z = 34 and 46). They are both amplified $1 \cdot 10^{11}$ times, while the least abundant, double labeled dioxygen and carbon dioxide species are collected with cups 3 and 7 (m/z = 36 and 48) which are amplified $1 \cdot 10^{12}$ times. For cups 1 and 3 it is possible to change the cup settings software controlled and to switch between a high (10^9 and 10^{12}) and a low ($3 \cdot 10^8$ and 10^{11}) amplification. Additionally it is possible to exchange the resistors of each cup in the instrument manually (not done in this study). The corresponding amplification factors allow direct comparison of dioxygen and carbon dioxide traces. Direct comparison of amplitudes is complicated by differences in molecule size and properties, which affect the membrane permeability and by different ionizabilities of analytes. Therefore, calibration with known standards is required for quantitative work. With cup 4 the abundant argon signal (m/z = 40) is detected with an amplification factor of $1 \cdot 10^{10}$. Since this signal does not change in response to light or by reaction with artificial

oxidants, it functions as control to how much air has been introduced to the system (e.g. by injection). It can be indicative for membrane permeability, e.g. due to heat effects.
A cooling trap filled with either ethanol/dry ice or liquid nitrogen is used. Due to its low temperature liquid nitrogen freezes out gases with melting points lower than 63 K e.g. CO_2 and acetonitrile.

2.2. Membrane Properties and Inlet Area

A semi-permeable membrane functions as analyte inlet system by separating the high vacuum from the sample. The membrane is permeable, not porous: the analyte molecules do not diffuse through the membrane, but follow a three step process, termed pervaporation (KONERMANN ET AL. 2008; JOHNSON ET AL. 2000; SILVA ET AL. 1999). In a first step, the gas is adsorbed on the surface of the membrane. In a second step, the analyte molecules enter the membrane (permeation). The third step is a desorption process of the molecules on the other side of the membrane. The rate constant of gas transmission (k_{trans}) through the membrane is given by Fick's law (Eq. 11) (HOCH AND KOCK 1963; KONERMANN ET AL. 2008; JOHNSON ET AL. 2000).

$$k_{trans} = (P\ A\ \Delta p)/l \qquad \textbf{(11)}$$

with P = gas permeability constant, A = area of the membrane inlet, Δp = partial pressure difference across the membrane, l = membrane thickness.

The analyte pervaporates readily through the membrane, because the partial pressure (concentration) of the analyte on the low pressure side of the membrane is very small. The difference between the two sides is even greater when the pressure is increased in the reaction chamber (100 fold from 0.21 bar to 20 bar in the case of O_2). k_{trans} is therefore proportional to the analyte concentration in the liquid phase and detected signals reflect the analyte's concentration.

Stirring of the sample solution, improved by the stir bar running directly in front of the membrane and a small sample volume, and on the other side of the membrane,

high rate pumps can increase the vacuum to enhance the process. Depending on application, it is necessary to optimize both parameters.

Optimization of the membrane itself is necessary depending on the task: different applications demand specific membrane properties (Table 2). *(i)* For time-resolved measurements it is most important to use a fast-response membrane, because the permeability of the membrane is usually rate limiting (KONERMANN ET AL. 2008). *(ii)* To measure artificial compounds that might be corrosive, because they are partly dissolved in organic solvents and at acidic conditions, with yet unknown reaction products, it is most important to use a repellant membrane material e.g. Teflon, which is unaffected by most chemicals. *(iii)* To measure liquid samples at high pressure it is necessary to stabilize the membrane, because the pressure forces the silicon molecules closer together, yielding a more tightly packed structure. The diffusion is limited and the signal response diminished. A membrane stabilized by a metal or plastic grid yields greater signal amplitudes.

The permeability of the membrane depends on the size and on the chemical nature of the anlalyte molecule. Therefore, for quantitative measurements calibrations need to be performed for each analyte. This has to be kept in mind when comparing different species.

Membrane area (inlet-size):
The high vacuum (10^{-7} to 10^{-8} mbar) in the instrument has to remain stable during measurements, especially to assure long lifetimes of the ion source. When the system is e.g. operated regularly at 10^{-6} mbar, the ion source has to be replaced approximately twice per year.

The size of the inlet strongly depends on the desired application. Measurements of gaseous phases require a small inlet, because a large amount of gas pervaporates the membrane. An inlet area of Ø 3 mm is optimal for a cell to detect the gaseous phase. In addition, the inlet to the high-pressure cell needs to be small, to reduce the surface between high vacuum and pressure. A small gas-inlet is also required, because it is essential that high gas concentration remain in solutions, which correspond to the increased gas pressure.

For time resolved measurements and measurements of FIOPs on the contrary, a large inlet is vital to detect photogenerated molecular oxygen immediately. Degassed liquid in the reaction chamber, provides the highest vacuum of down to $4 \cdot 10^{-8}$ mbar.

Table 2:

Membrane properties

APPLICATION	MEMBRANE MATERIAL & PROPERTIES
Study of artificial compounds	✓ Teflon ✓ repellant material, unaffected by most chemicals ✓ 12.5 µm thick ✓ H. Sauer Laborbedarf, Germany
Time-resolved measurements	✓ Silicon ✓ fast-response membrane ✓ 25 µm thick ✓ Mempro, MEM 213
Experiments at elevated pressure	✓ silicon membrane with embedded metal grid ✓ pressure stable ✓ Franatech GmbH, Germany

2.3. Construction of Reaction Cells (Inlet Design)

Several reaction cells have been constructed and an existing one improved respectively, of which the two most important ones for this study are displayed in Figs. 10 and 11. The first reaction cell was used for two very different applications: *(i)* artificial Mn-compounds dissolved in aqueous solution (water/acetonitrile mixtures) fill the reaction chamber (Fig. 10A). Appropriate oxidants are injected by a Hamilton syringe to induce dioxygen evolution. *(ii)* Kinetic measurements are performed with the same cell construction (Fig. 10B). The reaction chamber is filled with PSII samples and time resolution is achieved by rapid $H_2{}^{18}O$ injection with a computer controlled solenoid valve. All photosynthetic samples are illuminated through a quartz window.

The home-built reaction cell (Fig. 10) was constructed previously by Dr. Johannes Messinger as advancement of the cell described in (MESSINGER ET AL. 1995). The volume of the sample chamber has been decreased from 300 μl to 150 μl to reduce usage of limited reactants (*e.g.* $H_2{}^{18}O$).

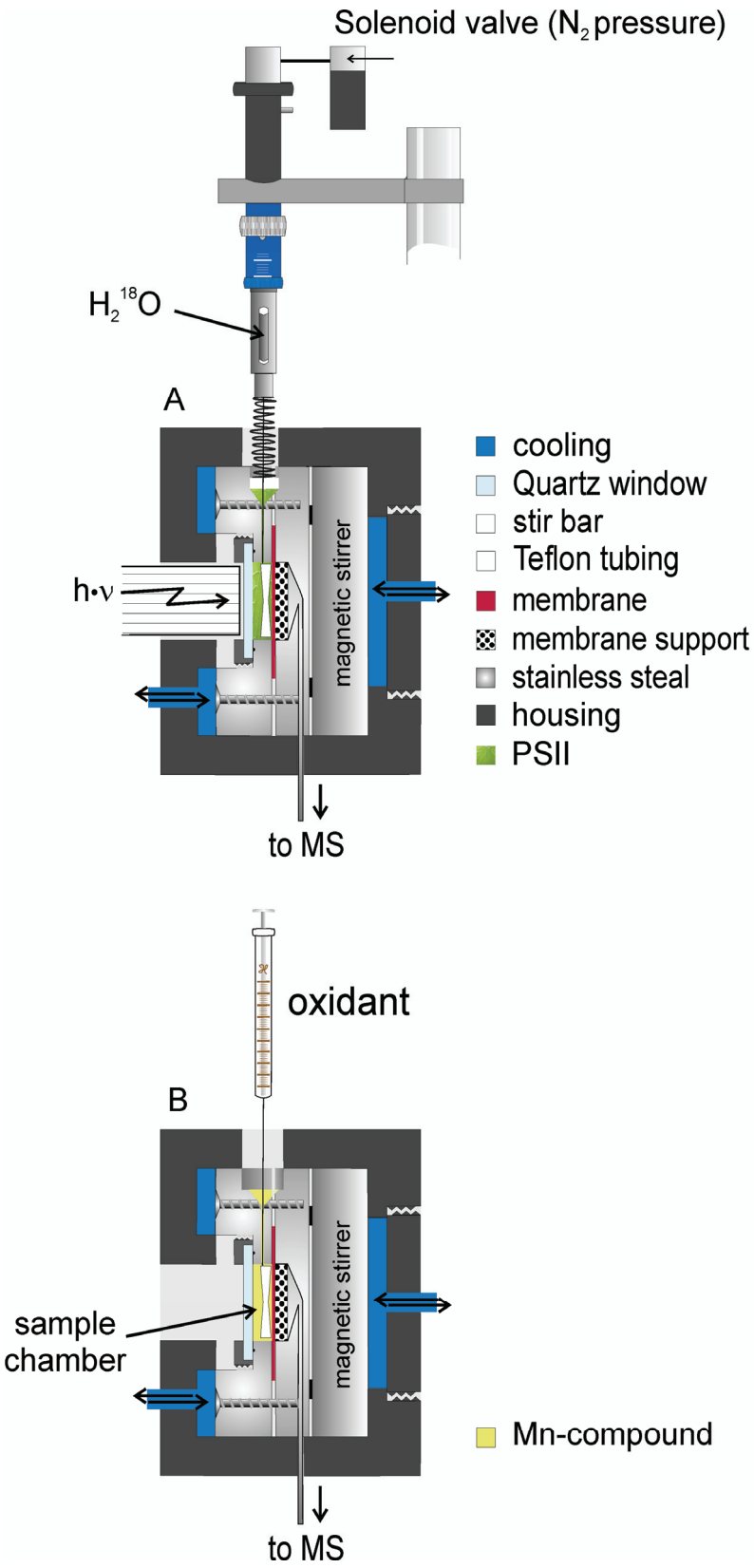

Figure 10:

Profile of the MIMS-reaction cell used for analysis of artificial Mn-compounds (A). Two steal units are combined to form one sample chamber that is flanked on the one side by a quartz window (light blue) and on the other side by a membrane (red). The membrane is permeable for gases. It separates the aqueous solutions from the high vacuum of the mass spectrometer. A porous Teflon support (black dots) stabilizes the membrane. The sample chamber has space for a Teflon coated cross-stir bar (white) which is driven by a magnetic stirrer kept next to the sample chamber. A hard plastic housing (black) to keep the reaction cell in an upright position holds the reaction cell, magnetic stirrer and a cooling system. This allows access to the reaction chamber from the top. The final volume of the reaction chamber is 150µl. For time-resolved measurements, $H_2{}^{18}O$ is injected by a Hamilton CR-700 syringe adapted to a computer-controlled solenoid, operated at up to 8 bar N_2 pressure. A computer triggered Xe-flash lamp and the rapid $H_2{}^{18}O$ injection are combined to run specific injection/flash-illumination protocols. The syringe is fixed in a mobile holder, which moves the syringe up and down. The bar containing the fixture is screwed to a stage, movable in X- and Y-direction. This positions the needle precisely above the small entrance to the sample chamber that has approximately the size of the needle.

Two units made of stainless steel to form the sample chamber. In one of the units a hole was drilled which seamlessly fits the porous Teflon support (Ø 10 mm). In the other half of the steel block a corresponding space with Ø 10 mm is cutout. Two openings arise from this side of the sample chamber: one is a small drilled hole

through the steel block to the top of Ø 0.8 mm. It provides access to the sample chamber via a needle (Hamilton syringe) for cell filling, cleaning and injection of substances. The second opening is closed by a quartz window (thickness: 3mm) sealed with an O-ring. The window enables sample illumination and bubble-free filling of the sample chamber with aqueous solutions. Screwed together, both steel parts form the sample chamber, which is then flanked by the Teflon membrane and the quartz window.

The membrane is larger than the Teflon support to cover it fully. The steel surface surrounding the Teflon support serves as sealing surface and small amounts of high vacuum grease (Lithelen, Leybold Vakuum GmbH, Germany) are used to stick the membrane to the steel. To prevent disturbances, the membrane fits smoothly to the steel and small air bubbles are released before screwing the two halves together. The set-up is equipped with a cross-stir bar (stirrer: “Micro” operated at 1000 rpm, H+P Labortechnik AG, Germany, stir bar: Bohlender GmbH, Germany) allowing rapid mixing of the aqueous solution in the sample chamber. To fit the sample chamber precisely a stir bar with a magnet size corresponding to the cell dimensions was bought. The Teflon coating was cut down to a thin layer and the edges rounded by rasping to fit the cell precisely. The size of the stir bar determines degassation speed of the solution and precise fitting allows smooth running to gain a good signal-to-noise ratio.

The stir bar moves directly on the membrane. To prevent tearing of the latter on an unevenness, the Teflon support has a smooth side (glossy appearance) facing the membrane. Further, a seamless rest of the Teflon support in its spacing is important to prevent lifting of the membrane off the steel surface.

The temperature is controlled with a cryostat (Ecoline Re 307, Lauda, Germany) pumping cooling liquid through two connected and one separate jacket (Fig. 10, blue blocks). A temperature sensor in contact with the reaction cell is held by the housing (Fig. 10, black). The magnetic stirrer is placed next to the steel block enclosing the reaction chamber. Because it heats up greatly during operation, it is combined with a cooling unit.

To achieve the necessary time resolution for kinetic measurements, the reaction cell is equipped with a computer controlled injection and illumination system (Fig. 10A).

The syringe (Hamilton CR-700, USA), loaded with $H_2{}^{18}O$, was adapted to be triggered by a computer-controlled solenoid operating with a N_2 pressure line of up to 8 bar (AEV-12-10-A-P, Festo, Germany) to enable rapid emptying of the $H_2{}^{18}O$ into the sample chamber. The triggering of the syringe and the Xe-flash lamp are both controlled by Lab View software (National Instruments, USA) that combines preflashes, the injection at defined times before one flash and a second flash sequence after a defined time for normalization. A short plastic glass rod is used to connect the Xe-flash lamp (~ 5 µs FWHM, EG&G, USA, model PS 302, light pack FY-604, polarization voltage of -750) directly to the quartz window of the reaction chamber. The syringe's $H_2{}^{18}O$ chamber is flanked by a window (Fig. 10A) and, aided by a magnifying glass, allows bubble free loading. A Teflon tip is forced down by the released N_2-pressure into a fitting Teflon counter piece, pushing the $H_2{}^{18}O$ in the sample chamber (Fig. 10A, syringe/white). Both need to be replaced when worn out by the force of injection, because untightness causes small amounts of $H_2{}^{18}O$ to leak into the reaction chamber prior to injection.

The high pressure with which the $H_2{}^{18}O$ is pushed into the cell causes a disturbance in the sample chamber that mixes the $H_2{}^{18}O$ with the thylakoids sample rapidly and forces some of the sample out the chamber. If no care is taken, the sample flows back immediately and then contains dioxygen from the air perturbing the dioxygen measurements. Therefore, a valve was constructed to release the pressure and at the same time prevent a flow back of the excess sample. This is solved by combining Teflon tubing that fits into the opening of the sample chamber with a spring (Fig. 10A, white tubing, dark gray spring). The pressure forces the spring up, and as soon as the spring is released the Teflon tubing blocks the entrance to the sample chamber and prevents flow back of excess sample as well as sample exiting the chamber. Another cause of disturbance are small vibrations of the needle containing $H_2{}^{18}O$ (*e.g.* when hitting the cell walls). Air enters the needle and is later injected together with the $H_2{}^{18}O$. This was solved by fixing the syringe in a mobile holder. The holder is movable up and down as well as in X- and Y-direction, to position the needle precisely above the small entrance to the sample chamber that has approximately the size of the needle.

Secondly, a reaction cell resisting high pressure was constructed together with Dr. Jürgen Clausen (group of Prof. Dr. Wolfgang Junge, University of Osnabrück, Germany) to connect to the isotope-ratio mass spectrometer (Fig. 11). Additionally, a

second high pressure cell for pre-incubation of buffer at elevated pressure was constructed. Both steel cells are approved to resist up to 20 bar gas pressure.

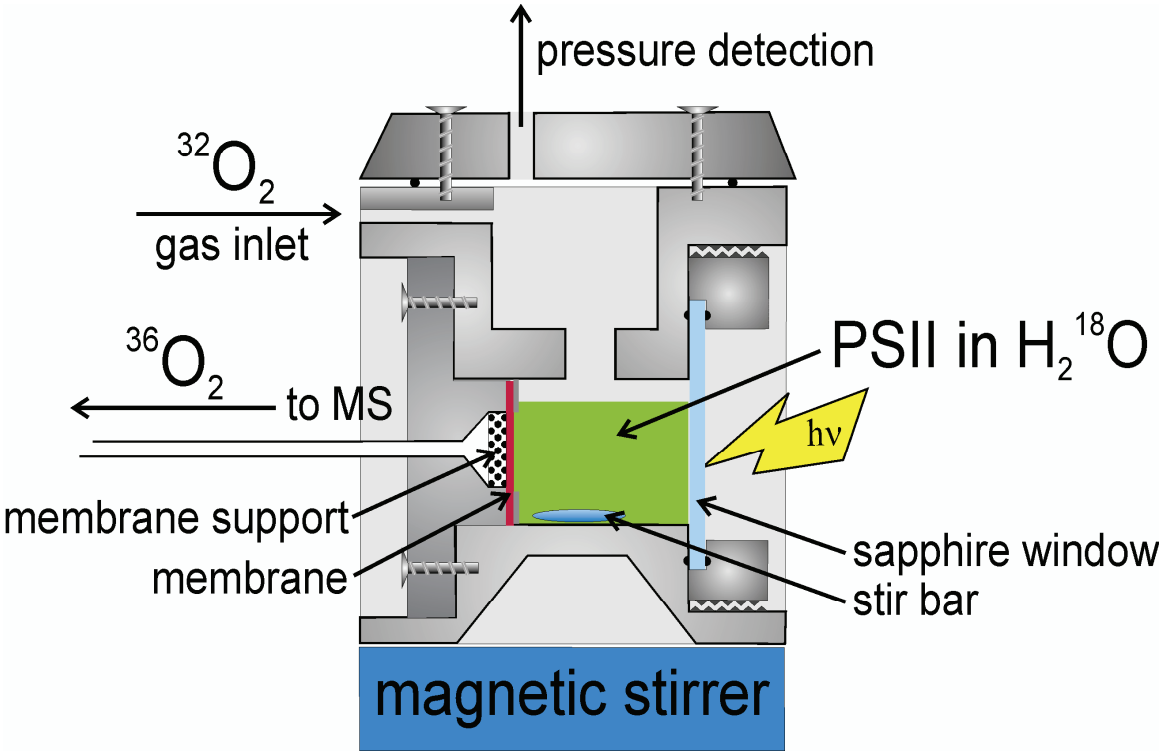

Figure 11:

For MIMS-measurements of thylakoid samples at elevated pressure, a gas tight cell was constructed. The steel block resisting up to 20 bar pressure consists of four parts: *(i)* a "main block" with three openings, forming the sample chamber, *(ii)* tubing to the MS opens up in a steel part to form a space for the porous Teflon support. The rigid membrane (medal grid cast in silicon, Franatech GmbH, Germany) rests on the steel surface. The steel part is larger than the opening of the base to the sample chamber (opening has precisely the size of the Teflon support, Ø 3 mm) to form a sealing surface. To stick the membrane to the steel before screwing it to the base, the membrane is sucked onto the support by a pre-vacuum prevailing in the tubing (before MS entrance) and high vacuum grease applied to the steel sealing surface. *(iii)* Opposite to the membrane a quartz window is screwed tightly in front of the second opening of the "main block". *(iv)* A steel lid to seal the 3rd opening of the "main block" and connect a pressure line and a pressure detector to the set-up. The nominal volume of the sample chamber is 1ml, while a filling volume of 700 µl is used to increase the interface between elevated pressure and liquid and thus enhance gas diffusion into the liquid.

On one side the chamber opens to a sapphire window, which resists at least 20 bar of pressure. On the opposite side the inlet to the mass spectrometer is located. The ⅛ inch tubing (Swagelok, USA) ends in a 3 mm opening in which the porous Teflon support (small parts INC., USA) is seamlessly resting. The support is covered by a membrane to separate the high vacuum needed for the mass spectrometry ($8x10^{-8}$ mbar) from the atmospheric pressure or elevated pressure of the sample chamber. The opening is part of a 13 mm round surface which is used to screw the tubing to the sample chamber and thereby tighten the membrane. Only the membrane (Ø 3 mm) is in contact to the liquid sample to reduce mechanical stress. Grease alone does not

stick the rigid membrane, which is strengthened by an embedded metal grid, to the sealing surface. Screwing the precisely fitting metal part to the steel block (Fig. 11) yields large air filled crinkles. To reach a high vacuum within the instrument it is necessary *(i)* for the membrane to precisely fit the sealing surface, *(ii)* to suck the membrane to the steel by a pre-vacuum and to *(iii)* connect the steel unit without moving the membrane by a flexible, short pressure proof hose.

On the bottom of the sample chamber with a nominal volume of 1 ml the steel has a thickness of 10 mm to allow driving of the stir bar by the magnetic stirrer. The top, screwed tightly to the steel block, is connected to a pressure detector (Huba control, Germany). The pressure is built up via a connection between the sample chamber and a gas cylinder (200 bar reduced to 20 bar by a pressure reducing regulator (Messer, Germany)).

The high pressure clearly reduces the sensitivity of the set-up, most likely by compressing the membrane and reducing this way its gas permeability. To separate pressure induced effects on the set-up from the influence of high O_2 concentrations on the PSII samples (Chapter 5); controls are performed at N_2 pressure.

2.4. $H_2{}^{18}O$- Injection

The injected $H_2{}^{18}O$ is rapidly mixed by the force of the injection, rather than by the stirring devise, with k_{inj} = 97 ± 3 at 5 bar. The rate of injection was determined by the injection of a saturated fluorescein solution (dissolved in ethanol) into the water filled sample chamber at standard conditions; the entrance to the mass spectrometer is closed (Fig. 12). Light of the wavelength 480 nm (LED) excites the fluorescein and depending on the time it takes to inject the solution into the sample chamber, fluorescence is emitted which is detected by a photo diode. Blue light is directed into the cell by a beam splitter (50% grey filter, Fig. 12, grey). The emitted fluorescence is detected by a photo diode at 530 nm. An edge filter (500 nm) blocks out the blue, excitation light in front of the photo diode. A lens focuses the beam onto the photo diode and a computer triggered oscilloscope (T210, Tektronix, USA) records both the computer controlled triggering event and the emitted fluorescence (Fig. 13).

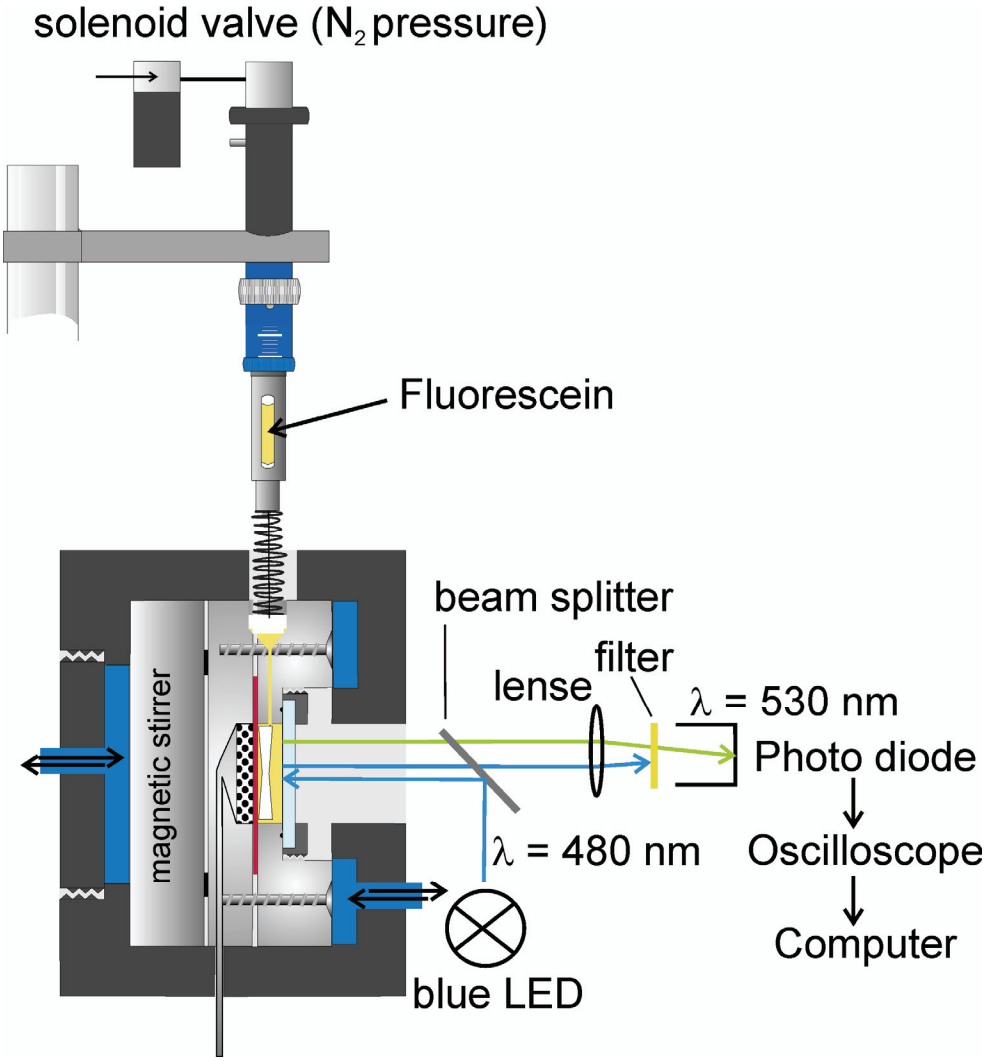

Figure 12:

Determining injection rate by fluorescein injection. Blue light (480 nm, LED) excites the fluorescein and according to the concentration of fluorescein in the sample chamber, a proportional amount of fluorescence is emitted and detected by a photo diode. A beam splitter (grey) reflects blue light into the sample chamber, while emitted fluorescence (530 nm) passes, which is detected by a photo diode. An edge filter (500 nm, yellow) is used to block out the excitation light in front of the photo diode and a lens to focus the beam onto the photo diode. An oscilloscope (T210, Tektronix, USA) triggered by a computer was employed to record the response of the photo-diode.

The fluorescence signal is detected in response to fluorescein injection at 1.5 bar, 5 bar and 8 bar pressure at the solenoid valve. The rise is best described by a monoexponential function (fitted in sigma plot, Systat Software, USA).

The force of the injection is absorbed by the use of a valve in the form of a spring pressing down a Teflon peace, which fits into the opening to the cell (Fig. 12). It is possible that the valve decreases the mixing speed of injected fluorescein ($H_2{}^{18}O$) by restraining sample outlet.

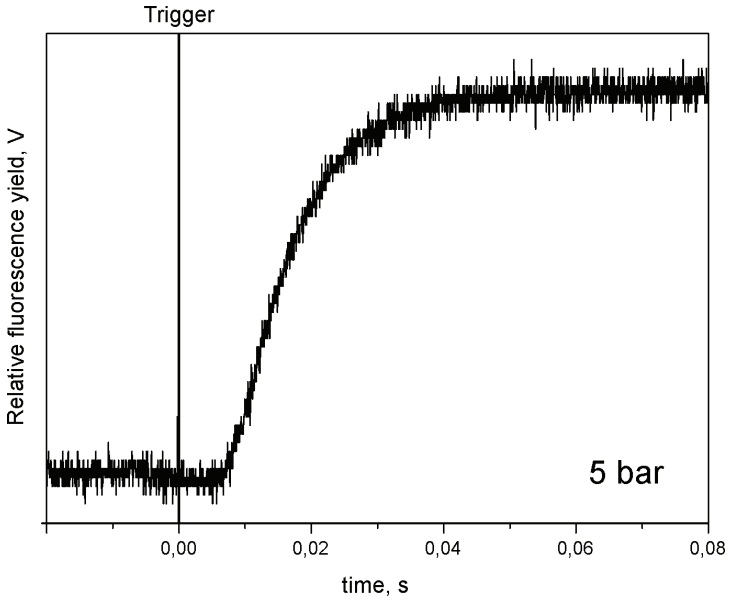

Figure 13:

Fluorescence trace initiated by fluorescein injection. The triggering event was computer controlled (Lab view software). An oscilloscope recorded trigger signal and fluorescence. Fluorescein was pushed into the sample chamber with 5 bar N_2-pressure.

2.5. Experimental Procedure

2.5.1 Time-Resolved Measurements

Thylakoid samples (thawed on ice and diluted to 0.2 mg (Chl) ml^{-1} with various buffers, see Section 2.7) were pre-illuminated with one saturating Xe-flash (Section 2.3), in thin glass-tubes (Ø 3 mm) and incubated for 45 min at room temperature to populate Y_D^{ox} and to maximize the S_1 state population (Section 1.1.5). Aliquots of the diluted, preflashed and dark-adapted sample were manually injected into the MIMS-sample chamber. The sample-temperature in the reaction chamber is kept constant at 10°C. The syringe is loaded bubble free with $H_2{}^{18}O$ that contains a few µl of an O_2 scavenging enzyme assay (see below). A small droplet is created on the needle tip to adjust for an air-filled cavity created by surface pressure in the capillary. The droplet cancels out small vibrations of the needle caused by movement of the syringe on the holder (Fig. 10). The syringe is carefully lowered into the sample chamber and fixed with a screw. To reach a stable baseline, the PSII sample is degassed for approximately 20 min prior to starting the flash-injection protocol.

2.5.2 O_2 scavenging assay

The $H_2{}^{18}O$ contains dissolved dioxygen which could not be distinguished from photosynthetically produced dioxygen upon injection of the labelled water. To reduce labeled background oxygen small quantities of a glucose/glucose oxidase/catalase assay are added (1 µl/Injection). The glucose oxidase (sigma-aldrich, USA) catalyses the reaction of O_2 and β-D- (+)-Glucose (sigma-aldrich, USA) to H_2O_2, while an H_2O_2 oxidoreductase (referred to as catalase, sigma-aldrich, USA) oxidizes two molecules hydrogen peroxide to two water molecules and one dioxygen. The catalyzed reaction converts dissolved dioxygen to water ("O_2 scavenging"). To prevent tainting of the results by enzyme access converting photosynthetically produced dioxygen to water, the enzyme concentration is adjusted carefully. It is as important to add enough enzymes, reducing the background dioxygen level, to enable measurements of small amounts of evolved dioxygen. Injections of $H_2{}^{16}O$-enzyme assay into water give the correct enzyme concentrations. To determine the remaining injection artifact the $H_2{}^{18}O$/enzyme mixture is repeatedly injected into buffer (blank) several times each measurement day.

A stock solution of glucose oxidase is kept at 4°C, while catalase is freshly dissolved in Mes-buffer (pH 6.5) before measurements. The two stock solutions (4.08 mg/ml glucose oxidase (181,000 units/g solid), 6.0 mg/ml Catalase (1,927 units/mg solid) are mixed and kept on ice during the day. Stock solutions (0.031 mg/ml glucose oxidase, 0.046 mg/ml catalase) and β-D- (+)-Glucose (13 mM) are mixed with $H_2{}^{18}O$ for ~ three injections. Between loadings of the syringe, the solution is kept on ice. Each injection yields 6.2 µg/ml glucose oxidase and 9.3 µg/ml catalase in the reaction chamber (V = 150µl), where further dilution takes place. The final enzyme concentration does not reduce produced oxygen significantly.

2.5.3 Flash and Injection Protocol

The degassed sample is illuminated with two short saturating Xe-flashes (Section 2.3) populating the S_3 state (Fig. 14). Back reactions to lower S-states are considerably slowed at low temperature and it is thereby ensured that most centres remain in S_3

during the flash/injection sequence (ISGANDAROVA ET AL. 2003; MESSINGER ET AL. 1993). Rapid injections of 32 μl ^{18}O-labeled water (98% $H_2{}^{18}O$ Isotrade, Germany), containing the O_2 scavenging mixture, yielded a final ^{18}O enrichment of 21.5%. The injection was performed at varying times before the 3rd, O_2 evolving flash. After 3 min, the sample is illuminated with eight Xe-flashes for normalization (2 Hz). This allows compensating for small changes in membrane permeability and sample concentration. Sample handlings were performed at very dim green light.

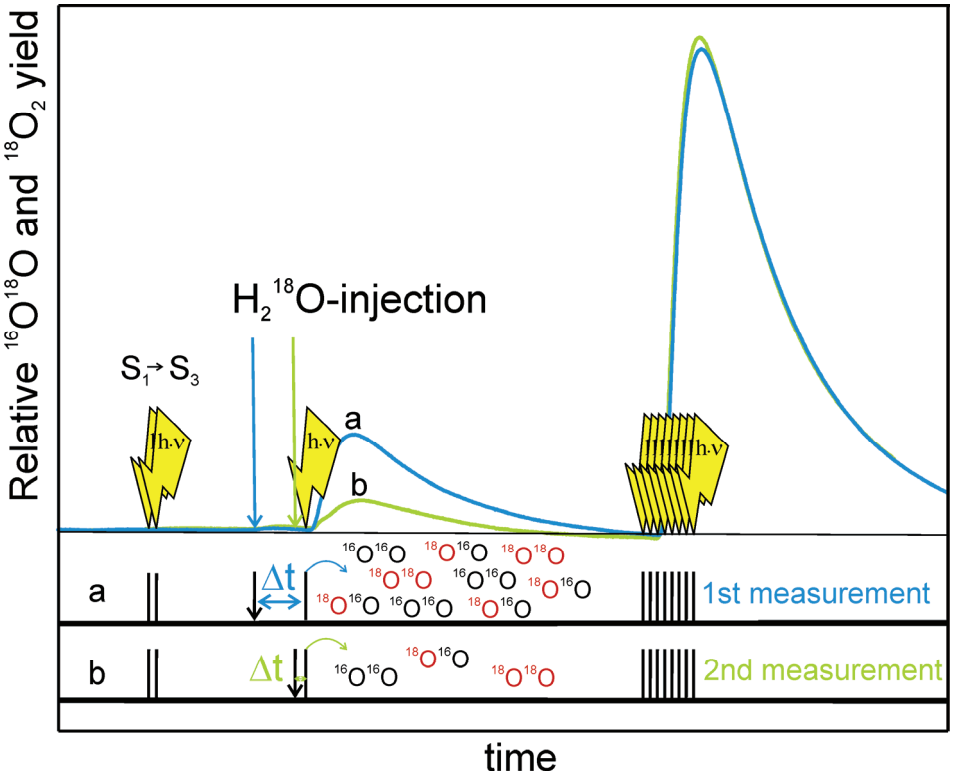

Figure 14:

To determine the substrate water exchange rate in the S_3 state, the time (Δt) between injection of $H_2{}^{18}O$ and the 3rd, turnover flash is varied. The sample is illuminated with two short Xe-flashes to convert centres from the dark-stable S_1 state into the S_3 state. Measurements are performed for Δt between 10ms and 10s. To account for small changes in chlorophyll concentrations or varying membrane permeability, the O_2 yield is normalized to the amplitude of O_2 evolution by 8 flashes given at 2Hz.

Time resolution is achieved by varying the time between $H_2{}^{18}O$-injection and the 3rd turnover flash. Depending on the exchange time, Δt, a defined amount of ^{18}O-labelled oxygen is generated by water-splitting at PSII. The corrected signal amplitudes at m/z = 34 and m/z = 36 corresponding to $^{16}O^{18}O$ and $^{18}O_2$ were plotted as a function of the exchange time Δt (Section 2.6) (MESSINGER ET AL. 1995).

2.5.4 MIMS-Measurements at Elevated Pressure

Measurements with varying overpressure are carried out between 2 bar and 20 bar (Chapter 5). Control measurements are performed at atmospheric pressure and corresponding N_2 pressure. The buffer is pre-incubated under O_2 or N_2 pressure for 40 min in a separate, stirred pressure cell of 100 ml volume (buffer: 50 mM Mes (pH = 6,5/10°C), 400 mM betain, 10 mM $CaCl_2$, 10 mM $MgCl_2$, 15 mM NaCl). The solution is saturated with the applied gas (at the chosen pressure) and thus bubbles are formed when releasing the pressure. Previous to the opening of the chamber, the pressure is released through a valve. For measurements at pH = 8 HEPES instead of Mes buffer is used (50 mM HEPES (pH = 8/10°C), 400 mM betain, 10 mM $CaCl_2$, 10 mM $MgCl_2$, 15 mM NaCl). Operation at elevated pressure requires wearing of a sufficient face protection.
In the sample chamber aliquots of either thylakoid preparations or PSII membrane fragments of spinach (final concentration of 0.2 mg (Chl) ml^{-1}), $H_2{}^{18}O$ (yielding a final enrichment of 20%), and an artificial electron acceptor are mixed with the pre-incubated buffer. As artificial electron acceptor either 7 mM ferricyanide (FeCy, dissolved in water) or 1 mM 2,5-Dichlorobenzoquinone (DCBQ, dissolved in Ethanol) were added. To ensure a high concentration of the applied gas, residual air containing O_2 and N_2 are removed by building up and releasing the pressure with the desired gas 3 times. The sample chamber is then closed by a valve and the appointed pressure controlled by a pressure detector (Section 2.3, Fig. 11). In the sample chamber, the solution is further incubated for another 30 min before illumination.

The continuous light measurements are carried out with a 250 W light source (slide projector). For the flash experiments a Xe-flash lamp (Section 2.3) is used. As photosynthetic inhibitor 3-(3,4-dichlorophenyl)-1,1-dimethylurea (DCMU, dissolved in Ethanol), is added to block the electron transfer from PSII to the PQ pool. $H_2{}^{18}O$ enrichment is used to detect light-induced oxygen evolution at m/z = 36 against the high m/z = 32 and 34 background, which is due to the applied elevated dioxygen pressure. To ensure a constant saturation level of gas during measurements m/z = 34 is detected with the 100 times less sensitive cup 1 (usually set for detection of $^{16}O_2$) before measurements, to ensure a high gas concentrations. At lower pressures (2, 5 and 10 bar) it is possible to detect $^{16}O_2$ throughout the measurement.

2.5.5 MIMS-Measurements of Artificial Mn-Compounds

Artificial compounds are dissolved in aqueous solutions (water or water/acetonitrile solutions). The production of oxygen species was induced by the addition of adequate oxidants.

The complexes Mn_2-bpmp-AcO, Mn_2-terpy, Mn_2-mcbpen and Mn_4-tphpn were synthesized according to literature procedures (BAFFERT ET AL. 2003; CHAN AND ARMSTRONG 1990; CHEN ET AL. 2005; NISHIDA AND NASU 1991; SUN ET AL. 2000). The dimeric manganese compounds were synthesized at the chair of Prof. Dr. Stenbjörn Styring in Uppsala, Sweden by Gustav Berggren (Mn_2-terpy, Mn_2-bpmp, Mn_2-mcbpen) and Dr. Magnus Anderlund (Mn_2-bpmp-AcO) while Mn_4-tphpn was provided by Prof. Dr. William H. Armstrong.

The sample chamber (V = 150 µl) was filled with the aqueous compound solution and defined amounts of isotopically labelled water ($H_2{}^{18}O$). After a stable baseline was reached the oxidant was injected and immediately reacted with the Mn-compound. Dioxygen and carbon dioxide as products of the reaction were simultaneously detected. Prior to the addition, the oxidant was purged with water or MeCN saturated N_2 to reduce the background level of dissolved gases. Each dissolved compound was concentrated to a final metal centre concentration of 2 mM. Three different oxidants were tested and compared in their ability to trigger an oxygen evolving reaction: tert-butyl hydroperoxide (TBHP, MERCK-Schuchardt, Germany), potassium peroxomonosulfate ($2KHSO_5{\cdot}KHSO_4{\cdot}K_2SO_4$, Fluka, Austria) referred to as oxone and lead tetraacetate ($Pb(OAc)_4$, MERCK-Schuchardt, Germany). With a gas tight glass syringe (Hamilton) 7.5 µl of 200 mM oxone, yielding 10 mM and 5 equivalents and 3 µl of 7 M TBHP yielding a final concentration of 5 mM, were injected. Variations of the standard concentrations are given in the figure legends. In addition Mn_2-bpmp-AcO and Mn_2-terpy were reacted with the oxidant lead tetraacetate ($Pb(OAc)_4$). Injection of 7.5 µl 200 mM $Pb(OAc)_4$ stock solution yielded a final concentration of 10 mM. Oxone was dissolved in water. Lead tetraacetate that hydrolyses in water to PbO_2 and acetic acid (AcOH) was dissolved in pure acetonitrile (MERCK-Schuchardt, Germany). Mn_2-bpmp-AcO and Mn_4-tphpn were dissolved in water/acetonitrile mixtures (3:1), while Mn_2-terpy and Mn_2-mcbpen were dissolved in water (Millipore). Additionally, Mn_2-bpmp-AcO was dissolved in an acetate buffer (100 mM, pH 4.3, purchased from MERCK-Schuchardt, Germany)/ acetonitrile solution of 3:1.

2.5.6 *MIMS-Measurements of O_2 Flash Patterns*

MIMS-measurements of oxygen flash patterns were carried out with spinach thylakoids, which were suspended in a buffer containing 5 mM $CaCl_2$, 50 mM Mes (pH 6.8/10°C), 5mM $MgCl_2$, 15 mM NaCl and 400 mM sucrose to give a final concentration of 0.02 mg Chl/ml. No artificial electron acceptors were added. Dark adapted aliquots of the sample were preflashed with one saturating Xe-flash and incubated for 20 min in the reaction chamber at 10°C. After the incubation time a stable baseline is reached and the dark-adapted samples are excited with a Xe flash-lamp (see Section 2.3). The individual flashes were separated by dark-intervals of 20 s to allow for a decline of the signal between dioxygen production (see following section, data analysis).

2.6. *Data analysis*

The signal's rise and decay kinetics depend on the intrinsic response time and the consumption of the instrument, respectively. The response time is mainly limited by the membrane pervaporation and the dioxygen signal is therefore slower detected than it is formed in the reaction chamber. Oxygen species are soluble in aqueous solutions and since the solubility of O_2 depends on its concentration in the gas phase (according to partial pressure) the amount dissolved in the sample might exceed the signal (photosynthetic/ artificial gas production). Degassing of the sample is facilitated by the adjacent high vacuum and enhanced by an effective stirring system (see Section 2.3).

After reaching a stable baseline, the gas production is triggered by e.g. oxidant injection or illumination. The oxygen (carbon dioxide) species are produced as immediate response to the oxidant injection. O_2 and CO_2 signals rise, and as the gases are consumed by the mass spectrometer, the signals decrease again.

For reactions of artificial compounds with oxidants, the reaction sequence is not necessarily known. It might consist of several intermediate steps and the production may occur over a considerable period. The rise and decay of the signal is best

described either by assigning the maximum value of the peak (subtraction of baseline) or by determining the area under the curve (integration) (Fig. 15, top and bottom). The value is then multiplied with a factor in accordance to the cup amplifications (m/z = 32 and 44 ·1000 and m/z = 34 and 46 ·10).

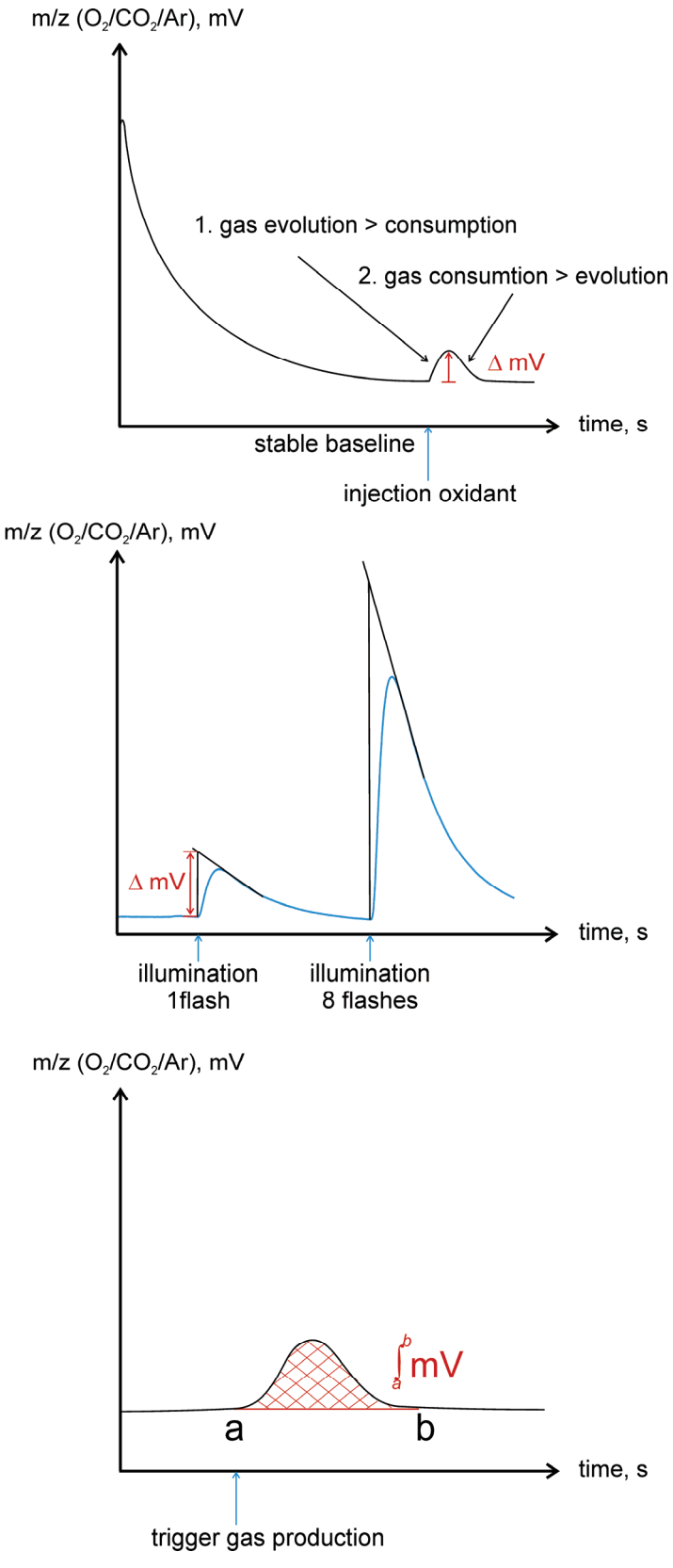

Figure 15:

Different possibilities of data analysis, depending on reaction sequence. Prior to signal triggering, the solution is degassed by the adjacent high vacuum and an effective stirring system. For complex reactions, involving possible intermediate steps, the gas production is evaluated by determining the value between baseline and maximum of the peak in mV or the area under the curve. Photosynthetic oxygen production, which is immediate in response to flash illumination is best accounted for by an extrapolated amplitude which reflects the O_2 burst within the reaction cell. The response time of the instrument is intrinsically limited mainly by the time it takes for the gas to pervaporate the membrane and by the sample volume.

The distribution of each oxygen (carbon dioxide) species is calculated in percent. The oxygen atoms of CO_2 exchange rapidly with solvent water and the calculated distribution for the CO_2 species matches the theoretical expected values for the given enrichment. It is thus possible to use the detected CO_2 species to determine the final enrichment of the

reaction solution.

In the case of oxygenic photosynthesis, the dioxygen is produced immediately in response to flash illumination. The oxygen burst in the reaction cell is not reflected by the detected signal, but tainted by slow pervaporation through the membrane and consumption by the instrument. An extrapolated amplitude represents the dioxygen evolution in the cell at the time of the flash (Fig. 15, middle part). After deriving the dioxygen yield (Y_M), the values are corrected for an injection artifact (Y_{Inj}). Though the dissolved O_2 in the $H_2{}^{18}O$ is depleted prior to injection by an enzyme assay (see Section 2.5.2), a minor amount of dioxygen is injected into the cell and cannot be directly distinguished from photosynthetically evolved molecular oxygen. The injection artifact is highly reproducible (blanks are separately recorded by injection into buffer) and can therefore be subtracted from the oxygen signal. At m/z = 36 two different molecules are detected, the desired $^{18}O_2$ and an isotope of Argon, ^{36}Ar. $H_2{}^{18}O$ is stored at argon atmosphere and the $^{18}O_2$ yield therefore needs to be corrected for the injected ^{36}Ar (Section 2.1). The amount is determined with blank injections. To account for small changes in chlorophyll concentrations, sample activity between the measurements, or membrane permeability, the O_2 yield is normalized to the amplitude of dioxygen evolution induced by 8 flashes (2 Hz) i.e. after subtraction of the injection artifact, the corrected dioxygen yield is divided by the dioxygen yield produced by 8 flashes. To allow comparison between samples, the Y_C values were normalized to one using the average dioxygen yield obtained, at long Δt where the exchange reaction is completed. Dilution and the delay between triggering event and injection are taken into account (HILLIER AND WYDRZYNSKI 2004 and Section 2.4) (Eq. 12).

$$Y_c(t) = \frac{\left[Y_M - Y_{Inj}\right]}{Y_{8\ flashes}} \times \frac{1}{\left[1 - \exp(-97t)(1 + \Delta\mathrm{Chl}\exp(-97t))\right]} \qquad \textbf{(12)}$$

The corrected $^{16}O^{18}O$ yield is plotted versus the exchange time, Δt, and the resulting biphasic response is fitted with the sum of two first order exponential functions in sigma plot (Systat, USA) with two parameters:

$$Y = 64\left[1 - \exp\left(-^{34}k_f \times t\right)\right] + 36\left[1 - \exp\left(-^{34}ks \times t\right)\right] \qquad \textbf{(13)}$$

The fast phase ($^{34}k_f$) represents the exchange of one of the two oxygen atoms. It is under normal conditions virtually complete before the slow phase ($^{34}k_s$) begins. With the exchange of only one bound substrate water molecule, unlabelled and single labeled species are evolved according to the water enrichment, i.e. at an enrichment of 21.5% the isotopic distribution is 78.5 : 21.5 : 0 for m/z 32 : 34 : 36.

At longer Δt the second substrate water molecule exchanges as well, increasing the probability of forming $^{16}O^{18}O$, since both water molecules are now exchangeable. This allows the formation of double-labeled oxygen species. The isotopic distribution is calculated according to:

$$^{16}O_2 : {}^{16}O^{18}O : {}^{18}O_2 = (1 - \varepsilon)^2 : 2(1 - \varepsilon)\varepsilon : \varepsilon^2 \quad \textbf{(14)}$$

with ε = ^{18}O enrichment

and changes to 61.6 : 33.8 : 4.6 for m/z 32 : 34 : 36. This change in enrichment explains the magnitudes of the normalized $^{34}O_2$ amplitudes that are 64% for the fast phase and 36% for the slow phase (i.e. 21.5/33.8 = 0.64).
At m/z = 36 double labeled oxygen species are detected. Both bound substrate water molecules need to be exchanged against labeled water to form one $^{18}O_2$ molecule. The exchange rate is therefore limited by the slow exchange rate and consequently a monophasic rise with $^{36}k = {}^{36}k_s$ is observed:

$$^{36}Y_c = [1 - \exp(-{}^{36}k \bullet t)] \quad \textbf{(15)}$$

2.6.1 Kok analysis

The dioxygen yields of the single flashes that are spaced apart by 20 s dark time are analyzed with an Excel spreadsheet program (Microsoft, USA), using a solver routine for error minimization of the Kok parameters. Deconvolution of the dioxygen flash pattern was based on the Kok model to determine the miss probability, α, and double hit probability, β, as well as the S_1 state population (ISGANDAROVA ET AL. 2003; MESSINGER ET AL. 1991).

The dioxygen yield of the n-th flash (Y_n) is the result of centers in S_3 undergoing a single or double turnover and centers in S_2 undergoing a double hit. Assuming that

the distribution of α and β is equal for all S-states, the oscillation can be calculated according to:

$$Y_n = (1 - \alpha)[S_3]_{n-1} + \beta[S_2]_{n-1} \quad \textbf{(16)}$$

The entire S-state distribution can be displayed as Kok matrix (K) that incorporates the α and β parameters as well as the single hit probability γ = 1 - α - β and the case of no transition 0. S_{n-1} and S_n represent the S_i state populations before and after the n-th flash of the train:

$$S_n = K \bullet S_{n-1} \text{ with } [S]_n = \begin{bmatrix} S_0 \\ S_1 \\ S_2 \\ S_3 \end{bmatrix} \text{ and } K = \begin{bmatrix} \alpha & 0 & \beta & 1-\alpha \\ 1-\alpha-\beta & \alpha & 0 & 0 \\ \beta & 1-\alpha-\beta & \alpha & 0 \\ 0 & \beta & 1-\alpha-\beta & \alpha \end{bmatrix} \quad \textbf{(17)}$$

2.6.2 Calibration

The calibration of the CO_2 and O_2 signals is performed by injecting various volumes of air-saturated water samples (tab-water incubated for several hours at 10°C) into the sample chamber filled with degassed buffer. The extrapolated amplitudes of the detected values in mV were plotted vs. gas concentration calculated according to Hendry's law in µM and linear fitted. The linear equation was used to determine the values for the detected analyte in µM. Taking into account the dependence of the solubility on Temperature, pressure and salt concentration, 21 µM CO_2 and 351 µM O_2 are dissolved in air saturated tap-water, at 10°C and atmospheric pressure (CROVETTO 1991). The relative sensitivity of the different cups was verified by measuring the same signal with all cups.

2.7. Sample Preparations

2.7.1. Thylakoid Membrane Preparation

Thylakoids were isolated from the thermophilic cyanobacterium *Thermosynechococcus elongatus* by Naoko Ishida and Dr. Alain Boussac in Saclay, France. To biosynthetically replace Ca^{2+} against Sr^{2+} and Cl^- against Br^- *Thermosynechococcus elongatus* (43-H strain, (SUGIURA ET AL. 1999)) has been grown in media containing either $CaCl_2$, $SrCl_2$, $CaBr_2$ or $SrBr_2$ at 45°C under continuous illumination (fluorescent white lamps, 80µmol of photons m^{-2} s^{-1}). Cells were harvested by centrifugation and washed once in buffer I and resuspended in the same buffer with the addition of 0.2% (w/v) bovine serum albumin, 1 mM benzamidine, 1 mM aminocaproic acid and 50 µg ml^{-1} DNaseI. Then cells were broken open with a French press (~ 700 p.s.i.) and unbroken cells removed by centrifugation (1000 x g, 5 min). Thylakoids were separated by centrifugation (180000 x g, 35 min, 4°C) and the pellet, containing the thylakoids were washed twice with buffer I. Finally, thylakoids were resuspended in the same buffer and stored at liquid N_2 at a Chl concentration of ~ 3 mg ml^{-1}. (BOUSSAC ET AL. 2004; ISHIDA ET AL., 2008)

Thylakoids were prepared by Birgit Nöring from spinach (*Spinacia oleracea*) according to Winget and co-workers (WINGET ET AL. 1965) with slight modifications (MESSINGER AND RENGER 1993). Leaves from market spinach are separated from leave stems, washed (last time in aqua dest.), weighed and buffer II added before grinding in a mixer for 4 x 10 s (500 ml buffer/kg spinach), to mechanically open up leave cells and release chloroplasts. The homogenate was quickly filtrated through a cheesecloth and centrifuged for 10 min at 8000 rpm (JLA-10.5, Avanti centrifuge™ J-20XP, Beckman-Coulter) to separate the chloroplasts from larger cell particles. The pellet is resuspended in buffer III and centrifuged at 6000 rpm for 10 min (JA-25.5, Avanti centrifuge™ J-20XP, Beckman-Coulter). The pellet is resuspended and homogenized in a small amount of buffer V and frozen in small beads in liquid N_2 and stored at -80°C. Preparation is performed at 4°C at dim green light.

2.7.2. PSII membrane fragments

Photosynthetic membrane fragments (BBY) were prepared from fresh thylakoids preparations as described in (BERTHOLD ET AL. 1981) with slight modifications (ONO AND INOUE 1983).
The chlorophyll content of freshly prepared thylakoids (in buffer IV) is determined and 25mg Triton X-100/mg Chl slowly added (use of a 25% stock solution). The solution is then incubated for 5 min in the dark to solubilise stromal thylakoid membranes containing PSI and ATPase. The solution was then centrifugation (15000 rpm, 15 min, JLA-10.5, Avanti centrifuge™ J-20XP, Beckman-Coulter) and the pellet (except for white, starch-containing bottom part) resuspended and homogenized in buffer III. A centrifugation step for 2 min at 15000 rpm follows (JLA-10.5, Avanti centrifuge™ J-20XP, Beckman-Coulter). The pellet is resuspended in buffer IV and the chlorophyll content determined. The PSII membrane fragments were frozen as beads in liquid N_2 and subsequently stored at -80°C until use.

2.7.3. Buffers

Buffer I: 40 mM Mes (pH 6.5), 15 mM $MgCl_2/MgBr_2$, 15 mM $CaCl_2/CaBr_2/SrCl_2/SrBr_2$, 10% glycerol, 1.2 M betaine
Buffer II: (grinding buffer): 50 mM Hepes (pH 7.5), 0.4 M Sucrose, 0.4 M NaCl, 4 mM $MgCl_2$ 1mM Na-EDTA, 5 mM Na-asorbic acid, 2 mg/ml BSA
Buffer III (incubation buffer): 50 mM Mes (pH 6.0), 150 mM NaCl, 8 mM $MgCl_2$
Buffer IV: 50 mM Mes (pH 6.0), 15 mM NaCl, 8 mM $MgCl_2$, 8 mM $CaCl_2$
Buffer V: 50 mM Mes (pH 6.0), 15 mM NaCl, 5 mM $MgCl_2$, 5 mM $CaCl_2$, 0.4 M sucrose

2.7.4. Chlorophyll determination

To determine the chlorophyll content (PORRA ET AL. 1989), the pigments of the thylakoids are extracted (2 x 20 µl Aliquots) with 80% buffered aceton solution (2.5 mM Na_2HPO_4/H_2NaPO_4, pH 7.8) and filtered to remove denatured protein. The absorption spectrum of the essence was then measured at 646.6 nm and 663.6 nm

and 750 nm (UV-Vis Spectrometer, Unicam, Germany) against 80% Aceton as blank. The detected absorption values (A) were then analyzed in mM according to:

For [Chla + b]: $[17.75\ (A_{646.6} - A_{750}) + 7.34\ (A_{663.6} - A_{750})]k$ **(18)**

For [Chla]: $[12.25\ (A_{663.6} - A_{750}) - 2.55\ (A_{646.6} - A_{750})]k$ **(19)**

For [Chlb]: $[20.31\ (A_{646.6} - A_{750}) - 4.91\ (A_{663.6} - A_{750})]k$ **(20)**

with $k = \mu l\ C - 1/\mu l_{sample}$) as dilution factor.

Chapter 3

Water, not Hydrogen Carbonate, is the Substrate of Photosynthetic Oxygen Evolution

3. WATER, NOT HYDROGEN CARBONATE, IS THE SUBSTRATE OF PHOTOSYNTHETIC OXYGEN EVOLUTION

3.1 Introduction

Photosynthetic oxygen production takes place in PS II (Chapter 1). The oxygen evolving complex (OEC) comprises a Mn_4O_xCa cluster, its amino-acid ligands, a redox-active tyrosine (Y_Z) and cofactors. A role of hydrogen carbonate at the acceptor side of PS II (VAN RENSEN ET AL. 2002) was reported were PS II inhibits when hydrogen carbonate is substituted for by formate (MENDE AND WIESSNER 1985). It was further suggested that hydrogen carbonate stabilises the OEC (KLIMOV AND BARANOV 2001), promotes the photo-assembly of the Mn_4O_xCa complex (ANANYEV ET AL. 2001), and interferes with the damping of the oscillatory pattern of oxygen evolution (STEMLER ET AL. 1974). It was also suggested that two tightly bound hydrogen carbonate ions, generating peroxydicarbonic acid could be the precursor for photosynthetic O_2 (CASTELFRANCO ET AL. 2007). Finally, in the structural model of PSII at 3.5 Å resolution (FERREIRA ET AL. 2004) hydrogen carbonate was presented as a ligand to the Mn_4O_xCa complex, though this could not be confirmed by the most recent crystal structure at 3.0 Å (LOLL ET AL. 2007).

It seems generally accepted that water serves as the electron donor for the production of reduced organic compounds by cyanobacteria and plants. Alternative concepts like that of Otto Warburg (WARBURG 1958; WARBURG ET AL. 1965), who proposed that 'activated CO_2' is converted to an aldehyde during oxygen evolution (see (STEMLER 2002) for a historical survey) have been discarded mainly because of mass spectrometric results. The isotopic composition of evolved dioxygen agrees with the one of water (BADER ET AL. 1987, HILLIER ET AL. 1998, HILLIER ET AL. 2000, MESSINGER ET AL. 1995, RADMER AND OLLINGER 1980) (Chapter 4). If the equilibrium between water, CO_2 and hydrogen carbonate (see below) is rapidly reached though, these data are still compatible with a catalytic role of hydrogen carbonate. Helmut Metzner (METZNER 1978) proposed a catalytic role for hydrogen carbonate on thermodynamic grounds according to the following reaction scheme:

$$2\ HCO_3^- + 2\ H^+ \xrightarrow{4h\nu} O_2 + 2\ CO_2 + 4\ H^+ + 4\ e^- \quad \textbf{(21)}$$

$$2\ CO_2 + 2\ H_2O \longleftrightarrow 2\ HCO_3^- + 2\ H^+ \quad \textbf{(22)}$$

$$2\ H_2O \xrightarrow{4h\nu} O_2 + 4\ H^+ + 4\ e^- \quad \textbf{(23)}$$

wherein *hν* stands for photon-driven processes.

In this mechanism oxygen is eventually derived from water, however, hydrogen carbonate is the primary educt and CO_2 an intermediate product according to reaction (21). The formed CO_2 is converted back into hydrogen carbonate by reaction (22). If the latter equilibrium is rapidly reached, as mediated by a carbonic anhydrase (CA) (TU AND SILVERMAN 1975; SILVERMAN AND TU 1975), then these partial reactions add up to the equation for water oxidation (equation (23)). An intrinsic carbonic anhydrase activity is indeed linked to the core and/or extrinsic proteins of PS II (DAI ET AL. 2001; KHRISTIN ET AL. 2004; LU AND STEMLER 2002; MOSKVIN ET AL. 2004; VILLAREJO ET AL. 2002). Because the reaction equilibrium ($K = [CO_2]/[H_2CO_3] = 600$; (COTTON ET AL. 1974) lies to 99.8 % on the side of CO_2, one might still expect a considerable amount of newly formed CO_2 escaping on each cycle into solution, to become detectable concomitant with O_2. In contrast to the situation in the scheme of H. Metzner, in the generally accepted view of photosynthetic oxygen evolution, with water as sole substrate, no CO_2 evolution is expected. The afore cited mass-spectrometric experiments were not designed to specifically answer the hydrogen carbonate question, neither was the CA activity assessed nor were flash-light induced O_2-release and CO_2-transients recorded simultaneously.
By membrane-inlet mass spectrometry the question is addressed whether there is a role of freely exchangeable (bulk) CO_2/hydrogen carbonate as substrate and/or intermediate product of oxygen evolution.

3.2 Results

A membrane-inlet isotope-ratio mass spectrometer was set up to simultaneously record O_2 and CO_2 at m/z = 32, 34, 36 and 44, 46, 48, respectively. Measurements under $H_2{}^{18}O$ enrichment and at low hydrogen carbonate/CO_2 concentration showed the normal oscillation of O_2-release.

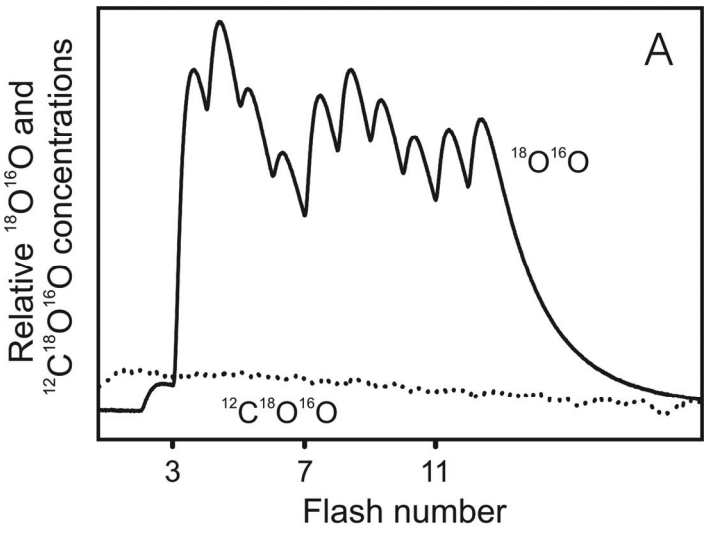

Figure 16:

Flash induced $^{18}O^{16}O$ (mass 34; solid line) and $^{12}C^{18}O^{16}O$ (mass 46; dashed line) evolution of spinach thylakoid samples. A series of twelve saturating Xe-flashes with intermittent dark times of 20s was given at 10 °C and pH 6.8. The $H_2{}^{18}O$ enrichment was 15 % and the chlorophyll concentration 0.02 mg Chl/ml. For better comparison a monoexponentially decaying baseline was subtracted from the CO_2 signal, which had a significantly higher starting value.

Figure 16 shows mass-spectrometric signals resulting from the excitation of dark-adapted spinach thylakoids with a series of 12 Xenon-flashes. For clarity Fig. 16 shows only signals of the single labelled species (cup amplification for O_2 and CO_2 are identical; see Section 2.1). Before the measurements, the PSII samples (20 µM Chl/ml at pH 6.8) were mixed with ~15% $H_2{}^{18}O$ (final concentration) and then degassed in the sample chamber under rapid stirring to about 1.4 µM CO_2 (~ 7 % of initial air-saturated value of 21 µM at 10°C) to achieve nearly constant baselines. A pre-flash and subsequent dark-adaptation were used to convert PSII centres into the $S_1Y_D^{ox}$ state, which strongly reduces the S state decay between the required long dark-times of 20 s between the flashes. The pre-flashed thylakoids were illuminated with a train of twelve Xe-flashes (~ 3 µs FWHM). The data in Fig. 16 show that oxygen is produced with high efficiency even at this low dissolved CO_2/HCO_3^- concentrations. This is evident from the clear period four oscillations in the O_2 signals, which can be well described with miss and double hit parameters of 14.3% and 3.8%, respectively, and 100% S_1 state dark-population. In contrast, the simultaneously recorded CO_2 trace does not show any flash induced signals. Thus, no evidence, under parallel detection, for any CO_2 release in response to a series of light flashes was revealed.

Figure 17 displays the decay of the normalised $^{12}C^{18}O_2$ concentration ([48]/([44] + [46] + [48])) that follows the injection and rapid mixing (< 10 ms) of 28 µl $H_2{}^{18}O$ into 150 µl unlabeled, degassed buffer containing different concentrations of spinach thylakoids. The initial rise (not shown) is due to the ambient ^{18}O-labeled CO_2 content of the $H_2{}^{18}O$ enriched water. Its decay reflects the rather complex isotopic equilibration process between all water and all CO_2, H_2CO_3, HCO_3^-, CO_2^{2-} molecules in the sample (for details see e.g. (MILLS AND UREY 1940)). Because of the above mentioned normalisation, the rates are unaffected by the simultaneous consumption

of CO_2 by the mass spectrometer. In the absence of thylakoids (trace c, Fig. 17) the isotopic equilibration is caused by chemical hydration/dehydration reactions of CO_2/H_2CO_3 and the interconversion to HCO_3^-. The observed significant increase in the rate of isotopic equilibration in the presence of thylakoids (traces b and a, Fig. 17) confirms the previously reported carbonic anhydrase activity of thylakoids. Rate constants describing the time course of this isotopic equilibration process as obtained by monoexponential fits of the normalised mass 48 signals are given in Table 3.

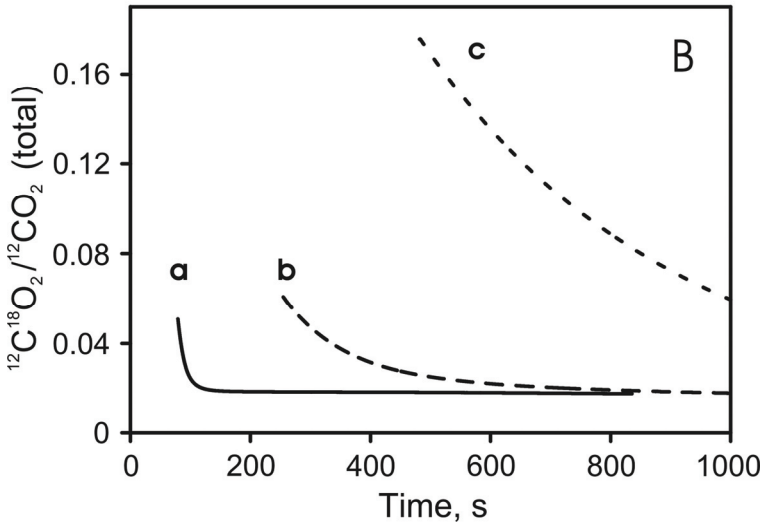

Figure 17:

Change in $^{12}C^{18}O_2$ concentration as a function of time after the injection of 28 µl $H_2{}^{18}O$ (15 % final enrichment). The concentration of spinach thylakoids was 0.20 mg Chl/ml (a), 0.02 mg Chl/ml (b) and 0 mg Chl/ml (c). Other conditions were as in Fig. 16.

Table 3:

Rates of monoexponential decay of the $^{12}C^{18}O_2$ signal after injection of $H_2{}^{18}O$ into degassed $H_2{}^{16}O$ buffer containing different concentrations of spinach thylakoids at 10 °C and pH 6.8.

CHLOROPHYLL CONCENTRATION (mg/ml)	DECAY RATE, *k* (s^{-1})	HALFLIFE-TIME (s)
0.00	0.0023	300
0.02	0.0074	95
0.20	0.0764	9

3.3 Discussion

In this chapter the question whether or not hydrogen carbonate and CO_2 are directly involved as substrate/intermediate in photosynthetic oxygen evolution is addressed. As outlined above a role of hydrogen carbonate/CO_2 as reaction intermediate during photosynthetic oxygen evolution is in principle compatible with the accepted view that dioxygen is produced at the expense of water. With MIMS it is possible to analyze

the role of freely exchangeable hydrogen carbonate/CO_2, in photosynthetic oxygen production.

If hydrogen carbonate and CO_2 are directly involved as substrate/intermediate in photosynthetic oxygen evolution it is expected that greatly decreased concentration of HCO_3^- inhibit oxygen evolution. But the mass spectrometric experiments of Fig. 16 show no effect on the typical pattern of oxygen evolution under flashing light, implying that, if hydrogen carbonate was involved, its binding to the OEC was saturated even at such low concentration (1.4 μM). It would further be expected that CO_2 is liberated concomitantly with oxygen. But the MS-experiments gave no evidence for any oscillating CO_2-release down to a level of 2% below the one of the oscillating oxygen production. This excludes the participation of freely exchangeable hydrogen carbonate/CO_2, although it does not exclude the participation of sequestered hydrogen carbonate/CO_2.

The total carbonic anhydrase activity of thylakoids from spinach was evident from the decay of the mass-spectroscopic signal at a normalised m/z = 48 ($^{12}C^{18}O_2$). Under the conditions employed in previous water exchange experiments (thylakoid concentrations of e.g. 0.25 mg Chl/ml; (MESSINGER ET AL. 1995) a comparatively long time (> 30 s) is required for reaching the isotopic equilibrium between CO_2/HCO_3^- and water. This contrasts with the rapid isotopic equilibrium in water, which is reached by physical mixing in the ms time scale (HENDRY AND WYDRZYNSKI 2002; HILLIER ET AL. 1998; HILLIER AND WYDRZYNSKI 2000; MESSINGER ET AL. 1995) (chapter 4), and is essentially unaffected by the subsequent equilibration with the CO_2 species because of the far smaller concentration of the latter. Since at 10°C the ^{18}O-label quantitatively appears in flash-induced oxygen signals within about 2 s (k_{slow} = 2.2 s^{-1}; (MESSINGER ET AL. 1995) these data also support the view that water, and not hydrogen carbonate, is directly oxidised by PSII. The function of the observed carbonic anhydrase activity of PSII in particular and of thylakoid membranes as a whole remains to be elucidated (see Table and Fig. 17, and (Stemler 1997; Stemler 2002)). It has been suggested that the lumenal carbonic anhydrase of thylakoids may play a role in the formation of a proton gradient across the thylakoid membrane in the dark in order to support ATP synthesis (VAN HUNNIK AND SULTEMEYER 2002). It may as well regulate the pH in the lumen similar to its known function in blood.

3.4 Conclusions

The results exclude any direct role of exchangeable hydrogen carbonate/CO_2 as substrate/intermediate of photosynthetic oxygen evolution, but do not exclude the participation of sequestered hydrogen carbonate/CO_2. Instead they corroborate the view that water is the direct source of electrons for the production of carbohydrates and likewise the source of the oxygen we breathe (CLAUSEN ET AL. 2005). The conclusion was confirmed by (HILLIER ET AL. 2006).

Chapter 4

Chloride influences the slowly exchanging Substrate Water

4. CHLORIDE INFLUENCES THE SLOWLY EXCHANGING SUBSTRATE WATER

4.1 Introduction

The OEC includes a Mn_4O_xCa complex, inorganic cofactors, an intermediate electron carrier (Y_Z) and the protein matrix. The OEC is located on the luminal side of PSII, well shielded from the aqueous phase of the lumen. The protein matrix seems to be of high importance and offers channels for the entry of substrate water as well as the exit of the produced oxygen and protons (for reviews see (MCEVOY ET AL. 2005; MEYER ET AL. 2007)). The protein matrix further positions the essential cofactors and supports structural changes of the active site's inorganic core during water oxidation (HILLIER AND MESSINGER 2005). (Reviewed in Chapter 1)

The structure of the catalytic center, consisting of manganese, calcium and bridging oxygen atoms is emerging. Most recently, on the basis of EXAFS spectroscopy, Yano and co-workes were able to limit the number of possible models for the structural arrangement of the Mn_4O_xCa cluster to four (YANO ET AL. 2006).
Even though this result was of high importance, the obtained knowledge is limited. Clausen and co-workers established water as the direct substrate of the reaction (CLAUSEN ET AL. 2005; HILLIER ET AL. 2006; Chapter 3), but the structure does not provide information on the substrate binding site. It is possible to learn more indirectly about the environment of water as substrate by following water exchange rates. Applying this technique, established by Messinger and co-workers in 1995 (see below), Hendry and coworkers have already successfully determined the role of calcium in the water splitting reaction. Thus, the binding site for the essential cofactor calcium was revealed on the basis of EXAFS measurements (CINCO ET AL. 1998; CINCO ET AL. 2002; CINCO ET AL. 2004; LATIMER ET AL. 1998; MIQYASS ET AL. 2007; MIQYASS AND VAN GORKOM 2007; YACHANDRA 2005; YANO ET AL. 2005B) and its role as water binding site has been established by determining substrate water exchange rates (HENDRY AND WYDRZYNSKI 2003).

In contrast to calcium, the structural knowledge obtained so far does not allow to draw conclusions on the binding site of the most controversially discussed cofactor chloride. To understand the function and role of chloride, it is of great interest to

know whether chloride interacts with or binds to the Mn_4O_xCa cluster. Most recently, two studies support a binding of chloride in the outer binding sphere of the OEC. In the first study, Haumann and coworkers propose a chloride binding site, which is not closer than ~ 5 Å from the nearest metal site (either Mn or Ca^{2+}) on the basis of Br EXAFS data. In the second study, Murray and coworkers suggest, based on bromide anomalous x-ray diffraction analysis, the existence of two halid binding sites with a distance of about 6 Å to 7 Å to the Mn_4O_xCa cluster. Due to x-ray induced reduction of the Mn_4O_xCa cluster and low resolution, the authors cannot exclude a change in the chloride binding. However, while the chloride requirement is of importance only for the $S_2 \rightarrow S_3$ and $S_3 \rightarrow S_4$ transition, the studies focused on the S_1 state, and in the second mentioned study on the reduced form of the Mn_4O_xCa-cluster (due to high radiation doses).

In contrast to the suggested two halide binding sites based on x-ray crystallography data, biochemical experiments with plants grown on radioactive $^{36}Cl^-$ yielded an estimation of one functional chloride *per* OEC (LINDBERG ET AL. 1990; LINDBERG AND ANDREASSON 1996; OLESEN AND ANDREASSON 2003). Under illumination, the OEC exhibits a high affinity for chloride with a K_d of 20 µM and one of K_d ~ 500 µM after chloride removal by dialysis against chloride free medium. The high affinity binding of K_d = 20 µM could be restored after adding chloride in darkness. Thus, a single chloride binding site may exist in a low and high affinity state (LINDBERG AND ANDREASSON 1996).

The long standing discussion about chloride as essential cofactor is nourished because the obtained results clearly depend on the depletion procedure. In order to study a possible chloride requirement by PSII, it is necessary to remove or substitute chloride, but Wydrzynski and co-workers have shown already in the beginning of the 90's (WYDRZYNSKI ET AL., 1990) that there is a complex dependence between secondary effects caused by depletion treatments and the chloride requirement itself. While the depletion complicates the interpretation, it does not exclude a chloride requirement of PSII.

Dialysis is a means to deplete samples of chloride while ensuring that the PsbP and PsbQ subunits remain bound to PSII (section 1.1.2). Cl^- depletion through dialysis against Cl^- free medium yields samples which continue to work, but with diminished O_2 evolving activity (LINDBERG AND ANDREASSON 1996). However, Ishida and co-

workers questioned the complete removal of chloride in this study (ISHIDA ET AL., 2008).

Depletion procedures, releasing Cl^- upon addition of sodium sulfate at high pH or through the removal of the chloride ligating extrinsic proteins of PSII, block the $S_2 \rightarrow S_3$ and $S_3 \rightarrow S_0$ transitions (WINCENCJUSZ ET AL. 1997; WINCENCJUSZ ET AL. 1998). A ~10 times lower binding affinity of Cl^- in the S_2 and S_3 state in comparison to the S_1 state was proposed (VAN GORKOM AND YOCUM 2005). Bromide addition restores the effect of Cl^--depletion on the oxygen evolving activity (HIND ET AL. 1969; KELLEY AND IZAWA 1978; WINCENCJUSZ ET AL. 1999). Chloride may be further replaced by NO_{3-}, NO_{2-} and I^- with decreasing binding affinity, while a substitution against fluoride and azide inhibits oxygen evolving activity (HADDY ET AL. 1999; HADDY ET AL. 2000; JAJOO ET AL. 2005; ONO ET AL. 1986; OLESEN AND ANDREASSON 2003). The exchange against other anions slows the S_i state turnover and/or the $Y_Z^{\bullet}$ reduction (WINCENCJUSZ ET AL. 1999).

To avoid harsh depletion procedures which clearly complicate interpretations, an optimal approach is to substitute the cofactors biosynthetically. Growing *T. elongatus*, a thermophilic cyanobacterium, in the presence of either Sr^{2+} or Br^- containing buffers instead of Ca^{2+} or Cl^--containing buffers results in an exchange of the cofactors Ca^{2+} and Cl^- by their surrogates Sr^{2+} and Br^- (ISHIDA ET AL., 2008).

With the tool to functionally replace chloride by bromide, and thereby avoid harsh depletion procedures, it is of highest interest to study the cofactors' role in the water-splitting reaction in combination with isotopic labelling. One way to unravel a possible direct involvement of chloride in the function of the OEC is to determine its interaction with substrate water.

Radmer and Olinger (1980, 1986) were the first to explore the nature of substrate water binding by introducing labeled oxygen species in one S-state, detecting photochemically produced dioxygen and determining its isotopic distribution by membrane-inlet mass spectrometry. By increasing time resolution to ≈ 30 ms and measuring evolved oxygen as a function of incubation time with labeled water, Messinger and coworkers were able to detect one exchangeable bound water molecule in the S_3 state (MESSINGER ET AL. 1995). They established a rate of $^{34}k_s = {}^{36}k = 2\ s^{-1}$ (10°C) for the slow exchanging substrate water and showed that one faster

exchanging ($k > 25\ s^{-1}$ at 10°C) water molecule had to be either bound in S_3 or enter only in the S_4 state. Further improved time resolution measurements revealed that two water molecules bind in the S_3 and S_2 state. This allowed detection of the slowly exchanging water molecule in the S_0 and S_1 state. For the slowly exchanging water molecule the S_i states exhibit relative exchange rates of 600 : 1 : 100 : 100 and for the fast exchanging water molecule (S_2 : S_3) 5000 : 2000 (HILLIER ET AL. 1998; HILLIER AND WYDRZYNSKI 2001; HILLIER AND MESSINGER 2005).

A great advantage of following the release of labeled oxygen species upon addition of $H_2{}^{18}O$ is that specifically the properties of substrate water are observed, since the product of the oxygen evolving reaction is monitored. Derived rate constants reflect the substrate water binding site. They would unravel a possible interaction between substrate water and chloride, if the cofactor was involved either directly or indirectly in the function of the OEC.

4.2 Results

To investigate a possible role of the cofactors calcium and chloride in substrate water binding, ^{18}O exchange kinetics in the S_3-state of PSII thylakoids isolated from *T. elongatus* grown in $CaCl_2$, $CaBr_2$, $SrCl_2$ or $SrBr_2$ containing buffers (Naoko Ishida & Alain Boussac, Saclay, (BOUSSAC ET AL. 2004, ISHIDA ET AL., 2008) were measured at 10°C by time-resolved membrane inlet mass spectrometry. Time resolution is achieved by varying the time between rapid $H_2{}^{18}O$-injection and the third, oxygen evolving flash (HILLIER ET AL. 1998; HILLIER AND WYDRZYNSKI 2004; KONERMANN ET AL. 2008; MESSINGER ET AL. 1995). Before the $H_2{}^{18}O$-injection, the dark adapted, $H_2{}^{16}O$ containing thylakoid suspensions are preflashed with two saturating Xe-flashes to populate the S_3 state. Measurements with intervals between injection and illumination (10 ms < Δt < 10 s) are performed each with a fresh aliquot of the sample. The injected $H_2{}^{18}O$ mixes rapidly with the PSII sample ($k_f << k_{inj}$, Table 4). For details see Chapter 2.

Figure 18 shows the corrected oxygen yields for m/z = 34 and m/z = 36 as a function of the exchange time, Δt (see Sections 2.5.3 and 2.6). The monophasic kinetics observed for $CaCl_2$-, $CaBr_2$- and $SrCl_2$-thylakoids at m/z = 36 ($^{18}O_2$) compare very well with each corresponding slow phase gained at m/z = 34 (Fig. 18, Table 4). It was

shown previously that the slow phase at m/z = 34 ($^{34}k_s$) and the monophasic kinetic observed for m/z = 36 (^{36}k) reflect the exchange of the substrate water at the slowly exchanging binding site (MESSINGER ET AL. 1995), since the evolution of $^{18}O_2$ is limited by the slowest ^{18}O exchange. The kinetics derived at m/z = 34 and 36, which are simultaneously detected, thus reflect the same (slowly exchanging) substrate water and it is therefore possible to combine ^{36}k with $^{34}k_{slow}$ at the fitting procedure to derive a reliable fast phase rate constant.

$CaCl_2$-, $CaBr_2$-, $SrCl_2$- and $SrBr_2$-thylakoids exhibit a biphasic rise of the $^{34}O_2$ yield, reflecting the exchange of the two unequivalent substrate water molecules (HILLIER ET AL. 1998; MESSINGER ET AL. 1995). A comparison of the rate constants reveals that the slow exchange rate Br^- - PSII, k_s is ~ 3 times faster, in Sr^{2+} - PSII ~ 2 times faster and in $SrBr_2$ - PSII ~ 4 times faster compared to PSII with the natural Ca^{2+} and Cl^- cofactors (Table 4). The increase in the rate of the slowly exchanging substrate water by either cofactor substitution is partly additive.

While the effect of the cofactor substitution is clearly measurable on the slowly exchanging substrate water molecule, the significantly altered rate of ^{18}O exchange is not observed for the fast exchanging substrate water. Here, only minor accelerations of the rate k_f upon cofactor substitution are detected. The values determined for the rate k_f are comparable for $CaCl_2$-, $CaBr_2$- and $SrCl_2$-thylakoids. The fast exchanging substrate water molecule is not profoundly affected by the substitution of the cofactors calcium and chloride.

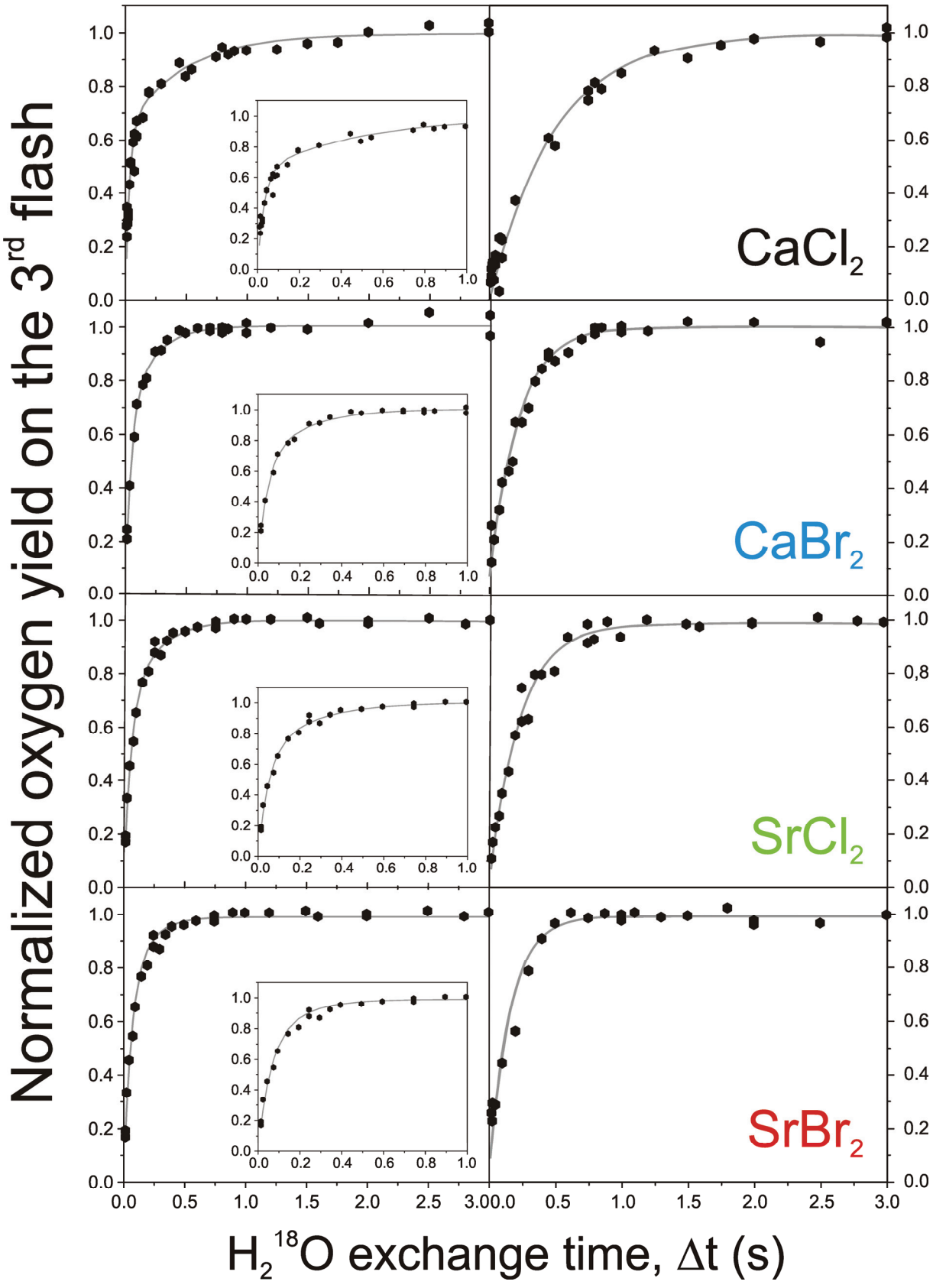

Figure 18:

Membrane-Inlet mass spectrometry measurements of the $H_2{}^{16}O/H_2{}^{18}O$ substrate water exchange rates in thylakoids isolated from *T. elongatus* cells grown in $CaCl_2$, $CaBr_2$, $SrCl_2$ and $SrBr_2$ containing media. Corrected oxygen yields are plotted for m/z = 34 ($^{16}O^{18}O$) on the left and 36 ($^{18}O_2$) on the right side as a function of exchange time, Δt with the fitting exchange kinetics shown by a solid gray line. The insets show a shorter time scale of the fast phase for better comparison. Experimental conditions: 10 °C, pH 6.5, final $H_2{}^{18}O$ enrichment after injection was 21.5% (for details notice section 2.5).

Table 4:

^{18}O substrate water exchange rate constants (m/z = 34 and 36)

PSII SAMPLE	$^{34}k_{fast}$ (s^{-1})	$^{34}k_{slow}$ (s^{-1}),	^{36}k (s^{-1})
$CaCl_2$	30.4 (± 1.9)	1.8 (± 0.2)	2.1 (± 0.1)
$CaBr_2$	22.8 (± 1.5)	4.8 (± 0.4)	4.7 (± 0.2)
$SrCl_2$	20.2 (± 1.2)	4.3 (± 0.4)	4.3 (± 0.2)
$SrBr_2$	17.6 (± 1.7)	6.9 (± 1.3)	6.2 (± 0.6)
$H_2{}^{18}O$ Injection (k_{inj})		97 (± 3)	

Rate constants for $H_2{}^{16}O/H_2{}^{18}O$ substrate water exchange at m/z = 34 (slow, $^{34}k_s$, fast $^{34}k_f$) and 36 (^{36}k) at 10 °C of thylakoids isolated from *T. elongatus* cells grown in $CaCl_2$, $CaBr_2$, $SrCl_2$ and $SrBr_2$ containing media (Section 2.7). The kinetic plots are displayed in Fig. 18. For the fitting procedure the derived rate constant of ^{36}k has been used to improve rate constants of $^{34}k_s$. The amplitudes have been fixed in agreement with the employed enrichment during the fitting procedure to 64 and 36 (Section 2.6). Rate of $H_2{}^{18}O$ (k_{inj}) derived from plotting fluorescence after fluorescein injection versus time after syringe trigger pulse at standard conditions (Section 2.4).

4.3 Discussion

The above presented substrate water exchange data on thylakoid-membranes from *T. elongatus* grown in either $CaCl_2$, $CaBr_2$, $SrCl_2$ or $SrBr_2$ containing media show that the slow exchange kinetic is significantly accelerated by both Cl^-/Br^- as well as Ca^{2+}/Sr^{2+} exchange. For an exchange of the cofactor chloride in PSII, k_s is ~ 3 times faster, for an exchange of calcium, k_s is ~ 2 times faster and for substitution of both cofactor k_s increases ~ 4 times (Table 4).

Hendry and coworkers previously presented exchange rate measurements of Ca^{2+} and Sr^{2+} containing PSII samples (HENDRY AND WYDRZYNSKI 2003). Even though they applied harsh, chemical substitution procedures, which may cause secondary effects, the acceleration of the slow phase by an exchange of Ca^{2+} against Sr^{2+} is confirmed. The conclusion that calcium plays a functional role in substrate water binding drawn earlier is therefore strengthened.

Despite rapidly increasing knowledge on the structure of the OEC, it is still unclear where and how precisely the two substrate water molecules bind. Most models established so far assume that at least one substrate water molecule binds to the Mn_4O_xCa complex. In agreement with the high oxidation state of the Mn_4O_xCa cluster it is most likely that substrate water is not fully protonated, but that at least one substrate water molecule is partly protonated up until the S_3 state. The proposal is

supported by H/D exchange ESEEM and ENDOR studies (for review see (BRITT ET AL. 2004)). The first EPR experiments supported a direct ligation of ^{17}O-water to manganese (EVANS ET AL. 2004; TURCONI ET AL. 1997), but did not allow final conclusions due to low resolution. A recent study with the two-dimensional EPR technique hyperfine sublevel correlation spectroscopy (HYSCORE) conclusively showed a direct ligation of one exchangeable ^{17}O to one or more Mn ions in the S_2 state. Depending on the binding mode it most likely corresponds to the slowly exchanging substrate water molecule (SU ET AL. 2008). The second water molecule (based on the proposed binding mode, the fast one) is either not resolved by the EPR study, not coupled to a Mn ion or not present in the S_2 state. It would also be undetectable to HYSCORE if it was bound to calcium. However, since the rates of the fast exchanging water molecule are not altered significantly upon either Ca^{2+}/Sr^{2+} or Cl^-/Br^- exchange a direct ligation to calcium is highly unlikely (unless the exchange is limited by other factors).

On the basis of the new finding that a Cl^-/Br^- exchange leads to a slightly greater acceleration of the slowly exchanging substrate water rate than the reported Ca^{2+}/Sr^{2+} exchange, three possibilities may be discussed:

1) In the S_1 state (and a reduced form of the cluster respectively), where chloride does not have special functional relevance (VAN GORKOM AND YOCUM 2005), XAS data seem to exclude a binding of Cl^-/Br^- to Mn (HAUMANN ET AL. 2006; MURRAY ET AL. 2008). Based on EXAFS measurements with the analogue N_3^-, direct binding of Cl^- to Mn seems unlikely, if N_3^- and Cl^- indeed compete on the same binding site (SHEVELA 2008). If one nevertheless assumes a direct binding of Cl^-/Br^- to Mn and takes into account that the slowly exchanging substrate water molecule may be μ-oxo-bridged between two Mn ions (SU ET AL. 2007), one will expect that Mn has a less positive charge and weakens the Mn-O bond in case of a Br^- *vs.* a Cl^- ligation. A protonation and thus an exchange against $H_2{}^{18}O$ (as protonation is a prerequisite for an exchange) would be less likely for Cl^- than in case of Br^- binding at the same position. This could explain the accelerated exchange rates upon chloride substitution. One may further speculate about Cl^-/Br^- having an additional bond to Ca^{2+}/Sr^{2+}. The observed partly additive effect on substrate exchange rate constants in $SrBr_2$ samples would support this.

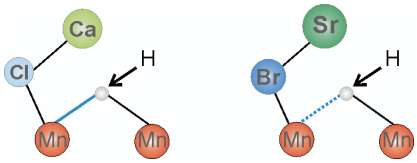

2) Possibly a hydroxo-group or three-binding oxygen, ligated by manganese and calcium represents the slowly exchanging substrate water molecule. If chloride ligates calcium, Br^- may in this case accelerate the exchange by weakening the Ca-O bond.

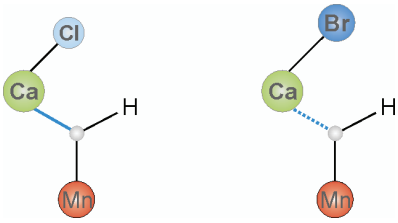

3) Another possibility is of an indirect effect: The function of the S-state cycling, giving rise to four protons per O-O bond formation, requires a proton abstraction mechanism. To circumvent a charge accumulation, which would make further electron abstractions increasingly difficult, protons are sequentially removed from the OEC (discussed in Section 1.1.6 and Messinger and Renger 2008). The proton's destination is the lumen and the water splitting reaction is therefore combined with long-range proton transfer through the protein matrix (for review see (Meyer et al. 2007)). If chloride participates in the proton network (Olesen and Andreasson 2003), the Cl^-/Br^- exchange will weaken the interaction and thereby influence the substrate water exchange rates by modulating its pKa value or the access of substrate water via changing the proton network around the Mn_4O_xCa cluster. It is feasible that the slowly exchanging substrate "water" is more affected by changes in the proton-(relay) network than the fast exchanging one, which may still be partially protonated.

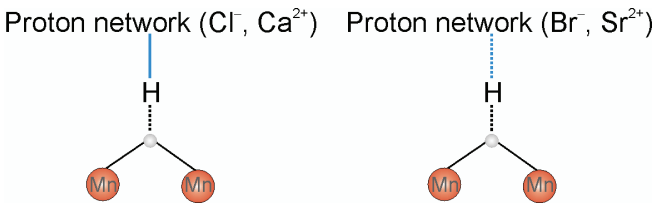

The partially additive effects of Ca^{2+}/Sr^{2+} and Cl^-/Br^- exchange would reflect additional effects of Ca^{2+}/Sr^{2+} exchange on the proton network.

Even though the Cl^-/Br^- substitution affects the substrate exchange rates greatly, a chloride binding site further away from the Mn_4O_xCa cluster as proposed earlier by XAS studies is not in contrast to a large effect on exchange rates. Singh et al. showed most recently that the mutation D1-D61N in the second coordination sphere influences the exchange rates greatly (SINGH ET AL. 2008). The amino acid residue probably lies at the entryway to a hydrogen bond network through the protein matrix, which is connected to substrate water (MEYER ET AL. 2007).

Possible models involving breaking of covalent -OH bonds are excluded based on measured kinetic isotope effects. The ratio of $k_i(H)/k_i(D)$ would be expected in the order of 10, while detected ratios for PSII membrane fragments are in the range of 1.3 – 1.4 for i = 1, 2 and 3 (KARGE ET AL. 1997; LYDAKIS-SIMANTIRIS ET AL. 1997; RENGER ET AL. 1994; RENGER AND MESSINGER 2008). The presence of terminal oxo ligands like Mn(IV)=O, Mn(V)=O and terminal oxo groups can be excluded in the S_2, S_3, S_4 states on the basis of comparison between Mn model compounds and PSII by XANES and time-resolved EXAFS measurements (HAUMANN ET AL. 2005A; HAUMANN ET AL. 2005B; MESSINGER ET AL. 2001B; ROELOFS ET AL. 1996; WENG ET AL. 2004). On the basis of this finding and results of substrate water exchange kinetics (the difference between the two rates for the substrate water molecules is much smaller than it would be expected from two very different binding sites) a mechanism based on "nucleophilic attack" is highly unlikely (HILLIER AND MESSINGER 2005) and thus does not have to be considered in respect to a chloride interaction.

4.4 Conclusion

The data shows that the exchange rate of the slowly exchangeable substrate water molecule is accelerated by replacement of Cl^- by Br^- and Ca^{2+} by Sr^{2+} and provides compelling evidence that both Ca^{2+} (Sr^{2+}) and Cl^- (Br^-) bind near the site where the slowly exchanging substrate water is bound to the Mn_4O_xCa cluster. The partly additive effect on the rates of $SrBr_2$ hints towards a binding of Ca^{2+} (Sr^{2+}) and Cl^- (Br^-). Alternatively, both ions might have significant effects on the proton-network of the OEC. The exchange of the slowly exchanging substrate water would then be rate limited by protonation.

Chapter 5

Chasing the intermediate S_4 State by employing elevated O_2 Pressure

5. CHASING THE INTERMEDIATE S_4 STATE BY EMPLOYING ELEVATED O_2 PRESSURE

5.1. Introduction

5.1.1. The transient S_4 state

According to the Kok scheme the Mn_4O_xCa cluster cycles during water splitting through five intermediate states. For a complete understanding of the water splitting reaction it is vital to gain information on possible intermediate step(s) of the water oxidation process. While the states S_0, S_1, S_2 and S_3 can be trapped with high yield using appropriate flash-freeze protocols, the reactive S_4 state remained illusive so far. Because of the close kinetic correlation between $Y_Z^{\bullet}$ reduction and O_2 release (it appears almost simultaneously) it has been even questioned if a distinct S_4 state intermediate exists or if this state would be better termed $S_3Y_Z^{\bullet}$ (HILLIER AND MESSINGER 2005; MESSINGER AND RENGER 2008). It is believed that the water oxidizing reaction occurs either in the last transition ($S_3Y_Z^{\bullet} \rightarrow [S_4] \rightarrow S_0$) with intermediate formation of complexed H_2O_2, or that a peroxidic intermediate is already formed at the level of $S_3Y_Z^{\bullet}$ (for details see Messinger and Renger, 2008). A concerted O-O bond formation may also prevent the release of harmful reactive species along the cycle.

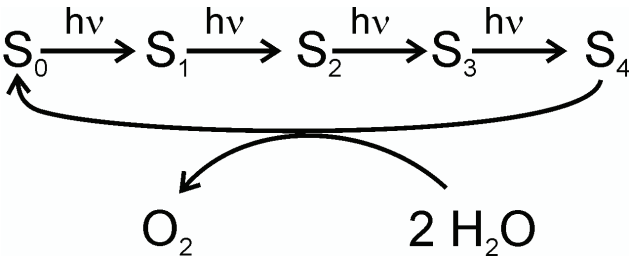

The short lived nature of the S_4 state immensely complicates its characterization and therefore the full understanding of photosynthetic water splitting. Since the S_4 state is chemically the most interesting, but least characterized state, gaining information about this intermediate has been attempted by several groups.

Clausen and Junge (2004) introduced recently the interesting idea of halting the cycle in the S_4 state by preventing the release of the produced oxygen by high applied oxygen pressures, up to 30 bar. On the basis of time-resolved UV absorption transients, which can be attributed to the oxidation of the Mn_4O_xCa cluster by $Y_Z^{\bullet}$, the authors conclude that a pressure of 2.3 bar is already sufficient to half-inhibit O_2

evolution. It is proposed, that the S_4 state can be described by an electronic configuration equivalent to S_2Y_Z (H_2O_2). Similar N_2 and CO_2 pressures were found to be ineffective.

5.1.2. Membrane-inlet mass spectrometry at elevated pressure

It would be most interesting to confirm the proposed inhibition of PSII by direct O_2 measurements. MIMS allows online detection of reaction products and an inhibitory effect can thus not be disguised. It is not possible to use e.g. an oxygen electrode (Clark type electrode), because applied oxygen pressure exceeding 1 bar, would hinder distinguishing between photosynthetically produced dioxygen and O_2 pressure. This was overcome by using a magnetic sector field mass spectrometer to distinguish between the different isotopic species and measure photo-induced $^{18}O_2$ production against a $^{16}O_2$ background caused by the applied $^{16}O_2$ pressure.

To perform measurements at elevated pressure with a MS-instrument, operating at high vacuum, several requirements have to be met:

(i) the reaction chamber has to be pressure stable,

(ii) a pressure stable membrane as interface between instrument and sample chamber is required to maintain the stable low pressure regime within the instrument,

(iii) the increased oxygen concentration (by the applied oxygen pressure) has to remain constant throughout the time-span of the measurement to ensure an oxygen concentration creating the inhibitory effect in the PSII solution. It thus has to be ensured, that dissolved oxygen is not significantly degassed during the measurement,

(iv) *t*o exclude pressure induced artefacts m/z = 40 (Argon) is monitored. The Argon concentration is independent of illumination and any changes in the Argon signal therefore indicate sensitivity problems of the experimental set-up, possibly caused by applied pressure. For details and set-up construction, see Sections 2.3 and 2.5.

5.2. Results

At 20 bar O_2 the $^{16}O_2$ in solution exceeds the cup sensitivity (50.000 mV). It is thus impossible to detect a distinct signal at m/z = 32. Decreasing the applied pressure allows detection at m/z = 32 (Fig. 19).

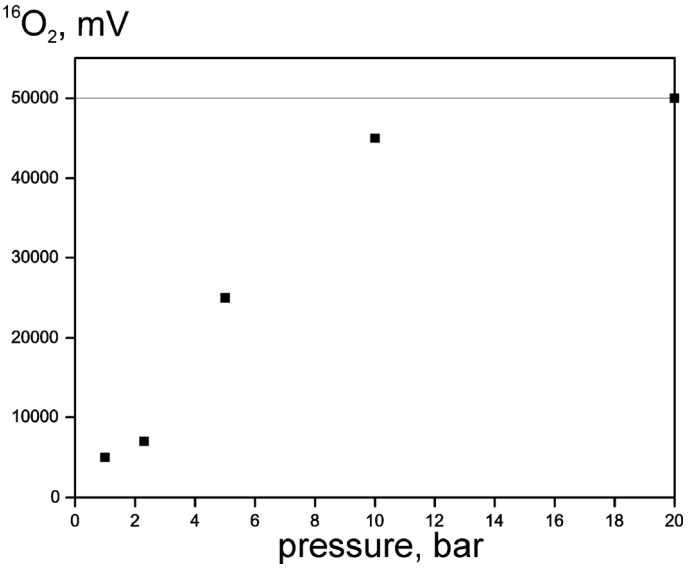

Figure 19:

The concentration of $^{16}O_2$ in solution depends on the applied pressure. The level of dissolved dioxygen increases corresponding to increasing pressure. The level of $^{16}O_2$ (in mV) before the measurement at the respective pressure is plotted vs. the applied pressure (in bar). The PSII sample was incubated for 20 min in the sample chamber before measurements (Section 2.5.4).

The high level of dissolved $^{16}O_2$ is a prerequisite for the experiments, because it has to be ensured that a high concentration of the product is present in the PSII solution. The $^{16}O_2$ concentration before illumination is plotted *vs.* applied pressure. This reveals a linear dependence between increasing pressure and the detected oxygen concentration in the solution.

5.2.1. CW illumination

MIMS-measurements of thylakoid samples were performed at 20 bar oxygen and 20 bar nitrogen pressure with a final $H_2{}^{18}O$ enrichment of 20%. Samples were illuminated continuously with a slide projector (250W).

MIMS-measurements of thylakoid samples at elevated oxygen pressure do not reveal an inhibition of photosynthetic oxygen production (Fig. 20). The PSII samples produce dioxygen with rates comparable to those of control measurements performed at elevated nitrogen pressure (20 bar).

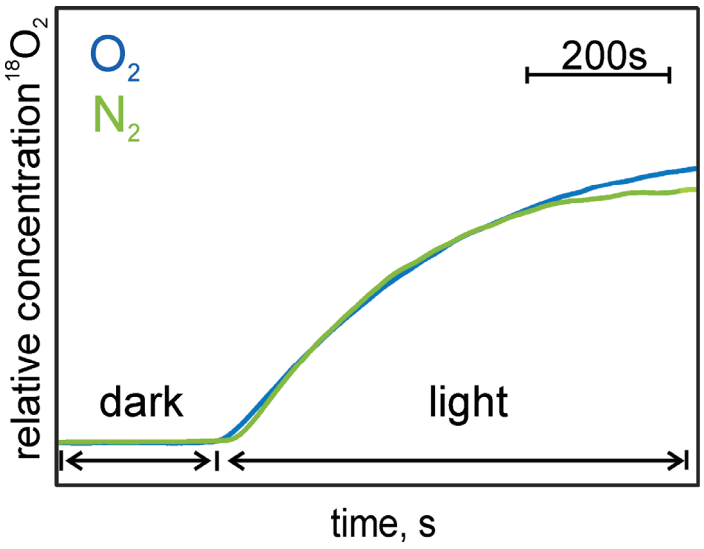

Figure 20:

Membrane-inlet mass spectrometry measurements of thylakoids samples (0.25 mg (Chl) ml^{-1}) with a final $H_2{}^{18}O$ enrichment of 20%. As artificial electron acceptor 7 mM Ferricyanid (dissolved in water) was added. Displayed are oxygen signals (m/z = 36) at 20 bar elevated oxygen (blue line) and 20 bar nitrogen pressure (green line).

A prerequisite for interfacing membrane-inlet mass spectrometry, operated at high vacuum of 2 x 10^{-10} bar and the reaction chamber operated at elevated pressure of 20 bar, is to construct the inlet to the instrument as small as possible. While this precaution enables mass spectrometric measurements at elevated pressure, the sensitivity is too low to detect O_2-evolution produced by single flashes. In addition to measurements at continuous illumination, the integrated O_2 yield induced by 200 Xe-flashes at 2 Hz frequency was measured. The obtained results confirm cw-illumination data in Fig. 20. A systematic difference in PSII activity between O_2- and N_2-pressure was not observed.

To rule out the possibility that an inhibition of the oxygen evolution occurs at different conditions than the ones applied, the parameters light, pH and pressure were varied. Different artificial electron acceptors as well as thylakoid and PSII membrane fragments preparations were compared.

5.2.2. Variation of Artificial Electron Acceptors

Measurements of thylakoid and PSII membrane fragments preparations at continuous light and sample-illumination with 200 flashes require the addition of artificial electron acceptors (they take up electrons from the electron transport chain in order to prevent the saturation of the plastoquinon-pool, which would block PSII, Chapter 1).

MIMS-measurements were performed with a hydrophilic artificial electron acceptor ferricyanide (FeCy), to avoid the use of solvents (e.g. Ethanol is detected at m/z = 46),

while UV-absorption transient measurements were performed with 2,5-Dichlorobenzoquinone (DCBQ), dissolved in ethanol as electron acceptor. To exclude a secondary effect (e.g. a reaction between dioxygen and the electron acceptor), MIMS-measurements were additionally performed with DCBQ at O_2 and N_2 pressure of 20 bar.

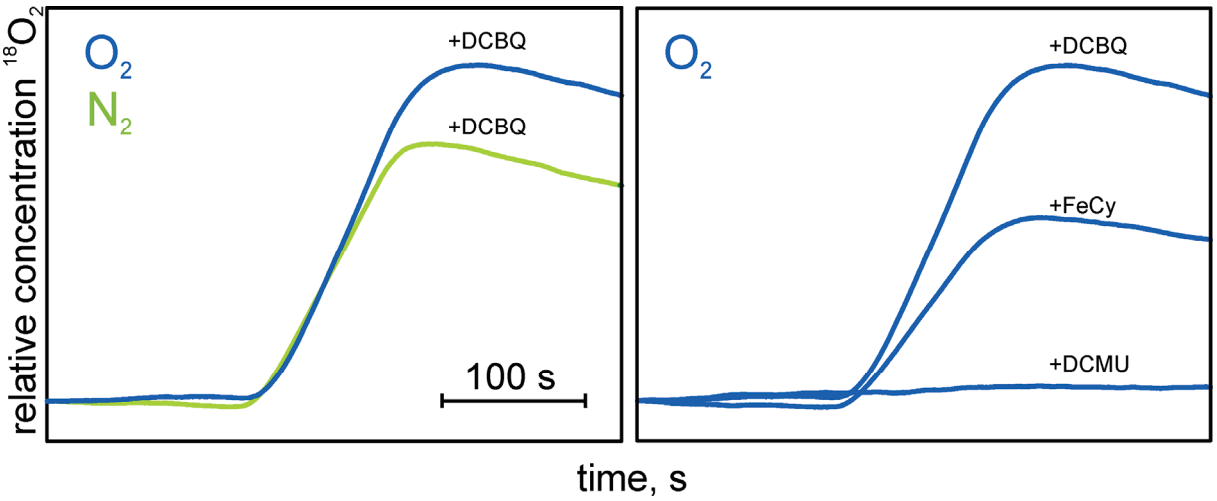

Figure 21:

Membrane-inlet mass spectrometry measurements of spinach PSII membrane fragments (200 µM) with a final $H_2{}^{18}O$ enrichment of 20%. As artificial electron acceptor either 7 mM Ferricyanid (FeCy) or 2,5 Dichlorobenzoquinone (DCBQ) resulting in a final concentration of 1mM is added. To inhibit photosynthetic oxygen evolution 10 µM 3-(3,4-dichlorophenyl)-1,1-dimethylurea (DCMU) is used. Displayed are oxygen signals (m/z = 36) at 20 bar elevated oxygen (blue lines) and 20 bar elevated nitrogen (green line) pressure respectively.

The addition of DCBQ leads to an even larger O_2 production under oxygen pressure (20 bar) than at nitrogen pressure (20 bar) (Fig. 21). Measurements of PSII sample with added FeCy exhibit similar oxygen evolution at elevated pressure for the two gases (20 bar). Photosynthetic oxygen evolution at elevated pressure therefore does not depend on the choice of electron acceptor. To ensure that an inhibition would be detectable, 3-(3,4-dichlorophenyl)-1,1-dimethylurea (DCMU) as photosynthetic inhibitor (to block the electron transfer from PSII to the PQ pool) is added. Measurements performed at 20 bar oxygen and nitrogen pressure reveal a complete inhibition of photosynthetic oxygen evolution upon addition of the inhibitor DCMU.

5.2.3. Influence of pH

An inhibitory effect on photosynthetic oxygen production by increased oxygen concentration at alkaline pH has been proposed earlier (BOICHENKO AND EFIMTSEV

1979). The pH of PSII samples was changed from pH 6.5 to pH 8 and measurements performed at elevated O_2 and N_2 pressure (20 bar).

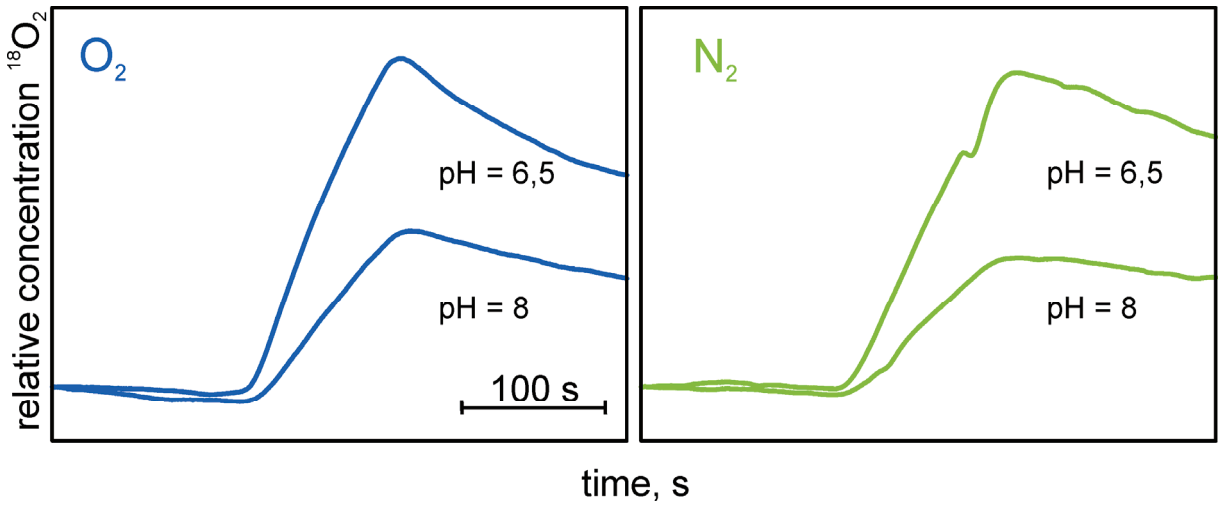

Figure 22:

Membrane-inlet mass spectrometry measurement of spinach PSII membrane fragments (200 µM) with a final $H_2{}^{18}O$ enrichment of 20%. As artificial electron acceptor 7 mM FeCy is added. Displayed for pH = 6.5 and pH = 8 are oxygen signals (m/z = 36) at 20 bar elevated oxygen (blue line) and 20 bar elevated nitrogen (green line) pressure respectively.

In response to elevated oxygen pressure, neither the MIMS-measurement of samples at pH 6.5 nor at pH 8 exhibits an inhibition of photosynthetic oxygen evolution. At pH = 8 the formation of dioxygen is clearly lower in comparison to measurements at pH 6.5, but both in the cases 20 bar yield similar results (Fig. 22).

5.2.4. Redox Titration

To ensure that not an artefact of the MIMS set-up caused by high pressure conceals

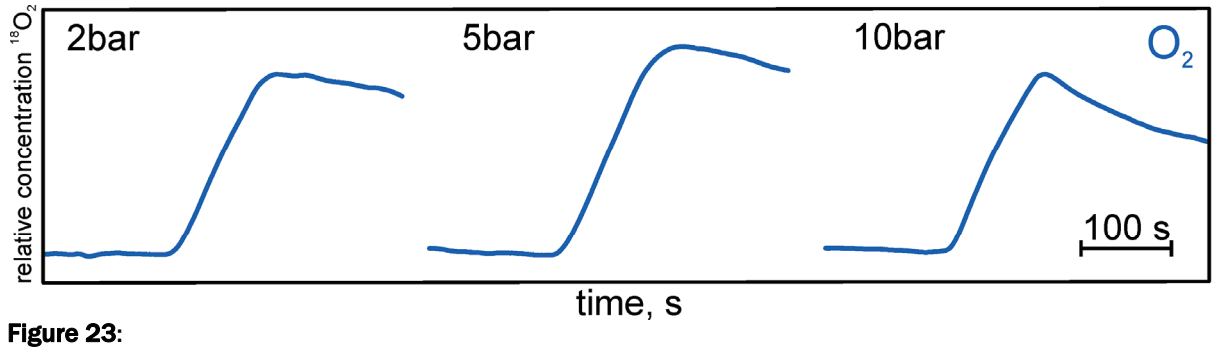

Figure 23:

Membrane-inlet mass spectrometry measurements of spinach PSII membrane fragments (200 µM) with a final $H_2{}^{18}O$ enrichment of 20%. As artificial electron acceptor 7 mM FeCy is added. Displayed are oxygen signals (m/z = 36) at 2, 5 and 10 bar elevated oxygen pressure (blue trace). Traces at 2, 5, and 10 bar elevated nitrogen pressure correspond to the ones displayed at elevated oxygen pressure (not displayed).

an inhibition of photosynthetic oxygen production, the O_2 and N_2 pressure is stepwise increased from 2 bar to 5 bar, to 10 bar and 20 bar.

A series of MIMS-measurements with increasing O_2 and N_2 pressure yields comparable O_2 production rates. An inhibitory effect could neither be detected at low (2, 5 bar), nor at high (10, 20 bar) dioxygen pressure. Comparing the oxygen and nitrogen measurements no obvious difference was revealed between applied O_2 and N_2 pressure (Fig. 23).

5.3. Discussion

The inhibitory effect of elevated oxygen pressure on photosynthetic oxygen release proposed by Clausen and Junge (2004) could not be confirmed. Control measurements at N_2 pressure proved the set-up to be capable of oxygen detection at elevated pressure. Samples produce comparable amounts of dioxygen at O_2 and N_2 pressure. It is also clearly shown that it is possible to detect a blocked oxygen production by measurements with an inhibitor of the electron transfer from PSII to plastoquinon (DCMU) (Fig. 21). The result obtained upon DCMU addition resembles what has been expected for MIMS-measurements at elevated dioxygen pressure, based on results obtained by UV-absorption measurements.

The OEC is a highly complex system and small variations in the environment may already cause changes. It is therefore difficult to identify the source of a possible secondary effect which might mislead interpretation of the UV-data. To draw conclusion on product release inhibition is very difficult if the released product is not measured and the oxidation state changes of the Mn_4O_xCa cluster and Y_Z are only indirectly monitored with UV-absorption transients.
In contrast to this, MIMS allows detecting O_2 online with isotopic labelling. This method is thus the most direct way to gain information on product release behaviour. If a blockade of the product release cannot be detected by MIMS it is either *(i)* not present and the result measured by UV absorption transients is caused by another, secondary effect or *(ii)* the MIMS set-up is unable to reproduce all parameters involved in creating the inhibitory effect.

One possibility explaining the detected stalling of the Kok-cycle by UV-absorption transients is that the effect is very weak and lasts only within the range of one or a few Kok-cycles. This explanation is in contrast to the reported half inhibition at 2.3 bar. An effect created by increasing oxygen pressure ~ 10 fold above ambient pressure hints towards a strong influence of oxygen on the product release. It is therefore unlikely that the set-up required difference in illumination protocol cancels an oxygen induced inhibition. Nevertheless, measurements have been performed at comparable low pressure, to exclude a disguised weak effect. The oxygen evolving activity at varying pressure of O_2 and N_2 did not influence the photosynthetic oxygen evolving activity.

The pH influences the photosynthetic reaction. A proton gradient is established across the thylakoids membrane and stored oxidizing equivalents are counterbalanced by charge abstraction to gain charge balance. The proton-relay network is sensitive towards pH changes in many ways. The proposed inhibitory effect of photosynthetic oxygen production by increased oxygen concentration at an alkaline pH on product release (BOICHENKO AND EFIMTSEV 1979) could not be confirmed. A stalling of the Kok-cycle at elevated oxygen pressure was not enhanced by creating an alkaline pH.

5.4. Conclusion

Clausen and Junge (2004) proposed an inhibitory effect on photosynthetic oxygen release at elevated oxygen pressure by UV-absorption transients. MIMS is the method of choice to determine an inhibition of product release, because it allows detecting a reactions' product *online*. The use of an isotopic ratio mass spectrometer allows distinguishing between the photosynthetic produced $^{18}O_2$ and the applied elevated O_2 pressure. The reported inhibitory effect was disproved by MIMS-measurements at elevated pressure.

Chapter 6

Artificial Photosynthesis

6. ARTIFICIAL PHOTOSYNTHESIS

6.1. Introduction

The alarming increase in the atmospheric CO_2 level since the start of the industrialization, has prompted diverse studies about possible environmental consequences. The necessity to reduce the atmospheric CO_2 concentration has been acknowledged by many industrial nations and the Nobel Peace Prize committee, who have assigned the honor equally to the Intergovernmental Panel on Climate Change (IPCC) and Albert Gore, for their efforts to build up awareness necessary to counteract predicted environmental changes. One vital step is to exchange the use of fossil fuels against "zero-CO_2 emission"-energy carriers in order to halt the continuous increase in atmospheric CO_2 level and at the same time, meet the rising energy demand. Thus the search for alternative power and fuel supplies is greatly intensified. (For an overview see (BARD AND FOX 1995; KRUSE ET AL. 2005; LEWIS AND NOCERA 2006) and "Climate Change 2007", the Fourth IPCC Assessment Report).

Technical approaches to reaching the goal of CO_2 emission reduction are diverse. Methods e.g. to bind carbon are devolved (carbon capture storage, CCS). The use of hydrogen as fuel supply remains attractive, even though H_2 storage has not been solved satisfactorily, yet. A promising approach to solar fuel production taking advantage of the infinite supply of sunlight and water, would be to mimic the natural photosynthetic system, possibly in combination with artificial hydrogenases, to directly convert solar energy into energy rich chemicals (BARD AND FOX 1995; LEWIS AND NOCERA 2006; MEYER 1989; SUN ET AL. 2001).

Kirch and co-workers (KIRCH ET AL. 1979) proposed already in 1979 an assembly in analogy to the catalytic sites of natural enzymes (biomimetic approach) consisting of three successive parts (Fig. 24):

i) Part I is a PSII mimic performing a first light reaction to drive the oxidation of water into four protons, molecular oxygen and four electrons, performed by a catalyst (Cat_{ox}). The electrons are transferred to an accepter (A^-) and passed *via*

ii) Part II, a relay system (R), on to

iii) Part III a PSI analog. It consists of a photo-excited electron-acceptor that donates the electrons to a hydrogenase (Hase) mimic (Cat_{red}). The second

catalyst finally reduces four protons, which originate from the water splitting reaction, to two hydrogen molecules.

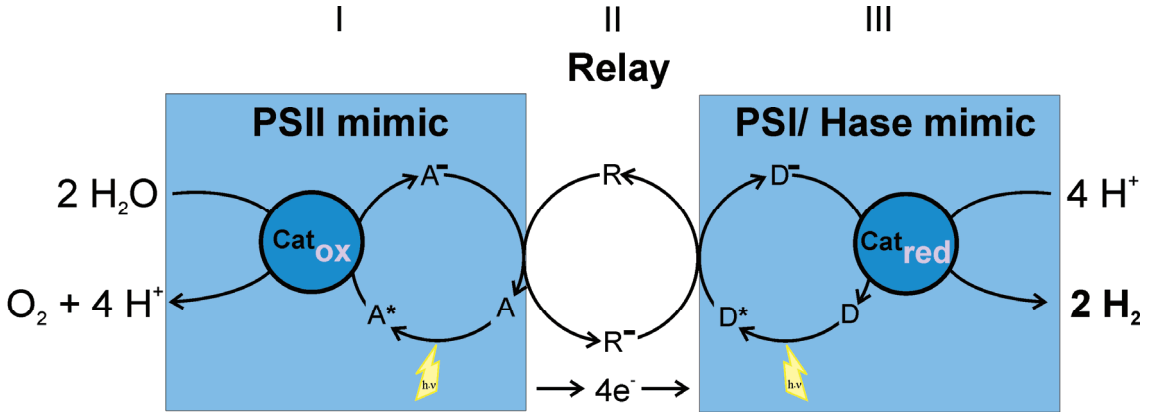

Figure 24:

Proposed reaction cycle to produce H_2 by mimicking both photosystems and combining the two light reactions with a hydrogenase mimic (KIRCH ET AL. 1979). Electrons from water serve for the reduction of protons (from water) to hydrogen.

In addition to the goal of efficient hydrogen production by artificial assemblies that mimic PSII, a PSII model can help to interpret the variety of information gained on PSII by diverse biophysical approaches. There is a mutual dependence that exists between understanding of the natural enzyme and the biomimetic approach of solar fuel production: a complete understanding of PSII would be helpful as template for mimicking PSII, while the artificial catalyst, exhibiting PSII like spectroscopic features, helps interpreting data obtained of the natural PSII.

Manganese is favoured by many chemists for the synthesis of the PSII like part in the artificial assembly, because it is chosen in the natural enzyme as an abundant metal which 'forms' stable clusters and has a wide oxidation state range from Mn^{II} to Mn^{VII} enabling one-electron oxidation steps. (ARMSTRONG 2008)

While the final goal, the development of industrial catalyst(s) for solar photoproduction on a large scale is still out of reach, a manifold of synthesized manganese-oxo compounds have been characterized and reported in literature (for a comprehensive overview see (MUKHOPADHYAY ET AL. 2004)). Oxygen evolution has been achieved with several of those compounds (KURZ ET AL. 2007), but so far, catalysis of water oxidation has mainly been reported for Ruthenium complexes, the most prominent being the "Blue Dimer" (BINSTEAD ET AL. 2000; CHRONISTER ET AL. 1997; COMTE ET AL. 1989; GERSTEN ET AL. 1982; GESELOWITZ AND MEYER 1990; GILBERT ET AL. 1985; HURST ET AL. 1992; LEI AND HURST 1994; NAZEERUDDIN ET AL. 1988; RAVEN AND MEYER 1988).

The reported oxygen evolving reactions are mainly not induced by photon absorption, but strong oxidants. Since some of the oxidants are capable of oxygen transfer reactions (CHEN ET AL. 2007), one vital step to characterize and understand the reaction mechanism is to distinguish between oxygen transfer reactions and true water oxidation reactions. Incorporation of an isotopic label (^{18}O) into O_2 proves, if a catalyst performs water splitting and might be useful as PSII mimic, if secondary effects can be excluded. Separation and simultaneous detection of labeled oxygen species by isotopic ratio mass spectrometry clarify a compound's water oxidizing ability. For this study, it is critical that only solvent water is isotopically labeled. If neither catalyst nor oxidant contains the label, and possible reaction intermediates do not undergo rapid exchange with the solvent. If none or half or fully labeled oxygen atoms appear in the formed O_2 a clear conclusion may be drawn.
Out of a manifold of synthesized Mn-compounds, so far, only Naruta and co-workers reported a dimeric Mn-compound to perform water splitting (NARUTA ET AL. 1994). This study focuses on the capacity of several described compounds to act as catalysts for the oxidation of H_2O to electrons, protons and O_2 in order to select compound(s) that mimic the PSII water splitting reaction and trigger the development of bio-mimetic assemblies to finally yield efficient solar fuel production on a broad scale.

6.2 Results

In an attempt to sort the manifold of compounds and establish standard conditions that enable direct comparison, Kurz and co-workers set up a grid study (KURZ ET AL. 2007). Six manganese complexes of various core type and ligand sphere have been chosen and screened for their ability to catalyse an oxygen yielding reaction. Upon addition of various oxidants O_2 evolution was recorded with a Clark type polarographic oxygen electrode revealing diverse traces, which hint towards complex reactions.

The established "O_2 evolution grid" enables focusing on most interesting compound/ oxidant-combination for mechanistic studies. From the grid the four O_2 evolving manganese compounds together with two oxidants have been selected to study the origin of the evolved O_2 by measuring oxygen evolution in presence of $H_2{}^{18}O$ by membrane-inlet mass spectrometry (MIMS).

In a typical MIMS-measurement the reaction between a defined amount of compound with a strong oxidant is followed by simultaneous detection of oxygen ($^{16}O_2$, $^{16}O^{18}O$ and $^{18}O_2$), carbon dioxide ($^{12}C^{16}O_2$, $^{12}C^{16}O^{18}O$ and $^{12}C\,^{18}O_2$) and argon (m/z = 40). The aqueous solutions of the studied compounds are enriched with ^{18}O-labeled water and the isotopic ratio of evolved oxygen is calculated. The maximal amount of the first O_2-rise for each oxygen species is determined and after taking into account the different amplification factors of the detecting faraday cups (see Section 2.1), the values for m/z = 32, 34 and 36 are summed up and the distribution of each species is calculated in percent. To determine the final ^{18}O-enrichment of the reaction mixture, a rapid association-dissociation equilibrium reaction, taking place between H_2O and CO_2 (scrambling) is utilized. As the oxygen atoms between the two molecules exchange rapidly ($t_{1/2}$ < 10 s (LIMBURG ET AL. 2001) the ^{18}O-labeled CO_2 species represent the portion of $H_2{}^{18}O$ in the solvent water.

An incorporation of ^{18}O into evolved O_2 enables drawing conclusions on the oxygen's origin if the oxidant is slow in exchange with solvent water in comparison to the rate of oxygen evolution. ESI-MS measurements have been performed at Varian (Darmstadt, Germany) to detect an oxygen exchange involving the oxo-groups of oxone and ^{18}O-enriched bulk water (Fig. 25).

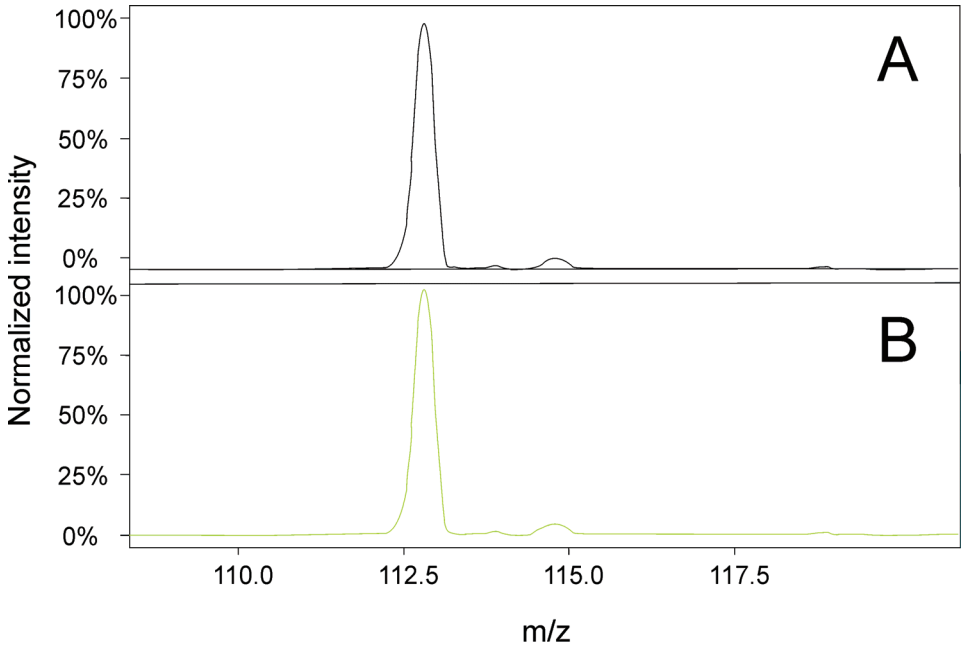

Figure 25:

ESI-MS measurement of oxone in $H_2{}^{16}O$ (A) and $H_2{}^{18}O$ (B) after 30 min incubation time. Measurements were performed at Varian in Darmstadt, Germany.

Within 30 min scrambling does not occur between solvent water and oxone, confirming earlier studies by Chen and coworkers who showed that oxone does not exchange within 1 h with labeled solvent water (CHEN ET AL. 2007). This premise limits the choice of oxidant compatible with isotopic studies and excludes the use of e.g. hypochlorite (OCl^-) (LIMBURG ET AL. 2000).

The following models describe possible reaction mechanisms based on the isotopic distribution of molecular oxygen:

Model A: Assuming that a water oxidizing reaction is catalyzed by a compound/oxidant solution, possible combinations are *(i)* two $H_2{}^{16}O$ forming one O–O bond, *(ii)* one $H_2{}^{16}O$ and one $H_2{}^{18}O$ forming one single labeled species $^{16}O^{18}O$ and *(iii)* two $H_2{}^{18}O$ combining to $^{18}O_2$. In absence of isotope effects the isotopic distribution of the evolved O_2 can therefore be calculated:

$$^{16}O_2 : {}^{16}O^{18}O : {}^{18}O_2 = (1 - \varepsilon)^2 : 2(1 - \varepsilon)\varepsilon : \varepsilon^2 \qquad \textbf{(24)}$$

with ε = ^{18}O enrichment.

The isotopic pattern of the produced O_2 consequently depends on the proportion of $H_2{}^{18}O$ in the ^{16}O external water phase, provided (*i*) that the substrate of the O_2 evolving reaction is water, (*ii*) external water freely accesses the active site of the compound and (*iii*) the bound substrate water is exchangeable.

As the oxidants, oxone and TBHP can act as oxygen transfer agents, further possibilities are: *Model B*, one oxygen atom is transferred from the unlabeled oxidant onto the Mn-compound and combines with solvent water to molecular oxygen. In this case only unlabelled and single labeled oxygen forms. Alternatively, both oxygen atoms stem from the unlabeled oxidant and yield only oxygen at natural enrichment *(Model C)*.

6.2.1 Analysis of O_2 evolved by the reaction of oxidants with manganese containing compounds

According to the grid study *Mn_2-terpy* ([(terpy) (H_2O) Mn^{III} $(O)_2$ Mn^{IV} (OH_2) (terpy)] $(NO_3)_3$ (terpy = 2,2':6,2''-terpyridin) (COLLOMB ET AL. 1999; COLLOMB ET AL. 2001;

LIMBURG ET AL. 1999; LIMBURG ET AL. 2001) *Mn_2-mcbpen* ($[Mn^{II}_2(mcbpen)_2(H_2O_2)]$ were mcbpen is the anion of *N*-methyl-*N'*-carboxymethyl-*N,N'*-bis(2-pyridylmethyl)ethane-1,2-diamine) (POULSEN ET AL. 2005), *Mn_2-bpmp-AcO* ($[Mn_2(bpmp)(\mu\text{-}OAc)_2]^+$ with 2,6-bis[(*N,N*-di(2-pyridinemethyl) amino)methyl]-4-methylphenol) as the anion of the complex (SUN ET AL. 2000) and *Mn_4-tbhpn* ($[Mn_4O_2(TBHPN)_2(H_2O)_2(CF_3SO_3)_2]^{3+}$ (CHAN AND ARMSTRONG 1990) are capable of oxygen production in reaction with the oxidants TBHP and oxone (both dissolved in water). Oxygen evolution has been reported earlier for Mn_2-terpy and Mn_2-mcbpen, while the grid study has revealed oxygen evolution for the di- and tetranuclear manganese compounds Mn_2-bpmp-AcO and Mn_4-tbhpn.

6.2.1.1 Mn_2-terpy

The dinuclear manganese complex Mn_2-terpy (Fig. 26) evolves O_2 in reaction with the oxidant oxone (KURZ ET AL. 2007; LIMBURG ET AL. 2001).

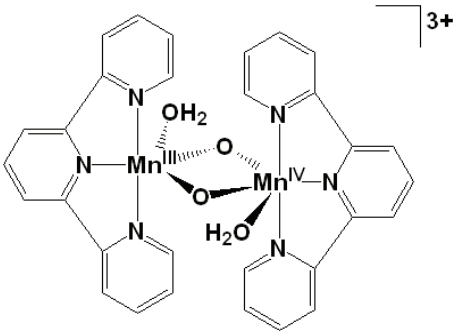

Mn_2-terpy

Figure 26:

The dimeric, bis-μ-oxo bridged manganese compound Mn_2-terpy ($[(terpy)(H_2O)Mn^{III}(O)_2Mn^{IV}(OH_2)(terpy)](NO_3)_3$ (terpy = 2,2':6,2''-terpyridin) (LIMBURG ET AL. 2001) with its tridentate ligand, terminally coordinates two water molecules in trans position per metal center. The compound was synthesized in the group of Prof. Dr. Stenbjörn Styring, Uppsala, Sweden by Gustav Berggren.

While MIMS confirms the reported evolution of labeled species (Fig. 27), stoichiometric evolution of labeled oxygen species according to model A is not detected. The isotopic distribution of the formed O_2 is compared on the right side of Fig. 27. View also Table 5) with model A "pure water oxidation" and model B, where one oxygen is transferred from the oxidant (unlabelled) and one from water (containing ^{18}O label).

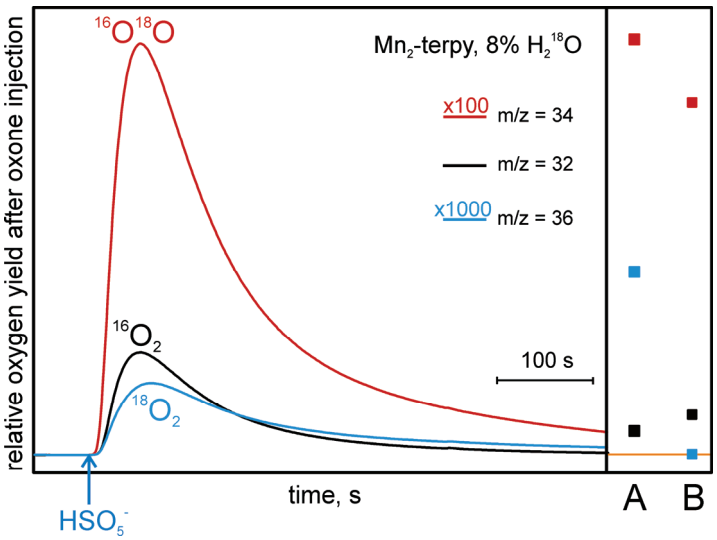

Figure 27:

Reaction of 5 equivalents oxone per metal center with 2mM Mn_2-terpy dissolved in H_2O with a final ^{18}O-water enrichment of 8%. Measurements are performed at 20 °C. Upon oxone injection mainly $^{16}O_2$ (black trace) and $^{16}O^{18}O$ (red trace) are produced. The amount of $^{18}O_2$ by the compound is ~1/3 of what is expected for a pure water splitting reaction (model B).

The comparison (Fig. 27) shows that neither model B, nor model A fully explains the data. Apparently a mixture of both reaction pathways occurs. A second oxone injection does not yield the same result, but an increase in unlabelled and a decrease in labeled oxygen species is observed (data not shown). Mn_2-terpy therefore does not act as a true catalyst for water-splitting. However, since a small percentage of water-splitting does occur, it may serve as model for future development.

6.2.1.2 Mn_2-mcbpen

Mn_2-mcbpen (Fig. 28) (POULSEN ET AL. 2005), evolves O_2 upon addition of the oxidant HSO_5^-.

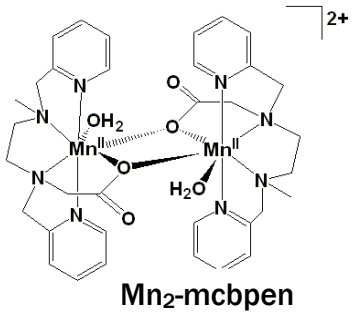

Mn_2-mcbpen

Figure 28:

The dimeric manganese compound Mn_2-mcbpen ($[Mn^{II}{}_2$ (mcbpen)$_2$ (H_2O_2)] were mcbpen is the anion of *N*-methyl-*N'*-carboxymenthyl-*N,N'*-bis(2-pyridyl methyl)ethane-1,2-diamine) (POULSEN ET AL. 2005) has two terminally coordinated water molecules in trans position per metal center. It contains carboxylate bridges instead of the µ-oxo bridges in Mn_2-terpy. The compound was synthesized in the group of Prof. Dr. Stenbjörn Styring, Uppsala, Sweden by Gustav Berggren.

When enriching the solvent water with $H_2{}^{18}O$, mainly unlabelled and single labeled oxygen species are detected (Fig. 29). The measured isotopic pattern of Mn_2-mcbpen resembles the distribution of "model B" best, despite the detection of a minor amount of $^{18}O_2$. The compound cannot be defined as a catalyst that would yield reproducible

amounts of oxygen for many cycles, because the oxygen evolution decreases with the third oxone injection (data not shown).

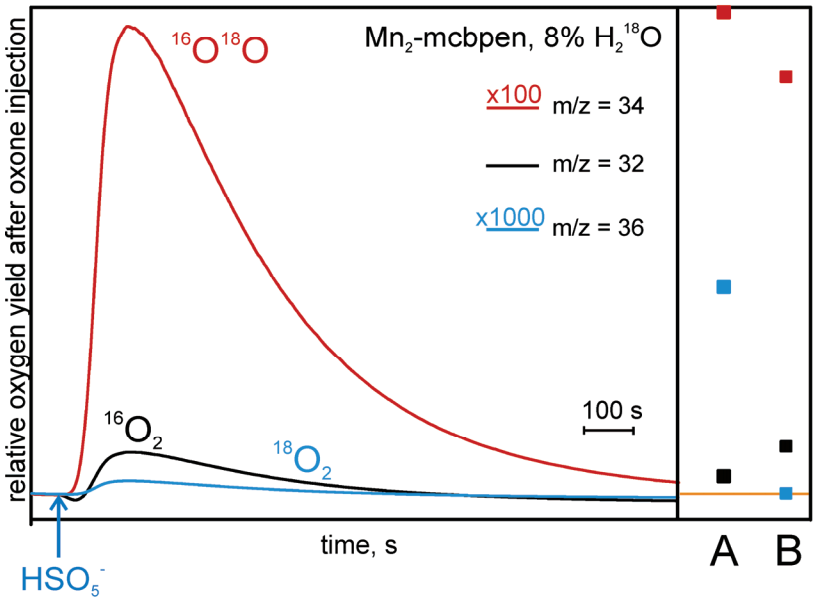

Figure 29:

Mn_2-mcbpen (2mM, in water) is reacted with oxone (5 equivalents per metal center, dissolved in water) at 20 °C. The final ^{18}O-water enrichment is 8%. Oxone injection (blue) invokes mainly $^{16}O_2$ (black trace) and $^{16}O^{18}O$ (red trace) evolution.

6.2.1.3 Mn_4-tbhpn

The tetra-nuclear manganese-compound Mn_4-tbhpn (Fig. 30) (CHAN AND ARMSTRONG 1990) with its heptadentate ligand exhibits oxygen evolution at oxone addition (KURZ ET AL. 2007).

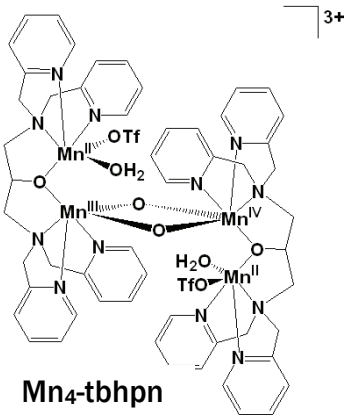

Figure 30:

The tetrameric manganese compound Mn_2-tbhpn ($[Mn_4O_2(TPHPN)_2(H_2O)_2(CF_3SO_3)_2]^{3+}$ (CHAN AND ARMSTRONG 1990) has two terminally coordinated water molecules. The compound was provided by Prof. Dr. William Armstrong.

MIMS measurements reveal the evolution of mainly unlabelled and single labeled oxygen species (Fig. 31). Like in the cases of the previously described results of the

compounds Mn_2-terpy and Mn_2-mcbpen, the O_2 generated by the reaction of Mn_4-tbhpn with oxone does neither match the theoretical assumption of a water splitting reaction (model A, Table 5) nor of an oxygen atom transfer reaction by oxone (model B, Table 5) entirely. However, the resulting pattern is close to model B. The compound responses to a second oxone injection with evolution of ~ ½ of the O_2 evolved at the first oxone addition (data not shown).

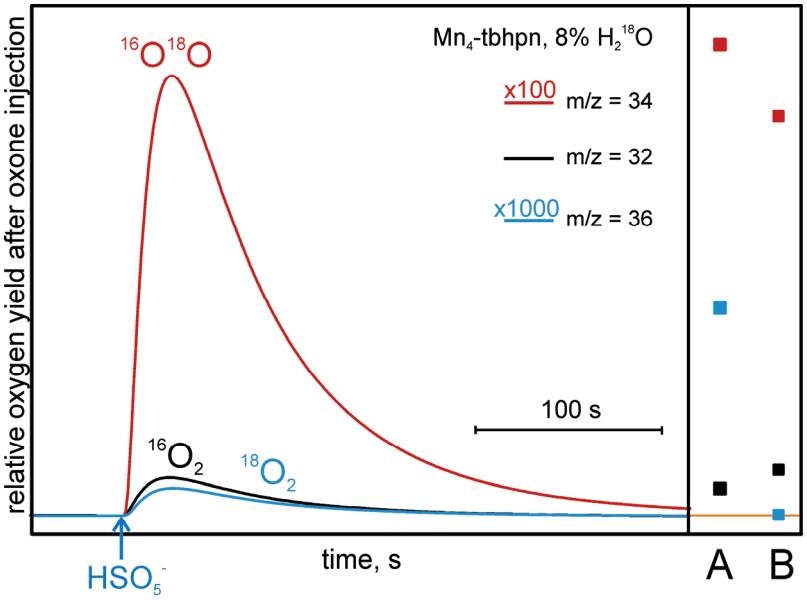

Figure 31:

Reaction of 5 equivalents oxone per metal center (dissolved in water) with 2mM Mn_4-tbhpn dissolved in H_2O/ MeCN (3:1) and 8% $H_2{}^{18}O$. The solution is constantly tempered at 20 °C. Upon oxone injection mainly $^{16}O_2$ (black line) and $^{16}O^{18}O$ (red line) are produced.

6.2.1.4 Mn_2-bpmp-AcO

Compound Mn_2-bpmp-AcO (Fig. 32) exhibits oxygen evolution in reaction with the oxidant oxone.

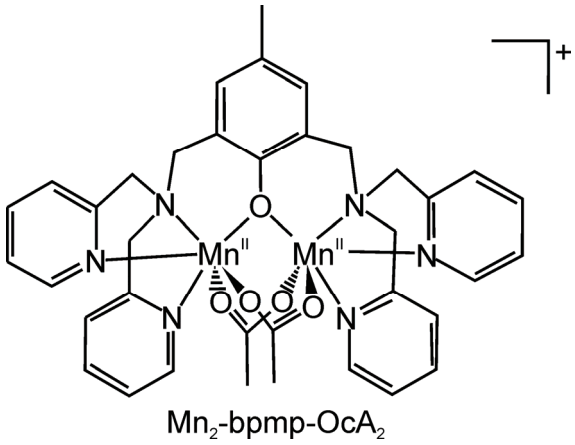

Mn_2-bpmp-OcA_2

Figure 32:

The dimeric manganese compound Mn_2-bpmp-AcO ($[Mn_2(bpmp)(\mu\text{-}OAc)_2]^+$ with 2,6-bis [(*N*,*N*-di(2-pyridinemethyl) amino)methyl]-4-methyl-phenol) as the anion of the complex (SUN ET AL. 2000) has two terminally coordinated acetate groups that are replaced by water derived ligands in solution. Gustav Berggren and Dr. Magnus Anderlund synthesized the com-pound at the chair of Prof. Dr. Stenbjörn Styring, Uppsala, Sweden.

The isotopic distribution of evolved O_2 is analyzed in measurements of Mn_2-bpmp-AcO with $H_2{}^{18}O$ and $HS^{16}O_5^-$.

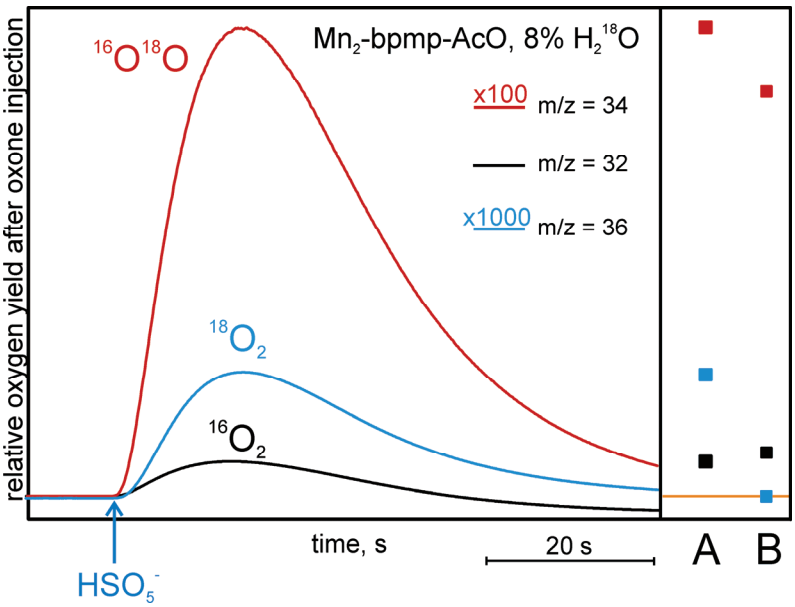

Figure 33:

Relative oxygen yield of Mn_2-bpmp-AcO after injection of 5 equivalents oxone (dissolved in water) per metal center to a 2mM Mn_2-bpmp-AcO in H_2O/MeCN (3:1)-solution. The mixture yields a final ^{18}O-water enrichment of 8%. The evolution of $^{16}O_2$ (black trace), $^{16}O^{18}O$ (red trace) and $^{18}O_2$ (blue trace) follow an oxone injection (blue). The isotopic distribution compares very well to model A ("true water splitting reaction").

The observed distribution of labeled oxygen species agrees well with the theoretically expected value based on the isotopic distribution of solvent water (model A, Table 5). Further oxone injection reveals a fast destruction of the compound.

Table 5:

Isotopic distribution of O_2 evolved by compounds Mn_2-mcbpen, Mn_2-terpy, Mn_4-tbhpn and Mn_2-bpmp-AcO

m/z	Mn_2-mcbpen	Mn_2-terpy	Mn_4-tbhpn	Mn_2-bpmp-AcO	MODEL A	MODEL B
32	91.2 (±0.4)	92.6 (±0.1)	91.7 (±0.1)	85.1 (±0.2)	84.6	92
34	8.8 (±0.4)	7.2 (±0.1)	8.2 (±0.1)	14.9 (±0.2)	14.7	8
36	0.03 (±0.0)	0.2 (±0.0)	0.06 (±0.0)	0.6 (±0.0)	0.6	0

Experimental and calculated isotopic distribution for the reaction of Mn_2-mcbpen, Mn_2-terpy, Mn_4-tbhpn and Mn_2- bpmp- AcO (each 2 mM) with oxone (each 5 equivalents). The final ^{18}O-enrichment was 8%. The calculated value model A reflects two oxygen-atoms deriving from water while model B represents one O-atom originating from water and another one transferred from the unlabelled oxidant $HS^{16}O_5^-$.

While the second addition of 5 equivalents oxidant yields clearly less ^{18}O-labeled oxygen species, the third oxone injection is similar to the isotopic distribution of oxygen species at natural abundance and the values gained for Mn_2O_3 (Fig. 34).

The most interesting compound is Mn_2-bpmp-AcO which matches the isotopic distribution of "model A", the water splitting reaction. To substantiate the interpretation that a water splitting reaction takes place, further measurements are performed.

6.2.2 *Stoichiometric $^{18}O_2$ evolution by Mn_2-bpmp-AcO*

The measurements reveal stoichiometric $^{18}O_2$ evolution by Mn_2-bpmp-AcO directly after addition of oxone. To ensure that the detected oxygen yield is caused by a specific reaction of Mn_2-bpmp-AcO with the oxidant, the following experiments were performed:

A the amount of evolved oxygen is plotted versus varying concentrations of Mn_2-bpmp-AcO and correspondingly,

B the amount of evolved oxygen is measured versus varying concentrations of oxone,

C Mn_2O_3, a manganese-oxo compound without chelating ligand is reacted with oxone and

D the chelating ligand bpmp-AcO without bound manganese is measured at conditions corresponding to the standard conditions (Section 2.5.5).

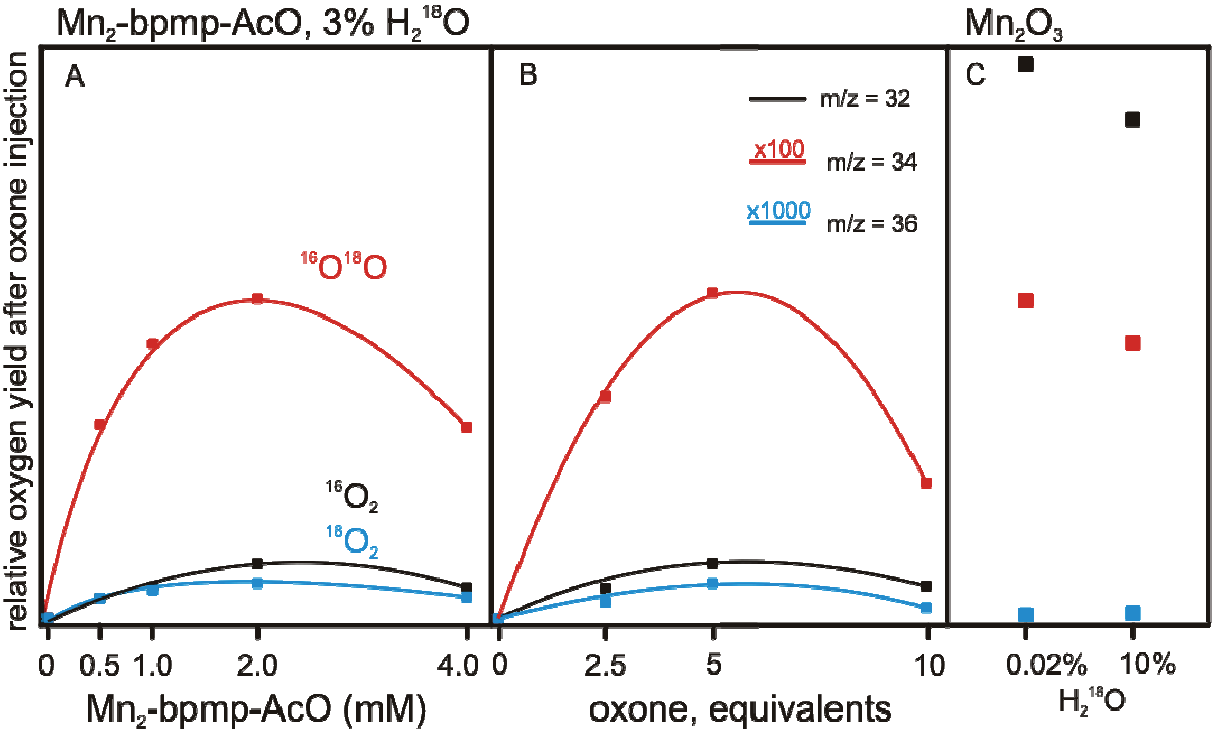

Figure 34:

Dependency between oxygen yield and concentration of Mn_2-bpmp-AcO. The oxone addition was kept at a constant ratio of 5 equivalents oxone per metal center (A). Corresponding dependence between O_2 evolution and oxone concentration is shown in (B). In each measurement the final ^{18}O-enrichment was 3%. When doubling the concentration of 2 mM compound and 5 equivalents oxone per metal centre, the O_2 yield is diminished. To prevent a limitation by oxone shortage the compound/oxone-ratio is kept constant in A. (C) Isotopic labeling studies of a manganese oxide without chelating ligand reveal (i) a different isotopic pattern in comparison to A and B and (ii) no significant change in isotopic pattern when comparing measurements without additional ^{18}O-water to samples with 8% ^{18}O-water enrichment. In C m/z = 32 ($^{16}O_2$, black squares) contributes to 99.6%, while the percentage distribution of m/z = 34 ($^{16}O^{18}O$, red squares) is 0.4% and the one of 36 ($^{18}O_2$, blue squares) below the detection limit. The experimental error is smaller than 1% for m/z = 32 and 34. Each measurement is performed at 20 °C with Mn_2-bpmp-AcO solved 3:1 in H_2O: MeCN while Mn_2O_3 and oxone are solved in H_2O.

Figure 34(A) reveals a correlation between relative O_2-yield upon oxone injection and Mn_2-bpmp-AcO concentration. Several compound concentrations varying from 0.5 – 4 mM are reacted each with 5 equivalents oxone per metal center. The amount of oxygen evolved increases by 1.4 times when doubling the concentration from 0.5 to 1 and by 1.2 times when increasing the concentration from 1 mM to 2 mM, while further increase in concentration, to 4 mM, yields a lower O_2 evolution by 1.7 times in comparison to the yield of measurements with 2 mM. (B): at low oxidant concentrations the amount of O_2 evolved increases by 1.5 times with further addition of oxidant equivalents while O_2 evolution decreases by 2.3 times at higher oxidant concentrations.

Measurements of manganese (III) oxide with oxone (C) exhibit mainly $^{16}O_2$ evolution. The values for the different oxygen species obtained at natural abundance (0.02%) and ^{18}O-enrichment of 10% are highly comparable, revealing that the detected oxygen does not originate from solvent water, but almost entirely from oxone.

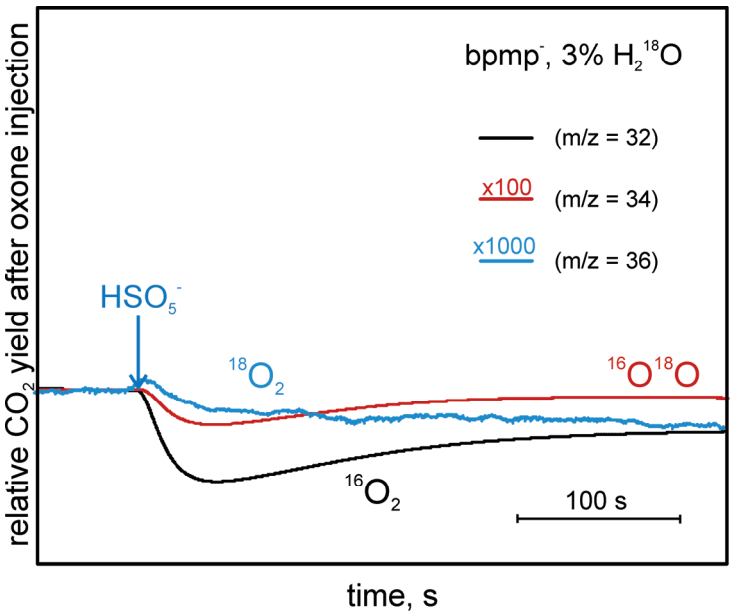

Figure 35:

Measurement of 2 mM bpmp-AcO dissolved in a H_2O/MeCN (3:1)-solution with a final ^{18}O-enrichment of 3%. Upon oxone addition (5 equivalents per metal center, dissolved in water) an oxygen uptake by the ligand scaffold is detected. Concomitant with oxone a minor amount of Argon is injected causing a small artifact on m/z = 36. Black traces represent $^{16}O_2$, red traces $^{16}O^{18}O$ and blue traces $^{18}O_2$.

Measurements of bpmp-AcO clearly lack O_2 evolution when treated with oxone (Fig. 35). On the contrary, upon oxone addition an oxygen uptake is detected revealing that oxygen is not produced by bpmp-AcO. The decrease in oxygen signal is most likely based on oxygen consumption by the compound, showing that oxone efficiently oxidizes the ligand. This is also visible when only small amounts of oxygen are liberated e.g. at low oxidant/compound concentrations (data not shown).

6.2.3 *Influence of pH*

At standard conditions (Section 2.5.5), Mn_2-bpmp-AcO evolves oxygen according to model A, but further oxone addition leads to a loss of the production of labeled species. One possible reason for this could be that the oxone solution is highly acidic (pH ~2) and might cause destruction of the compound. In an attempt to stabilize the compound and possibly increase turnover number the solution pH was kept above pH > 4 by the use of acetate buffer.

The comparison of measurements with acetate buffer (100 mM, pH 4.3) (A) and at standard conditions (B) (Fig. 36) reveals that the reaction is perturbed in the presence of the buffer.

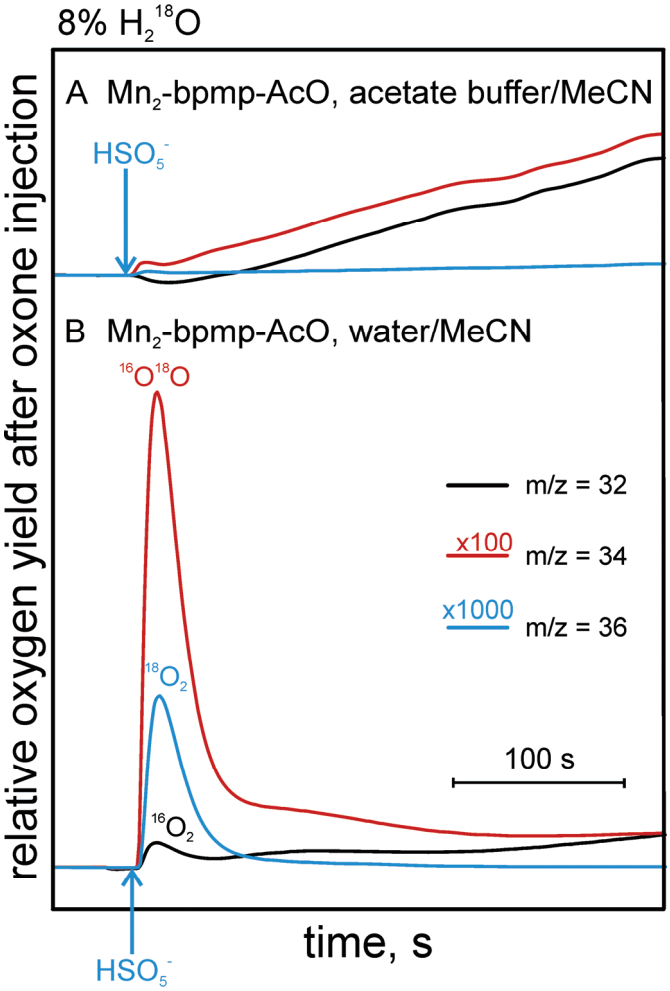

Figure 36:

Reaction of 2mM Mn_2-bpmp-AcO with 5 equivalents oxone per metal center (dissolved in water) at 20 °C. The ^{18}O-enrichment yields 8%. Compared are measurements of Mn_2-bpmp-AcO in a 3:1 acetate buffer (pH 4.75): MeCN solution (A) to standard conditions of 3:1 water/ MeCN solution (B). Black traces represent $^{16}O_2$, red traces $^{16}O^{18}O$ and blue traces $^{18}O_2$.

Upon addition of 100 mM acetate buffer, only negligible amounts of labeled species are formed by oxone injection despite 8% ^{18}O-water enrichment. This is in clear contrast to the measurements in an unbuffered solution, which represent model A.

6.2.4 *CO_2 evolution by Mn_2-bpmp-AcO*

The reaction of Mn_2-bpmp-AcO with oxone yields not only O_2, but labeled carbon dioxide species ($C^{16}O^{18}O$ and $C^{18}O_2$) were also produced at significant levels. This CO_2

evolution can be recorded at m/z = 44, 46 and 48 (data not shown). Nearly twelve times more CO_2 (m/z = 44) than O_2 (m/z = 32) is generated upon oxone addition. The active site of Mn_2-bpmp-AcO comprises two manganese atoms which are directly ligated by two acetate groups. Acetate can easily produce CO_2 and may therefore be the source for the observed CO_2 evolution. This hypothesis was tested by the exchange of the acetate ligands against *(i)* ^{13}C-enriched acetate ($H_3{}^{12}C{}^{13}COO^-$) and *(ii)* chloride as replacement for the acetate groups.

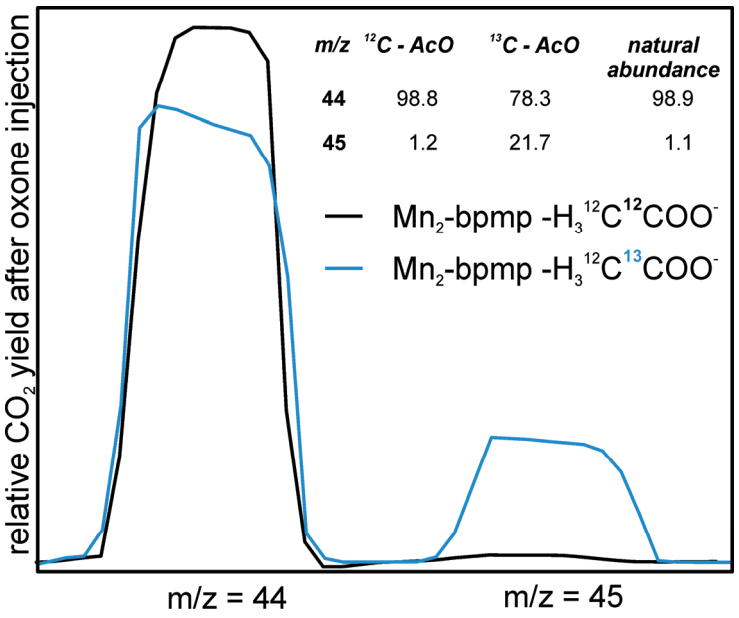

Figure 37:

Mass scan from m/z = 44 and to m/z = 45 at 20°C. Mn_2-bpmp-AcO (2 mM in H_2O/MeCN (3:1)) is measured either with ^{12}C-AcO (black traces) or ^{13}C-AcO (blue traces). An increase by ~ 20 times of m/z = 45 for Mn_2-bpmp-^{13}C-AcO labeled samples in comparison to Mn_2-bpmp-^{12}C-AcO is revealed.

The difference of one mass unit between m/z = 44 (^{12}C) and m/z = 46 (^{13}C) can be separated when scanning the mass range. Comparison of Mn_2-bpmp-^{12}C-AcO to Mn_2-bpmp-^{13}C-AcO reveals a clear increase in m/z = 45 by ~ 20 times (Fig. 37), together with a corresponding decrease of the m/z = 44 peak. Replacement of acetate ligands against chloride diminished CO_2 emission by ~ 20% (data not shown). It is interesting to note that measurements of Mn-free bpmp-AcO yields CO_2 in reaction with oxone as well. However, compared to the reactions of fully assembled Mn_2-bpmp-AcO the CO_2 yield is reduced to 1/14 .

6.2.5 Oxidation with the strict two-electron transfer agent lead tetraacetate

Mn_2-bpmp-AcO2 appears to split water upon reaction with oxone. However, the situation is complicated by the fact, that oxone is a two-electron transfer agent that is also capable of oxygen transfer reactions. To exclude that doubly labeled oxygen is

formed by an oxygen transfer reaction which is followed by a fast solvent exchange, lead tetraacetate ($Pb(OAc)_4$), a strict two-electron transfer agent is used to oxidize the Mn_2-bpmp-AcO.

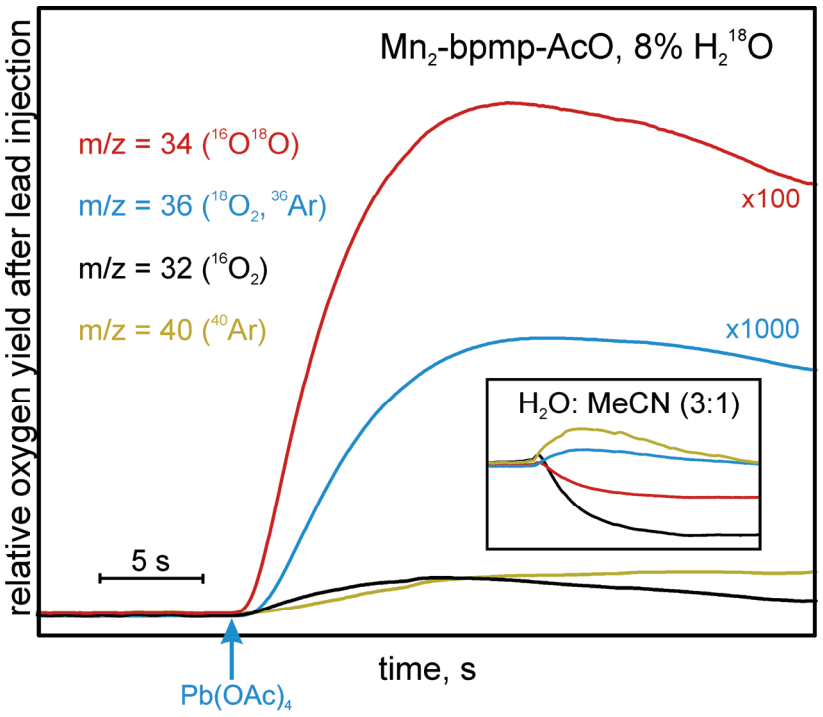

Figure 38:

Relative oxygen yield of Mn_2-bpmp-AcO after injection of ~ 5 equivalents lead tetraacetate ($Pb(OAc)_4$) dissolved in MeCN. The mixture of 2 mM Mn_2-bpmp-AcO per metal center (H_2O/MeCN-solution, 3:1) had a final ^{18}O-water enrichment of 8%. The evolution of $^{16}O_2$ (black trace), $^{16}O^{18}O$ (red trace), $^{18}O_2$ (blue trace) was induced by Pb $(OAc)_4$ addition (blue). As control, lead tetraacetate is injected into a solution of H_2O/MeCN (3:1) (inset). Detection of m/z = 40 (^{40}Ar) functions as control.

The reaction of Mn_2-bpmp-AcO with the strict two-electron transfer agent lead tetraacetate yields an isotopic pattern for O_2 that is close to model A ("pure water splitting"). In comparison, the reaction of Mn_2-mcbpen with lead tetraacetate does not yield oxygen.

6.2.6 Oxidant tert-butyl hydroperoxide

The tested compounds Mn_2-bpmp-AcO, Mn_2-mcbpen, Mn_2-terpy and Mn_4-tbhpn evolve oxygen upon oxidant tert-butyl hydroperoxide (TBHP) addition as an oxidant, but ^{18}O-enrichment does not lead to an increased evolution of labelled oxygen species. The relative amount of evolved $^{16}O^{18}O$ and $^{18}O_2$ is essentially identical between measurements at natural abundance and a final enrichment of 92% $H_2{}^{18}O$ (data not shown). Therefore, in case of TBHP both oxygen atoms stem from the oxidant.

6.2.7 O_2/CO_2 evolution and the ^{18}O content of evolved O_2

The four compounds Mn_2-terpy, Mn_2-mcbpen, Mn_2-bpmp-AcO and Mn_4-tbhpn evolve O_2 and CO_2 to very different extends.

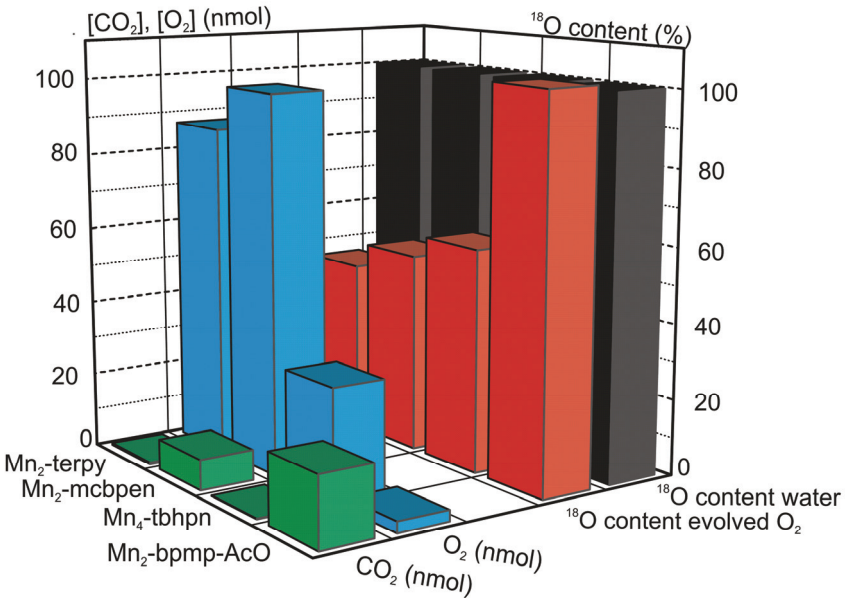

Figure 39:

Comparison of the Mn_2-terpy, Mn_2-mcbpen, Mn_2-bpmp-AcO and Mn_4-tbhpn. CO_2 and O_2 concentrations in nmol (for evaluation of peak heights, see Section 2.6) evolved by the com-pounds are displayed. For details about calibration by injection of defined amounts of O_2 and CO_2, view Section 2.6.2. Dis-played for each com-pound are the ^{18}O content of evolved O_2 ($^{18}O_2$ + ½ · $^{16}O^{18}O$) and the ^{18}O content of solvent water enriched with $H_2{}^{18}O$.

Compounds Mn_2-terpy and Mn_2-mcbpen produce the highest oxygen yields (Fig. 39). In both cases, clearly less CO_2 than O_2 is liberated. While the tetrameric manganese compound Mn_4-tbhpn evolves less O_2, the CO_2 emission is lowest in comparison to other tested compounds. Mn_2-bpmp-AcO evolves by far the least molecular oxygen, while the carbon dioxide yield clearly exceeds the one of the other three compounds, and its O_2-production. If selecting a compound only on dioxygen yield and benefiting O_2/CO_2-ratio Mn_2-bpmp-AcO would be excluded, but because of its ability to produce labeled oxygen species, in accordance with the ^{18}O enrichment, it is the most interesting compound. Mn_2-terpy, Mn_2-mcbpen and Mn_4-tbhpn also evolve labeled oxygen, but the ^{18}O content of the produced dioxygen amounts to only about half of the amount of added $H_2{}^{18}O$.

6.3. Discussion

The aim of this study was to classify the observed O_2 evolution activities of several Mn-compounds according to three categories: A: true water splitting, B: only one O from water and C: decomposition of oxidant (both O from oxidant). Therefore, Mn_2-

bpmp-AcO, Mn_2-mcbpen, Mn_2-terpy and Mn_4-tbhpn have been mixed with various oxidants (HSO_5^-, $Pb(AcO)_4$, TBHP) in the presence of ^{18}O enriched water and oxygen evolution was followed by MIMS.

Mn_2-bpmp-AcO, Mn_2-mcbpen, Mn_2-terpy and Mn_4-tbhpn produce dioxygen in very different amounts (Fig. 39). While none of the tested compounds is a true catalyst that repeatedly evolves reproducible amounts of dioxygen and all of the tested compounds liberate CO_2 to very different extends, only Mn_2-bpmp-AcO yields as much ^{18}O as present in the solvent water (Model A), but is the least stable of the tested compounds. For the other three compounds, about half of the ^{18}O content of solvent water is detected in the produced dioxygen (Model B). The mechanism of a one-oxygen-transfer reaction has been proposed for the compounds Mn_2-mcbpen (POULSEN ET AL. 2005) and for Mn_2-terpy (LIMBURG ET AL. 2001). The performed MIMS measurements of Mn_2-mcbpen and Mn_2-terpy in reaction with oxone (Figs. 27 and 29) reveal the evolution of mainly unlabeled and single labeled oxygen species and thereby confirm these previous proposals. Very similar results were obtained with Mn_4-tbhpn and oxone (Fig. 31). In all three cases varying, but small amounts of $^{18}O_2$ are detected, which do not match the yield expected for true water splitting reactions (Model A). An exchange reaction between transferred oxygen and solvent water must therefore clearly be slower than the oxygen release kinetic. Alternatively, a small percentage of true water-splitting activity of these complexes cannot be excluded. They may serve as models for future development.

The reaction of Mn_2-bpmp-AcO in $H_2{}^{18}O$ with the oxidant oxone and the oxidant lead tetraacetate reveals $^{18}O_2$ evolution at theoretical level (Model A, Fig. 33, Table 5). The possibility of a fast exchange reaction, where oxygen is transferred by oxone in a first step and then rapidly exchanged against labeled bulk water, cannot be excluded. Lead tetraacetate is a true two-electron transfer agent, not capable of oxygen transfer reactions. The oxygen evolution of Mn_2-bpmp-AcO in reaction with lead tetraacetate therefore excludes fast exchange reactions and indicates strongly that water is the source of the liberated oxygen and that Mn_2-bpmp-AcO oxidizes water to O_2. The oxygen evolving mechanism for Mn_2-mcbpen on the other hand has been shown to involve oxygen transfer. This compound does not evolve oxygen in reaction with lead tetra acetate, confirming the drawn conclusion.

So far, the final reaction mechanism for the most interesting compound Mn_2-bpmp-AcO has not been established, though several reaction steps have been suggested earlier. The stepwise oxidation of $Mn^{II/II}$ to $Mn^{III/III}$ is proposed to be facilitated by the exchange of acetate ligands against water-derived ligands (H_2O, OH^-, O^{2-}). The mechanism is thought to be a μ-acetate bridge modification by rapid association-dissociation equilibrium. The mechanistic proposal is based on a dependency of the reaction on water. Measurements of Mn_2-bpmp-AcO performed in dry acetonitrile have shown that manganese cannot be oxidized beyond $Mn^{II/III}$ (EILERS ET AL. 2005; HUANG ET AL. 2002; HUANG ET AL. 2004). MIMS measurements reveal that the water splitting ability is lost in the presence of acetate buffer. Analogues to the finding that the ligating acetate groups have to be exchanged against water derived ligands previous to the water splitting reaction, the use of acetate buffer perturbs the water oxidizing reaction greatly. The increased concentration of acetate ions shifts the association-dissociation equilibrium between bound acetate and water so strongly towards acetate that only a slight amount of labeled oxygen species is evolved in the presence of acetate buffer (Fig. 36).

Based on the finding of a reaction from $Mn^{II/II}$ to $Mn^{III/III}$ that involves the exchange of acetate ligands against water derived ligands, the first step of the reaction towards water splitting is likely to be a two-electron transfer reaction from $Mn^{II/II}$ to $Mn^{III/III}$. Lead tetraacetate is a strict two-electron transfer agent that yields labeled oxygen species. It therefore is likely that a second 2 e^- transfer reaction yields $Mn^{IV/IV}$ that could be able to oxidize water. However, the entire reaction mechanism and the active species involved remains unclear at this early stage.

While Mn_2-bpmp-AcO performs water splitting upon addition of a chemical oxidant, the final goal of developing a light driven catalyst mimicking PSII for industrial production is still out of reach. Mn_2-bpmp-AcO already performs two key reactions of the sought hydrogen producing assembly: it oxidizes water and has been successfully coupled to a photo-sensitizer (P680 mimic) and electron acceptor; a stepwise photooxidation of the Mn_2-compound, mimicking the PSII electron transfer reaction has been proposed (HAMMARSTROM ET AL. 2001; SUN ET AL. 2000).

6.3. Conclusion

One dimeric Mn-compound (Mn_2-bpmp-AcO) has been identified to generate O_2 closely resembling the theoretical values, and thus suggesting strongly a true water-splitting reaction. Though the ^{18}O exchange from water into oxone is slow, the possibility of O-transfer and subsequent exchange against ^{18}O from water could be excluded on the basis of $^{18}O_2$ evolution in reaction with the 2 e^- oxidant $Pb(OAc)_4$, which is not capable of O-transfer reactions.

Literature

LITERATURE

Allin, C., and Gerwert, K. (2001). Ras catalyzes CTP hydrolysis by shifting negative charges from gamma- to beta-phosphate as revealed by time-resolved FTIR difference spectroscopy. Biochemistry **40,** 3037-3046.

Ananyev, G.M., and Dismukes, G.C. (1996). Assembly of the tetra-Mn site of photosynthetic water oxidation by photoactivation: Mn stoichiometry and detection of a new intermediate. Biochemistry **35,** 4102-4109.

Ananyev, G.M., Zaltsman, L., Vasko, C., and Dismukes, G.C. (2001). The inorganic biochemistry of photosynthetic oxygen evolution/water oxidation. Biochim. Biophys. Acta **1503,** 52-68.

Artz, K., Williams, J.C., Allen, J.P., Lendzian, F., Rautter, J., and Lubitz, W. (1997). Relationship between the oxidation potential and electron spin density of the primary electron donor in reaction centers from *Rhodobacter sphaeroides*. Proc. Natl. Acad. Sci. U. S. A. **94,** 13582-13587.

Atkins, P.W., and de Paula, J. (2006). Physical Chemistry. (Oxford: Oxford University Press).

Audi, G. (2006). The history of nuclidic masses and of their evaluation. Int. J. Mass Spectr. **251,** 85-94.

Audi, G., and Wapstra, A.H. (1993). The 1993 Atomic Mass Evaluation .1. Atomic Mass Table. Nucl. Phys. A **565,** 1-65.

Bader, K.P., Thibault, P., and Schmid, G.H. (1987). Study on the properties of the S_3 state by mass-spectrometry in the filamentous cyanobacterium *Oscillatoria chalybea*. Biochim. Biophys. Acta **893,** 564-571.

Baffert, C., Collomb, M.N., Deronzier, A., Kjaergaard-Knudsen, S., Latour, J.M., Lund, K.H., McKenzie, C.J., Mortensen, M., Nielsen, L., and Thorup, N. (2003). Biologically relevant mono- and di-nuclear manganese II/III/IV complexes of mononegative pentadentate ligands. Dalton Trans., 1765-1772.

Bard, A.J., and Fox, M.A. (1995). Artificial Photosynthesis - Solar Splitting of Water to Hydrogen and Oxygen. Acc. Chem. Res. **28,** 141-145.

Beck, W.F., and Brudvig, G.W. (1988). Ligand substitution reactions of the oxygen evolving center of photosystem II. Chem. Scripta **28A,** 93-98.

Bernat, G., Morvaridi, F., Feyziyev, Y., and Styring, S. (2002). pH dependence of the four individual transitions in the catalytic S-cycle during photosynthetic oxygen evolution. Biochemistry **41,** 5830-5843.

Berry, E.A., Guergova-Kuras, M., Huang, L.S., and Crofts, A.R. (2000). Structure and function of cytochrome bc complexes. Annu. Rev. Biochem. **69,** 1005-1075.

Berthold, D.A., Babcock, G.T., and Yocum, C.F. (1981). A highly resolved, oxygen-evolving photosystem II preparation from spinach thylakoid membranes. FEBS Lett. **134,** 231-234.

Binstead, R.A., Chronister, C.W., Ni, J.F., Hartshorn, C.M., and Meyer, T.J. (2000). Mechanism of water oxidation by the mu-oxo dimer $[(bpy)(2)(H_2O)(RuORuIII)\text{-}O\text{-}III(OH_2)(bpy)_2]^{4+}$. J. Am. Chem. Soc. **122,** 8464-8473.

Blubaugh, D.J., and Cheniae, G.M. (1992). Photoassembly of the PSII Mn/Ca Cluster. Photosynth. Res. **34,** 147-147.

Boichenko, V.A., and Efimtsev, E.I. (1979). Inhibition of photosystem II activity in *Chlorella* at high oxygen concentrations. Sov. Plant Physiol. **26,** 658-666.

Bouges, B. (1971). Action de faibles concentrations d'hydroxylamine sur l'emission d'oxygene des algues chlorella et des chloroplastes d'epinards. Biochim. Biophys. Acta **936,** 228-235.

Boussac, A., and Rutherford, A.W. (1988). Nature of the inhibition of the oxygen-evolving enzyme of photosystem II induced by NaCl washing and reversed by the addition of Ca^{2+} or Sr^{2+}. Biochemistry **27,** 3476-3483.

Boussac, A., Rappaport, F., Carrier, P., Verbavatz, J.M., Gobin, R., Kirilovsky, D., Rutherford, A.W., and Sugiura, M. (2004). Biosynthetic Ca^{2+}/Sr^{2+} exchange in the photosystem II oxygen-evolving enzyme of *Thermosynechococcus elongatus*. J. Biol. Chem. **279,** 22809-22819.

Bricker, T.M., and Frankel, L.K. (2002). The structure and function of CP47 and CP43 in Photosystem II. Photosynth. Res. **72,** 131-146.

Britt, R.D. (1996). Oxygen Evolution. In Oxygenic Photosynthesis: The Light Reactions, D.R. Ort and C.F. Yocum, eds (Dordrecht: Kluwer Academic Publishers), pp. 137-164.

Britt, R.D., Campbell, K.A., Peloquin, J.M., Gilchrist, M.L., Aznar, C.P., Dicus, M.M., Robblee, J., and Messinger, J. (2004). Recent pulsed EPR studies of the Photosystem II oxygen-evolving complex: implications as to water oxidation mechanisms. Biochim. Biophys. Acta **1655,** 158-171.

Buick, R. (1992). The Antiquity of Oxygenic Photosynthesis - Evidence from Stromatolites in Sulfate-Deficient Archean Lakes. Science **255,** 74-77.

Butler, W.L., and Strasser, R.J. (1977). Tripartite Model for Photochemical Apparatus of Green Plant Photosynthesis. Proc. Natl. Acad. Sci. U. S. A. **74,** 3382-3385.

Cammarata, K.V., and Cheniae, G.M. (1987). Studies on 17, 24 kD Depleted Photosystem II Membranes. Plant Physiol. **84,** 587-595.

Castelfranco, P.A., Lu, Y.K., and Stemler, A.J. (2007). Hypothesis: the peroxydicarbonic acid cycle in photosynthetic oxygen evolution. Photosynth. Res. **94,** 235-246.

Chan, M.K., and Armstrong, W.H. (1990). Tetranuclear Manganese Oxo Complex with a 2.7A Mn=Mn Separation and Intramolecular H_2O=(Mu-O) Hydrogen-Bonded Contacts - $[Mn_4O_2(Tphpn)_2(H_2O)_2(Cf_3SO_3)_2](Cf_3SO_3)_3$ - Possible Mode for Binding of Water at the Active-Site of the Oxygen-Evolving Complex in Photosystem II. J. Am. Chem. Soc. **112,** 4985-4986.

Chen, C., Kazimir, J., and Cheniae, G.M. (1995). Calcium Modulates the Photoassembly of Photosystem II $(Mn)_4$-Clusters by Preventing Ligation of Nonfunctional High-Valency States of Manganese. Biochemistry **34,** 13511-13526.

Chen, H.Y., Faller, J.W., Crabtree, R.H., and Brudvig, G.W. (2005). Synthesis and properties of $[(MnO_4)$-O-IV_4(ETO-TERPY$)_4(OH)_2(OH_2)_2](ClO_4)_6$: A new high-valent manganese tetramer structure related to the oxygen-evolving complex of photosystem II. Abstr. Pap. Am. Chem. Soc. **229,** U1050-U1050.

Chen, H.Y., Tagore, R., Olack, G., Vrettos, J.S., Weng, T.C., Penner-Hahn, J., Crabtree, R.H., and Brudvig, G.W. (2007). Speciation of the catalytic oxygen evolution system: $[Mn_2(III/IV)(mu\text{-}O)_2(terpy)_2(H_2O)_2](NO_3)_3$+$HSO_5$. Inorg. Chem. **46,** 34-43.

Cheniae, G.M., and Martin, I.F. (1969). Photoreactivation of manganese catalyst in photosynthetic oxygen evolution. Plant Physiol. **44,** 351-360.

Cheniae, G.M., and Martin, I.F. (1970). Sites of function of manganese within photosystem II - roles in O_2 evolution and system II. Biochim. Biophys. Acta **197,** 219-239.

Cheniae, G.M., and Martin, I.F. (1973). Absence of oxygen-evolving capacity in dark-grown *Chlorella* - photoactivation of oxygen-evolving centers. Photochem. Photobiol. **17,** 441-459.

Christen, G., and Renger, G. (1999). The role of hydrogen bonds for the multiphasic $P680^{+\cdot}$ reduction by Y_Z in photosystem II with intact oxygen

evolution capacity. Analysis of kinetic H/D isotope exchange effects. Biochemistry **38,** 2068-2077.

Christen, G., Seeliger, A., and Renger, G. (1999). $P680^{+\cdot}$ reduction kinetics and redox transition probability of the water oxidizing complex as a function of pH and H/D isotope exchange in spinach thylakoids. Biochemistry **38,** 6082-6092.

Chronister, C.W., Binstead, R.A., Ni, J., and Meyer, T.J. (1997). Mechanism of Water Oxidation Catalyzed by the μ-Oxo Dimer $[(bpy)_2(OH_2)Ru^{III}ORu^{III}(OH_2)(bpy)_2]^{4+}$. Inorg. Chem. **36,** 3814-3815.

Cinco, R.M., Robblee, J.H., Rompel, A., Fernandez, C., Yachandra, V.K., Sauer, K., and Klein, M.P. (1998). Strontium EXAFS reveals the proximity of calcium to the manganese cluster of oxygen evolving photosystem II. J. Phys. Chem. B **102,** 8248-8256.

Cinco, R.M., Robblee, J.H., Messinger, J., Fernandez, C., Holman, K.L.M., Sauer, K., and Yachandra, V.K. (2004). Orientation of calcium in the Mn_4Ca cluster of the oxygen-evolving complex determined using polarized strontium EXAFS of photosystem II membranes. Biochemistry **43,** 13271-13282.

Cinco, R.M., McFarlane Holman, K.L., Robblee, J.H., Yano, J., Pizarro, S.A., Bellacchio, E., Sauer, K., and Yachandra, V.K. (2002). Calcium EXAFS establishes the Mn-Ca cluster in the oxygen evolving complex of photosystem II. Biochemistry **41,** 12928-12933.

Clausen, J., and Junge, W. (2004). Detection of an intermediate of photosynthetic water oxidation. Nature **430,** 480-483.

Clausen, J., Beckmann, K., Junge, W., and Messinger, J. (2005). Evidence that bicarbonate is not the substrate in photosynthetic oxygen evolution. Plant Physiol. **139,** 1444-1450.

Collomb, M.N., Deronzier, A., Richardot, A., and Pecaut, J. (1999). Synthesis and characterization of a new kind of Mn-2(III, IV)mu-oxo complex: $[Mn_2O_2(terpy)_2(H_2O)_2](NO_3)_3$ x $6H_2O$, terpy = 2,2 ': 6 ',2 "-terpyridine. New J. Chem. **23,** 351-353.

Collomb, M.N., Richardot, A., Baffert, C., and Deronzier, A. (2001). Electrochemical properties in aqueous solution of the di-mu-oxo complex $[Mn_2(III,IV)(O)_2(terpy)_2(H_2O)_2](NO_3)_3$ x $6H_2O$ (terpy=2,2 ': 6 ',2 "-terpyridine), model of the oxygen-evolving-center of photosystem II. J. Inorg. Biochem. **86,** 184-184.

Comte, P., Nazeeruddin, M.K., Rotzinger, F.P., Frank, A.J., and Gratzel, M. (1989). Artificial Analogs of the Oxygen-Evolving Complex in Photosynthesis - the Oxo-Bridged Ruthenium Dimer 2,2'-Bipyridyl-4,4'-Dicarboxylate-$2(H_2O)$RuIII-O-RuIII$(H_2O)L_2$. J. Mol. Cat. **52,** 63-84.

Cotton, F.A., and Wilkinson, G. (1974). Anorganische Chemie. (Weinheim: Verlag Chemie).

Crovetto, R. (1991). Evaluation of Solubility Data of the System CO_2-H_2O from 273-K to the Critical-Point of Water. J. Phys. Chem. Ref. Data **20,** 575-589.

Dai, X.B., Yu, Y., Zhang, R.X., Yu, X.J., He, P.M., and Xu, C.H. (2001). Relationship among photosystem II carbonic anhydrase, extrinsic polypeptides and manganese cluster. Chin. Sci. Bull. **46,** 406-409.

de Wijn, R., and van Gorkom, H.J. (2002). The rate of charge recombination in Photosystem II. Biochim. Biophys. Acta **1553,** 302-308.

Debus, R. (2005). The catalytic manganese cluster: protein ligation. In Photosystem II. The Light Driven Water:Plastiquinone Oxidoreductase, T. Wydrzynski and K. Satoh, eds (Dordrecht: Springer), pp. 261-284.

Debus, R.J. (1992). The manganese and calcium ions of photosynthetic oxygen evolution. Biochim. Biophys. Acta **1102,** 269-352.

Debus, R.J., Barry, B.A., Sithole, I., Babcock, G.T., and Mcintosh, L. (1988). Directed mutagenesis indicates that the donor to $P680^+$ in photosystem II is tyrosine-161 of the D1 polypeptide. Biochemistry **27,** 9071-9074.

DeRose, V.J., Latimer, M.J., Zimmermann, J.-L., Mukerji, I., Yachandra, V.K., Sauer, K., and Klein, M.P. (1995). Fluoride substitution in the Mn cluster from Photosystem II: EPR and X-ray absorption studies. Chem. Phys. **194,** 443-459.

Diner, B.A. (1977). Dependence of deactivation reactions of photosystem II on redox state of plastoquinone pool A varied under anaerobic conditions. Equilibria on the acceptor side of photosystem II. Biochim. Biophys. Acta **460,** 247-258.

Dismukes, G.C., Klimov, V.V., Baranov, S.V., Kozlov, Y.N., DasGupta, J., and Tyryshkin, A. (2001). The origin of atmospheric oxygen on earth: The innovation of oxygenic photosynthesis. Proc. Natl. Acad. Sci. U. S. A. **98,** 2170-2175.

Eilers, G., Zettersten, C., Nyholm, L., Hammarstrom, L., and Lomoth, R. (2005). Ligand exchange upon oxidation of a dinuclear Mn complex - detection of structural changes by FT-IR spectroscopy and ESI-MS. Dalton Trans., 1033-1041.

Evans, M.C.W., Nugent, J.H.A., Ball, R.J., Muhiuddin, I., and Pace, R.J. (2004). Evidence for a direct manganese-oxygen ligand in water binding to the S_2 state of the photosynthetic water oxidation complex. Biochemistry **43,** 989-994.

Fernandez, C., Cinco, R.M., Robblee, J.H., Messinger, J., Pizarro, S.A., Sauer, K., Yachandra, V.K., and Klein, M.P. (1998). Calcium and chloride cofactors of the oxygen evolving complex: X-ray absorption spectroscopy evidence for a Mn/Ca/Cl heteronuclear cluster. In Photosynthesis: Mechanisms and Effects, G. Garab, ed (Dordrecht: Kluwer Academic Publishers), pp. 1399-1402.

Ferreira, K.N., Iverson, T.M., Maghlaoui, K., Barber, J., and Iwata, S. (2004). Architecture of the photosynthetic oxygen-evolving center. Science **303,** 1831-1838.

Gersten, S.W., Samuels, G.J., and Meyer, T.J. (1982). Catalytic-Oxidation of Water by an Oxo-Bridged Ruthenium Dimer. J. Am. Chem. Soc. **104,** 4029-4030.

Geselowitz, D., and Meyer, T.J. (1990). Water Oxidation by $[(Bpy)_2(O)Ruvoruv(O)(Bpy)_2]^{4+}$ - an Oxygen-Labeling Study. Inorg. Chem. **29,** 3894-3896.

Gilbert, J.A., Eggleston, D.S., Murphy, W.R., Geselowitz, D.A., Gersten, S.W., Hodgson, D.J., and Meyer, T.J. (1985). Structure and Redox Properties of the Water-Oxidation Catalyst $[(Bpy)_2(OH_2)Ruoru(OH_2)(Bpy)_2]^{4+}$. J. Am. Chem. Soc. **107,** 3855-3864.

Golbeck, J.H. (2006). Photosystem I. The Light-Driven Plastocyanin:Ferredoxin Oxidoreductase. (Dordrecht: Springer).

Grabolle, M., Haumann, M., Müller, C., Liebisch, P., and Dau, H. (2006). Rapid loss of structural motifs in the manganese complex of oxygenic photosynthesis by x-ray irradiation at 10-300 K. J. Biol. Chem. **281,** 4580-4588.

Gregor, W.G., Cinco, R.M., Yu, H., Yachandra, V.K., and Britt, R.D. (2005). Influence of the 33 kDa manganese-stabilizing protein on the structure and substrate accessibility of the oxygen-evolving complex of photosystem II. Biochemistry **44,** 8817-8825.

Haddy, A., Kimel, R.A., and Thomas, R. (2000). Effects of azide on the S_2 state EPR signals from Photosystem II. Photosynth. Res. **63,** 35-45.

Haddy, A., Hatchell, J.A., Kimel, R.A., and Thomas, R. (1999). Azide as a competitor of chloride in oxygen evolution by photosystem II. Biochemistry **38,** 6104-6110.

Hammarstrom, L., Sun, L.C., Akermark, B., and Styring, S. (2001). A biomimetic approach to artificial photosynthesis: Ru(II)-polypyridine photosensitisers linked to tyrosine and manganese electron donors. Spectrochim. Acta A **57,** 2145-2160.

Han, K.-C., and Katoh, S. (1993). Different Localization of Two Ca^{2+} in Spinach Oxygen-Evolving Photosystem II Membranes. Evidence for Involvement of Only One Ca^{2+} in Oxygen Evolution. Plant Cell Physiol. **34,** 585-593.

Haumann, M., Liebisch, P., Müller, C., Barra, M., Grabolle, M., and Dau, H. (2005a). Photosynthetic O_2 formation tracked by time-resolved X-ray experiments. Science **310,** 1019-1021.

Haumann, M., Barra, M., Loja, P., Loscher, S., Krivanek, R., Grundmeier, A., Andreasson, L.E., and Dau, H. (2006). Bromide does not bind to the Mn_4Ca complex in its S_1 state in Cl^--depleted and Br^--reconstituted oxygen-evolving photosystem II: Evidence from X-ray absorption spectroscopy at the Br K-edge. Biochemistry **45,** 13101-13107.

Haumann, M., Müller, C., Liebisch, P., Iuzzolino, L., Dittmer, J., Grabolle, M., Neisius, T., Meyer-Klaucke, W., and Dau, H. (2005b). Structural and oxidation state changes of the photosystem II manganese complex in four transitions of the water oxidation cycle ($S_0 \rightarrow S_1$, $S_1 \rightarrow S_2$, $S_2 \rightarrow S_3$, and S_3, $S_4 \rightarrow S_0$) characterized by X-ray absorption spectroscopy at 20 K and room temperature. Biochemistry **44,** 1894-1908.

Hendry, G., and Wydrzynski, T. (2002). The two substrate water molecules are already bound to the oxygen evolving complex in the S_2 state of photosystem II. Biochemistry **41,** 13328-13334.

Hendry, G., and Wydrzynski, T. (2003). ^{18}O isotope exchange measurements reveal that calcium is involved in the binding of one substrate-water molecule to the oxygen-evolving complex in photosystem II. Biochemistry **42,** 6209-6217.

Hill, R., and Bendall, F. (1960). Function of the 2 Cytochrome Components in Chloroplasts - Working Hyothesis. Nature **186,** 136-137.

Hillier, W., and Wydrzynski, T. (2000). The affinities for the two substrate water binding sites in the O_2 evolving complex of photosystem II vary independently during S-state turnover. Biochemistry **39,** 4399-4405.

Hillier, W., and Wydrzynski, T. (2001). Oxygen ligand exchange at metal sites: implications for the O_2 evolving mechanism of photosystem II. Biochim. Biophys. Acta **1503,** 197-209.

Hillier, W., and Wydrzynski, T. (2004). Aspects of substrate water interactions within the photosystem II oxygen evolving complex. Phys. Chem. Chem. Phys. **6,** 4882-4889.

Hillier, W., and Messinger, J. (2005). Mechanism of photosynthetic oxygen production. In Photosystem II. The Light-Driven Water:Plastoquinone Oxidoredutase, T. Wydrzynski and K. Satoh, eds (Dordrecht: Springer), pp. 567-608.

Hillier, W., Messinger, J., and Wydrzynski, T. (1998). Kinetic determination of the fast exchanging substrate water molecule in the S_3 state of photosystem II. Biochemistry **37,** 16908-16914.

Hillier, W., McConnell, I., Badger, M.R., Boussac, A., Klimov, V.V., Dismukes, G.C., and Wydrzynski, T. (2006). Quantitative assessment of

intrinsic carbonic anhydrase activity and the capacity for bicarbonate oxidation in photosystem II. Biochemistry **45,** 2094-2102.

Hind, G., Nakatani, H.Y., and Izawa, S. (1969). The role of Cl^- in photosynthesis. The Cl^- requirement of electron transport. Biochim. Biophys. Acta **172,** 277-289.

Hoch, G., and Kok, B. (1963). A Mass Spectrometer Inlet System for Sampling Gases Dissolved in Liquid Phases. Arch. Biochem. Biophys. **101,** 160-170.

Hoganson, C.W., and Babcock, G.T. (1997). A metalloradical mechanism for the generation of oxygen from water in photosynthesis. Science **277,** 1953-1956.

Huang, P., Hogblom, J., Anderlund, M.F., Sun, L.C., Magnuson, A., and Styring, S. (2004). Light-induced multistep oxidation of dinuclear manganese complexes for artificial photosynthesis. J. Inorg. Biochem. **98,** 733-745.

Huang, P., Magnuson, A., Lomoth, R., Abrahamsson, M., Tamm, M., Sun, L., van Rotterdam, B., Park, J., Hammarstrom, L., Akermark, B., and Styring, S. (2002). Photo-induced oxidation of a dinuclear Mn2(II,II) complex to the Mn2(III,IV) state by inter- and intramolecular electron transfer to RuIII tris-bipyridine. J. Inorg. Biochem. **91,** 159-172.

Hurst, J.K., Zhou, J.Z., and Lei, Y.B. (1992). Pathways for Water Oxidation Catalyzed by the $[(Bpy)_2ru(OH_2)]_2O_4$+ Ion. Inorg. Chem. **31,** 1010-1017.

Isgandarova, S., Renger, G., and Messinger, J. (2003). Functional differences of photosystem II from *Synechococcus elongatus* and spinach characterized by flash-induced oxygen evolution patterns. Biochemistry **42,** 8929-8938.

Ishida, N., Sugiura, M., Rappaport, F., Lai, T.L., Rutherford, A.W., and Boussac, A. (2008). Biosynthetic exchange of bromide for chloride and strontium for calcium in the photosystem II oxygen-evolving enzymes. J. Biol. Chem. **283,** 13330-13340.

Jajoo, A., Bharti, S., and Kawamori, A. (2005). EPR characteristics of chloride-depleted photosystem II membranes in the presence of other anions. Photochem. Photobiol. Sci. **4,** 459-462.

Johnson, R.C., Cooks, R.G., Allen, T.M., Cisper, M.E., and Hemberger, P.H. (2000). Membrane introduction mass spectrometry: Trends and applications. Mass Spectr. Rev. **19,** 1-37.

Joliot, P., Barbieri, G., and Chabaud, R. (1969). Un nouveau modele des centres photochimiques du systeme II. Photochem. Photobiol. **10,** 309-329.

Junge, W., and Nelson, N. (2005). Nature's rotary electromotors. Science **308,** 642-644.

Jursinic, P. (1981). Investigation of double turnovers in photosystem II charge separation and oxygen evolution with excitation flashes of different duration. Biochim. Biophys. Acta **635,** 38 - 52.

Kaltashov, I.A., and Eyles, S.J. (2005). Mass Spectrometry in Biophysics. Conformation and Dynamics of Biomolecules. (Hoboken: John Wiley & Sons, Inc.).

Kamiya, N., and Shen, J.-R. (2003). Crystal structure of oxygen-evolving photosystem II from *Thermosynechococcus vulcanus* at 3.7 Å resolution. Proc. Natl. Acad. Sci. U. S. A. **100,** 98-103.

Karge, M., Irrgang, K.-D., and Renger, G. (1997). Analysis of the reaction coordinate of photosynthetic water oxidation by kinetic measurements of 355 nm absorption changes at different temperatures in photosystem II preparations suspended in either H_2O or D_2O. Biochemistry **36,** 8904-8913.

Katoh, S., Satoh, K., Ohno, T., Chen, J.-R., and Kashino, Y. (1987). Numbers of Calcium Ions Associated with Oxygen Evolving Photosystem II Preparations with Different Affinities. In Progress in Photosynthesis Research, J. Biggins, ed (Dordrecht: Martinus Nijhoff Publishers), pp. I.5.625-628.

Kelley, P.M., and Izawa, S. (1978). The role of chloride ion in Photosystem II: effects of chloride ion on Photosystem II electron transport and hydroxylamine inhibition. Biochim. Biophys. Acta **502,** 198-210.

Kessler, E. (1955). On the role of manganese in the xygen-evolving system of photosynthesis. Arch. Biochem. Biophys. **59,** 527-529.

Kessler, E. (1957). Stoffwechselphysiologische Untersuchungen an Hydrogenase Enthaltenden Grünalgen. 1. Über die Rolle des Mangans bei Photoreduktion und Photosynthese. Planta **49,** 435-454 (in German).

Khristin, M.S., Ignatova, L.K., Rudenko, N.N., Ivanov, B.N., and Klimov, V.V. (2004). Photosystem II associated carbonic anhydrase activity in higher plants is situated in core complex. FEBS Lett. **577,** 305-308.

Kirch, M., Lehn, J.M., and Sauvage, J.P. (1979). Hydrogen Generation by Visible-Light Irradiation of Aqueous-Solutions of Metal-Complexes - Approach to the Photo-Chemical Conversion and Storage of Solar-Energy. Helv. Chim. Acta **62,** 1345-1384.

Klimov, V.V., and Baranov, S.V. (2001). Bicarbonate requirement for the water-oxidizing complex of photosystem II. Biochim. Biophys. Acta **1503,** 187-196.

Kok, B., and Velthuys, B.R. (1976). Present status of the O_2 evolution model. In Research in Photobiology, A. Castellani, ed (New York: Plenum Press), pp. 111-119.

Kok, B., Forbush, B., and McGloin, M. (1970). Cooperation of charges in photosynthetic O_2 evolution. Photochem. Photobiol. **11,** 457-476.

Konermann, L., Messinger, J., and Hillier, W. (2008). Mass spectrometry based methods for studying kinetics and dynamics in biological systems. In Biophysical Techniques in Photosynthesis (Volume II), T.J. Aartsma and J. Matysik, eds (Dordrecht: Springer), pp. 167-190.

Kotting, C., Kallenbach, A., Suveyzdis, Y., Eichholz, C., and Gerwert, K. (2007). Surface change of Ras enabling effector binding monitored in real time at atomic resolution. Chembiochem **8,** 781-787.

Krishtalik, L.I. (1986). Energetics of multielectron reactions. Photosynthetic oxygen evolution. Biochim. Biophys. Acta **849,** 162-171.

Krishtalik, L.I. (1990). Activation energy of photosynthetic oxygen evolution: an attempt at theoretical analysis. Bioelectrochem. Bioenerg. **23,** 249-263.

Kruse, O., Rupprecht, J., Mussgnug, J.R., Dismukes, G.C., and Hankamer, B. (2005). Photosynthesis: a blueprint for solar energy capture and biohydrogen production technologies. Photochem. Photobiol. Sci. **4,** 957-970.

Kühn, P., Pieper, J., Kaminskaya, O., Eckert, H.J., Lechner, R.E., Shuvalov, V., and Renger, G. (2005). Reaction pattern of photosystem II: oxidative water cleavage and protein flexibility. Photosynth. Res. **84,** 317-323.

Kurz, P., Berggren, G., Anderlund, M.F., and Styring, S. (2007). Oxygen evolving reactions catalysed by synthetic manganese complexes: A systematic screening. Dalton Trans., 4258-4261.

Latimer, M.J., DeRose, V.J., Yachandra, V.K., Sauer, K., and Klein, M.P. (1998). Structural effects of calcium depletion on the manganese cluster of photosystem II: determination by x-ray absorption spectroscopy. J. Phys. Chem. B **102,** 8257-8265.

Lei, Y.B., and Hurst, J.K. (1994). Dynamical Investigations of the Catalytic Mechanisms of Water Oxidation by the [(Bpy)(2)Ru(Oh2)]2o(4+) Ion. Inorg. Chim. Acta **226,** 179-185.

Lewis, N.S., and Nocera, D.G. (2006). Powering the planet: Chemical challenges in solar energy utilization. Proc. Natl. Acad. Sci. U. S. A. **103,** 15729-15735.

Limburg, J., Crabtree, R.H., and Brudvig, G.W. (2000). Kinetic analysis of the O_2-forming reaction between $[Mn(III)(dpa)_2]^-$ (dpa = dipicolinate) and potassium peroxomonosulfate. Inorg. Chim. Acta **297,** 301-306.

Limburg, J., Vrettos, J.S., Liable-Sands, L.M., Rheingold, A.L., Crabtree, R.H., and Brudvig, G.W. (1999). A functional model for O–O bond formation by the O_2 evolving complex in photosystem II. Science **283,** 524-527.

Limburg, J., Vrettos, J.S., Chen, H., Paula, J.C.d., Crabtree, R.H., and Brudvig, G.W. (2001). Characterization of the O_2-Evolving Reaction Catalyzed by $[(terpy)(H_2O)MnIII(O)_2MnIV(OH_2)(terpy)](NO_3)_3$ (terpy = 2,2':6,2' '-Terpyridine). J. Am. Chem. Soc. **123,** 423-430.

Lindberg, K., and Andréasson, L.-E. (1996). A one-site, two-state model for the binding of anions in photosystem II. Biochemistry **35,** 14259-14267.

Lindberg, K., Wydrzynski, T., Vänngård, T., and Andréasson, L.-E. (1990). Slow release of chloride from ^{36}Cl-labeled photosystem II membranes. FEBS Lett. **264,** 153-155.

Loll, B., Kern, J., Saenger, W., Zouni, A., and Biesiadka, J. (2005). Towards complete cofactor arrangement in the 3.0 Å resolution structure of photosystem II. Nature **438,** 1040-1044.

Loll, B., Kern, J., Saenger, W., Zouni, A., and Biesiadka, J. (2007). Lipids in photosystem II: Interactions with protein and cofactors. Biochim. Biophys. Acta **1767,** 509-519.

Lu, Y.K., and Stemler, A.J. (2002). Extrinsic photosystem II carbonic anhydrase in maize mesophyll chloroplasts. Plant Physiol. **128,** 643-649.

Lubitz, W. (2006). EPR Studies of the Primary Electron Donor P700 in Photosystem I. In Photosystem I. The Light-Driven Plastocyanin:Ferredoxin Oxidoreductase, J.H. Golbeck, ed (Dordrecht: Springer), pp. 245-269.

Lydakis-Simantiris, N., Ghanotakis, D.F., and Babcock, G.T. (1997). Kinetic isotope effects on the reduction of the Y_Z radical in oxygen evolving and Tris washed photosystem II membranes by time resolved EPR. Biochim. Biophys. Acta **1322,** 129-140.

Martin, W., Scheibe, R., and Schnarrenberger, C. (2000). The Calvin Cycle and Its Regulation. In Photosynthesis: Physiology and Metabolism, R.C. Leegood, T.D. Shakey, and S. von Caemmerer, eds (Dordrecht: Kluwer Academic Publishers), pp. 9-51.

McCarty, R.E., Evron, Y., and Johnson, E.A. (2000). The chloroplast ATP synthase: A rotary enzyme? Ann. Rev. Plant Physiol. Plant Mol. Biol. **51,** 83-109.

McEvoy, J.P., Gascon, J.A., Batista, V.S., and Brudvig, G.W. (2005). The mechanism of photosynthetic water splitting. Photochem. Photobiol. Sci. **4,** 940-949.

Mende, D., and Wiessner, W. (1985). Bicarbonate *in vivo* requirement of photosystem II in the green alga *Chlamydobotrys stellata*. J. Plant Physiol. **118,** 259-266.

Messinger, J., and Renger, G. (1990). The reactivity of hydrazine with PS II strongly depends on the redox state of the water oxidizing system. FEBS Lett. **277,** 141 - 146.

Messinger, J., and Renger, G. (1993). Generation, oxidation by the oxidized form of the tyrosine of polypeptide D2, and possible electronic configuration of the redox States S_0, S_{-1} and S_{-2} of the water oxidase in isolated spinach thylakoids. Biochemistry **32,** 9379-9386.

Messinger, J., and Renger, G. (2008). Photosynthetic Water Splitting. In Primary Processes of Photosynthesis, Part 2 Principles and Apparatus, G. Renger, ed (Cambridge: RSCPublishing), pp. 291-351.

Messinger, J., Wacker, U., and Renger, G. (1991). Unusual low reactivity of the water oxidase in the redox state S_3 toward exogenous reductants. Analysis of the NH_2OH and NH_2NH_2 induced modifications of flash induced oxygen evolution in isolated spinach thylakoids. Biochemistry **30,** 7852-7862.

Messinger, J., Schröder, W.P., and Renger, G. (1993). Structure-function relations in photosystem II. Effects of temperature and chaotropic agents on the period four oscillation of flash induced oxygen evolution. Biochemistry **32,** 7658-7668.

Messinger, J., Badger, M., and Wydrzynski, T. (1995). Detection of *one* slowly exchanging substrate water molecule in the S_3 state of photosystem II. Proc. Natl. Acad. Sci. U. S. A. **92,** 3209-3213.

Messinger, J., Seaton, G., Wydrzynski, T., Wacker, U., and Renger, G. (1997). S_{-3} state of the water oxidase in photosystem II. Biochemistry **36,** 6862-6873.

Messinger, J., Robblee, J.H., Bergmann, U., Fernandez, C., Glatzel, P., Isgandarova, S., Hanssum, B., Renger, G., Cramer, S.P., Sauer, K., and Yachandra, V.K. (2001a). Manganese oxidation states in photosystem II. (Collingwood, Australia: CSIRO Publishing).

Messinger, J., Robblee, J.H., Bergmann, U., Fernandez, C., Glatzel, P., Visser, H., Cinco, R.M., McFarlane, K.L., Bellacchio, E., Pizarro, S.A., Cramer, S.P., Sauer, K., Klein, M.P., and Yachandra, V.K. (2001b). Absence of Mn centered oxidation in the S_2 to S_3 transition: implications for the mechanism of photosynthetic water oxidation. J. Am. Chem. Soc. **123,** 7804-7820.

Metz, J.G., Nixon, P.J., Rögner, M., Brudvig, G.W., and Diner, B.A. (1989). Directed alteration of the D1 polypeptide of photosystem II: evidence that tyrosine-161 is the redox component, Z, connecting the oxygen evolving complex to the primary electron donor, P680. Biochemistry **28,** 6960-6969.

Metzner, H. (1978). Photosynthetic Oxygen Evolution. (London: Academic Press).

Meyer, B., Schlodder, E., Dekker, J.P., and Witt, H.T. (1989). O_2 evolution and Chl *a* II^+ ($P680^+$) nanosecond reduction kinetics in single flashes as a function of pH. Biochim. Biophys. Acta **974,** 36-43.

Meyer, T.J., Huynh, M.H.V., and Thorp, H.H. (2007). The possible role of proton-coupled electron transfer (PCET) in water oxidation by photosystem II. Angew. Chem. Int. Ed. **46,** 5284-5304.

Michel, H., and Deisenhofer, J. (1988). Relevance of the Photosynthetic Reaction Center from Purple Bacteria to the Structure of Photosystem II. Biochemistry **27,** 1-7.

Miqyass, M., and van Gorkom, H. (2007). Calcium requirement for S-state transitions. Photosynth. Res. **91,** 175-175.

Miqyass, M., van Gorkom, H.J., and Yocum, C.F. (2007). The PSII calcium site revisited. Photosynth. Res. **92,** 275-287.

Miyashita, H., Ikemoto, H., Kurano, N., Adachi, K., Chihara, M., and Miyachi, S. (1996). Chlorophyll *d* as a major pigment. Nature **383,** 402-402.

Moskvin, O.V., Shutova, T.V., Khristin, M.S., Ignatova, L.K., Villarejo, A., Samuelsson, G., Klimov, V.V., and Ivanov, B.N. (2004). Carbonic anhydrase activities in pea thylakoids - A Photosystem II core complex-associated carbonic anhydrase. Photosynth. Res. **79,** 93-100.

Mukhopadhyay, S., Mandal, S.K., Bhaduri, S., and Armstrong, W.H. (2004). Manganese clusters with relevance to photosystem II. Chem. Rev. **104,** 3981-4026.

Murray, J.W., Maghlaoui, K., Kargul, J., Ishida, N., Lai, T.L., Rutherford, A.W., Sugiura, M., Boussac, A., and Barber, J. (2008). X-ray

crystallography identifies two chloride binding sites in the oxygen evolving centre of Photosystem II. Energy Environ. Sci. **1,** 161-166.

Naruta, Y., Sasayama, M., and Sasaki, T. (1994). Oxygen Evolution by Oxidation of Water with Manganese Porphyrin Dimers. Angew. Chem. Int. Ed. **33,** 1839-1841.

Nazeeruddin, M.K., Rotzinger, F.P., Comte, P., and Gratzel, M. (1988). Spontaneous Oxidation of Water to Oxygen by the Mixed-Valence Mu-Oxo Ruthenium Dimer L2(H_2O)RuIII-O-Ruiv(OH)L2 (L = 2,2'-Bipyridyl-5,5'-Dicarboxylic Acid). J. Chem. Soc., 872-874.

Nelson, N., and Yocum, C.F. (2006). Structure and function of photosystems I and II. Annu. Rev. Plant Biol. **57,** 521-565.

Nishida, Y., and Nasu, M. (1991). Redox Interaction between Binuclear Mn_2(III/IV) Complexes and Binuclear Mn_2(II/II) Complexes. Z. Naturforsch. **46,** 231-234.

Nixon, P.J., Barker, M., Boehm, M., de Vries, R., and Komenda, J. (2005). FtsH-mediated repair of the photosystem II complex in response to light stress. J. Exp. Bot. **56,** 357-363.

Nugent, J.H.A., Demetriou, C., and Lockett, C.J. (1987). Electron donation in photosystem II. Biochim. Biophys. Acta **894,** 534-542.

Nugent, J.H.A., Ball, R.J., and Evans, M.C.W. (2004). Photosynthetic water oxidation: the role of tyrosine radicals. Biochim. Biophys. Acta **1655,** 217-221.

Olesen, K., and Andréasson, L.-E. (2003). The function of the chloride ion in photosynthetic oxygen evolution. Biochemistry **42,** 2025-2035.

Olson, J.M., and Blankenship, R.E. (2004). Thinking about the evolution of photosynthesis. Photosynth. Res. **80,** 373-386.

Ono, T.-A., and Inoue, Y. (1983). Mn-preserving extraction of 33-, 24- and 16-kDa Proteins from O_2-evolving PS II particles by divalent salt-washing. FEBS Lett. **164,** 255-260.

Ono, T.-A., Zimmermann, J.-L., Inoue, Y., and Rutherford, A.W. (1986). EPR evidence for a modified S-state transition in chloride depleted photosystem II. Biochim. Biophys. Acta **851,** 193-201.

Ort, D.R., and Yocum, C.F. (1996). Oxygenic Photosynthesis: The Light Reactions. (Dordrecht: Kluwer Academic Publishers).

Petrouleas, V., and Crofts, A.R. (2005). The Iron-Quinone Acceptor Complex In Photosystem II. The Light-Driven Water:Plastoquinone Oxidoreductase, T. Wydrzynski and K. Satoh, eds (Dordrecht: Springer), pp. 177-206.

Porra, R.J., Thompson, W.A., and Kriedemann, P.E. (1989). Determination Of Accurate Extinction Coefficients and Simultaneous Equations For Assaying Chlorophyll-a and Chlorophyll-B Extracted With 4 Different Solvents - Verification Of the Concentration Of Chlorophyll Standards By Atomic Absorption Spectroscopy. Biochim. Biophys. Acta **975,** 384-394.

Poulsen, A.K., Rompel, A., and McKenzie, C.J. (2005). Water oxidation catalyzed by a dinuclear Mn complex: A functional model for the oxygen-evolving center of photosystem II. Angew. Chem. Int. Ed. **44,** 6916-6920.

Radmer, R., and Ollinger, O. (1980). Isotopic composition of photosynthetic O_2 flash yields in the presence of $H_2{}^{18}O$ and $HC^{18}O_3^-$. FEBS Lett. **110,** 57-61.

Radmer, R., and Ollinger, O. (1986). Do the higher oxidation states of the photosynthetic O_2 evolving system contain bound water? FEBS Lett. **195,** 285-289.

Rappaport, F., Guergova-Kuras, M., Nixon, P.J., Diner, B.A., and Lavergne, J. (2002). Kinetics and pathways of charge recombination in photosystem II. Biochemistry **41,** 8518-8527.

Rashid, A., and Homann, P.H. (1992). Properties of iodide activated photosynthetic water oxidizing complexes. Biochim. Biophys. Acta **1101,** 303-310.

Renger, G. (1997). Mechanistic and structural aspects of photosynthetic water oxidation. Physiol. Plant. **100,** 828-841.

Renger, G. (2001). Photosynthetic water oxidation to molecular oxygen: apparatus and mechanism. Biochim. Biophys. Acta **1503,** 210-228.

Renger, G., and Hanssum, B. (1988). Studies on the deconvolution of flash induced absorption changes into the difference spectra of individual redox steps within the water oxidizing enzyme system. Photosynth. Res. **16,** 243-259.

Renger, G., and Holzwarth, A.R. (2005). Primary electron transfer. In Photosystem II. The Light-Driven Water:Plastoquinone Oxidoreductase, T.J. Wydrzynski and K. Satoh, eds (Dordrecht: Springer), pp. 139-175.

Renger, G., and Kuhn, P. (2007). Reaction pattern and mechanism of light induced oxidative water splitting in photosynthesis. Biochim. Biophys. Acta **1767,** 458-471.

Renger, G., Bittner, T., and Messinger, J. (1994). Structure-function relationships in photosynthetic water oxidation. Biochem. Soc. Trans. **22,** 318-322.

Roelofs, T.A., Liang, W., Latimer, M.J., Cinco, R.M., Rompel, A., Andrews, J.C., Sauer, K., Yachandra, V.K., and Klein, M.P. (1996). Oxidation states of the manganese cluster during the flash-induced S-state cycle of the photosynthetic oxygen evolving complex. Proc. Natl. Acad. Sci. U. S. A. **93,** 3335-3340.

Roose, J.L., Wegener, K.M., and Pakrasi, H.B. (2007). The extrinsic proteins of photosystem II. Photosynth. Res. **92,** 369-387.

Rutherford, A.W., and Inoue, Y. (1984). Oscillation of delayed luminescence from PS II: recombination of $S_2Q_B^-$ and $S_3Q_B^-$. FEBS Lett. **165,** 163-170.

Rutherford, A.W., Zimmermann, J.-L., and Boussac, A. (1992). Oxygen Evolution. In The Photosystems: Structure, Function, and Molecular Biology, J. Barber, ed (Amsterdam: Elsevier B. V.), pp. 179-229.

Sauer, K. (1980). A Role for Manganese in Oxygen Evolution in Photosynthesis. Acc. Chem. Res. **13,** 249-256.

Schlichting, I., Almo, S.C., Rapp, G., Wilson, K., Petratos, K., Lentfer, A., Wittinghofer, A., Kabsch, W., Pai, E.F., Petsko, G.A., and Goody, R.S. (1990). Time-Resolved X-Ray Crystallographic Study of the Conformational Change in Ha-Ras P21 Protein on Gtp Hydrolysis. Nature **345,** 309-315.

Seidler, A. (1996). The extrinsic polypeptides of photosystem II. Biochim. Biophys. Acta **1277,** 35-60.

Shastry, M.C.R., Luck, S.D., and Roder, H. (1998). A continuous-flow capillary mixing method to monitor reactions on the microsecond time scale. Biophys. J. **74,** 2714-2721.

Shevela, D. (2008). Role of Inorganic Cofactors and Species Differences in Photosynthetic Water Oxidation. In Fachbereich 6 (Berlin: TU Berlin).

Shevela, D., Su, J.-H., Klimov, V., and Messinger, J. (2008). Hydrogencarbonate is not a tightly bound constituent of the water-oxidizing complex in photosystem II. Biochim. Biophys. Acta **1777,** 532-539.

Shi, L.X., and Schröder, W.P. (2004). The low molecular mass subunits of the photosynthetic supracomplex, photosystem II. Biochim. Biophys. Acta **1608,** 75-96.

Shinkarev, V., and Wraight, C.A. (1993). Oxygen evolution in photosynthesis: from unicycle to bicycle. Proc. Natl. Acad. Sci. U. S. A. **90,** 1834-1838.

Silva, A.C.B., Augusti, R., Dalmazio, I., Windmoller, D., and Lago, R.M. (1999). MIMS evaluation of pervaporation processes. Phys. Chem. Chem. Phys. **1,** 2501-2504.

Silverman, D.N., and Tu, C.K. (1975). Buffer Dependence of Carbonic-Anhydrase Catalyzed Oxygen-18 Exchange at Equilibrium. J. Am. Chem. Soc. **97,** 2263-2269.

Singh, S., Debus, R.J., Wydrzynski, T., and Hillier, W. (2008). Investigation of substrate water interactions at the high-affinity Mn site in the photosystem II oxygen-evolving complex. Philos. Trans. R Soc. Lond. B Biol. Sci. **363,** 1229-1234.

Siuzdak, G., Bothner, B., Yeager, M., Brugidou, C., Fauquet, C.M., Hoey, K., and Chang, C.M. (1996). Mass spectrometry and viral analysis. Chem. Biol. **3,** 45-48.

Stemler, A., Babcock, G.T., and Govindjee. (1974). Effect of bicarbonate on photosynthetic oxygen evolution in flashing light in chloroplast fragments. Proc. Natl. Acad. Sci. U. S. A. **71,** 4679-4683.

Stemler, A.J. (1997). The case for chloroplast thylakoid carbonic anhydrase. Physiol. Plant. **99,** 348-353.

Stemler, A.J. (2002). The bicarbonate effect, oxygen evolution, and the shadow of Otto Warburg. Photosynth. Res. **73,** 177-183.

Stewart, D.H., and Brudvig, G.W. (1998). Cytochrome b_{559} of photosystem II. Biochim. Biophys. Acta **1367,** 63-87.

Strasser, R.J., and Sironval, C. (1972). Induction of photosystem 2. Activity in flashed leaves. FEBS Lett. **28,** 56-60.

Styring, S., and Rutherford, A.W. (1987). In the oxygen evolving complex of photosystem II the S_0 state is oxidized to the S_1 State by Y_D^+ (Signal II_{slow}). Biochemistry **26,** 2401-2405.

Su, J.H., Lubitz, W., and Messinger, J. (2008). Probing mode and site of substrate water binding to the oxygen-evolving complex in the S_2 state of photosystem II by O^{17}-HYSCORE Spectroscopy. J. Am. Chem. Soc. **130,** 786-787.

Sugiura, M., Minagawa, J., and Inoue, Y. (1999). Properties of *Chlamydomonas* photosystem II core complex with a His-tag at the C-terminus of the D2 protein. Plant Cell Physiol. **40,** 311-318.

Sun, L.C., Hammarström, L., Akermark, B., and Styring, S. (2001). Towards artificial photosynthesis: ruthenium-manganese chemistry for energy production. Chem. Soc. Rev. **30,** 36-49.

Sun, L.C., Raymond, M.K., Magnuson, A., LeGourrierec, D., Tamm, M., Abrahamsson, M., Kenez, P.H., Martensson, J., Stenhagen, G., Hammarstrom, L., Styring, S., and Akermark, B. (2000). Towards an artificial model for Photosystem II: a manganese(II,II) dimer covalently linked to ruthenium(II) tris-bipyridine *via* a tyrosine derivative. J. Inorg. Biochem. **78,** 15-22.

Tamura, N., and Cheniae, G.M. (1987). Photoactivation of the water-oxidizing complex in Photosystem II membranes depleted of Mn and extrinsic proteins. I. Biochemical and kinetic characterization. Biochim. Biophys. Acta **890,** 179-194.

Tamura, N., Inoue, Y., and Cheniae, G.M. (1989). Photoactivation of the water oxidizing complex in photosystem II membranes depleted of Mn, Ca and extrinsic proteins. II. Studies on the functions of Ca^{2+}. Biochim. Biophys. Acta **976,** 173-181.

Tang, X.S., Zheng, M., Chisholm, D.A., Dismukes, G.C., and Diner, B.A. (1996). Investigation of the differences in the local protein environments surrounding tyrosine radicals $Y_Z^{\cdot}$ and $Y_D^{\cdot}$ in photosystem II using wild type and

the D2-Tyr160Phe mutant of *Synechocystis* 6803. Biochemistry **35,** 1475-1484.

Thomson, J.J. (1900). The mass of the carriers of negative electrification in gases of low pressure. Physikalische Zeitschrift **1,** 20-22.

Trissl, H.W., and Wilhelm, C. (1993). Why Do Thylakoid Membranes from Higher-Plants Form Grana Stacks. Trends Biochem. Sci. **18,** 415-419.

Tu, C.K., and Silverman, D.N. (1975a). Mechanism of Carbonic-Anhydrase Studied by C-13 and O-18 Labeling of Carbon-Dioxide. J. Am. Chem. Soc. **97,** 5935-5936.

Tu, C.K., and Silverman, D.N. (1975b). Kinetics of Exchange of Oxygen between Carbon-Dioxide and Carbonate in Aqueous-Solution. J. Phys. Chem. **79,** 1647-1651.

Turconi, S., MacLachlan, D.J., Bratt, P.J., Nugent, J.H.A., and Evans, M.C.W. (1997). Analysis of the interaction of water with the manganese cluster of photosystem II using isotopically labeled water. Biochemistry **36,** 879-885.

Un, S., Boussac, A., and Sugiura, M. (2007). Characterization of the tyrosine-Z radical and its environment in the spin-coupled $S_2Tyr_Z^{\cdot}$ state of photosystem II from *Thermosynechococcus elongatus*. Biochemistry **46,** 3138-3150.

van Gorkom, H.J., and Yocum, C.F. (2005). The calcium and chloride cofactors. In Photosystem II. The Light-Driven Water:Plastoquinone Oxidoreductase, T. Wydrzynski and K. Satoh, eds (Dordrecht: Springer), pp. 307-328.

van Hunnik, E., and Sultemeyer, D. (2002). A possible role for carbonic anhydrase in the lumen of chloroplast thylakoids in green algae. Funct. Plant Biol. **29,** 243-249.

van Rensen, J.J.S. (2002). Role of bicarbonate at the acceptor side of Photosystem II. Photosynth. Res. **73,** 185-192.

van Rensen, J.J.S., and Klimov, V.V. (2005). Bicarbonate interactions. In Photosystem II. The Light-Driven Water:Plastoquinone Oxidoreductase, T. Wydrzynski and K. Satoh, eds (Dordrecht: Springer), pp. 329-346.

van Rensen, J.J.S., Xu, C., and Govindjee. (1999). Role of bicarbonate in photosystem II, the water-plastoquinone oxido-reductase of plant photosynthesis. Physiol. Plant. **105,** 585-592.

Vass, I., Deak, Z., Jegerschold, C., and Styring, S. (1990). The accessory electron-donor tyrosine D of photosystem II is slowly reduced in the dark during low-temperature storage of isolated thylakoids. Biochim. Biophys. Acta **1018,** 41-46.

Vermaas, W.E.J., Renger, G., and Dohnt, G. (1984). The reduction of the oxygen evolving system in chloroplasts by thylakoid components. Biochim. Biophys. Acta **764,** 194-202.

Vermaas, W.F.J., Rutherford, A.W., and Hansson, O. (1988). Site directed mutagenesis in photosystem II of the cyanobacterium *Synechocystis sp.* PCC 6803: donor D is a tyrosine residue in the D2 protein. Proc. Natl. Acad. Sci. U. S. A. **85,** 8477-8481.

Villarejo, A., Shutova, T., Moskvin, O., Forssen, M., Klimov, V.V., and Samuelsson, G. (2002). A photosystem II-associated carbonic anhydrase regulates the efficiency of photosynthetic oxygen evolution. EMBO J. **21,** 1930-1938.

Warburg, O. (1964). Prefactory Chapter. Annu. Rev. Biochem. **33,** 1-18.

Warburg, O., and Krippahl, G. (1958). Hill-Reaktionen. Z. Naturforschung **13,** 509-514.

Webb, M.S., and Green, B.R. (1991). Biochemical and Biophysical Properties of Thylakoid Acyl Lipids. Biochim. Biophys. Acta **1060,** 133-158.

Weng, T.C., Hsieh, W.Y., Uffelman, E.S., Gordon-Wylie, S.W., Collins, T.J., Pecoraro, V.L., and Penner-Hahn, J.E. (2004). XANES evidence against a manganyl species in the S_3 state of the oxygen-evolving complex. J. Am. Chem. Soc. **126,** 8070-8071.

Wincencjusz, H., van Gorkom, H.J., and Yocum, C.F. (1997). The Photosynthetic Oxygen Evolving Complex Requires Chloride for Its Redox State S_2–S_3 and S_3-S_0 Transitions But Not for S_0-S_1 or S_1-S_2 Transitions. Biochemistry **36,** 3663-3670.

Wincencjusz, H., Yocum, C.F., and van Gorkom, H.J. (1998). S-state dependence of chloride binding affinities and exchange dynamics in the intact and polypeptide-depleted O_2 evolving complex of photosystem II. Biochemistry **37,** 8595-8604.

Wincencjusz, H., Yocum, C.F., and van Gorkom, H.J. (1999). Activating anions that replace Cl^- in the O_2 evolving complex of photosystem II slow the kinetics of the terminal step in water oxidation and destabilize the S_2 and S_3 states. Biochemistry **38,** 3719-3725.

Wincencjusz, H., Allakhverdiev, S.I., Klimov, V.V., and van Gorkom, H.J. (1996). Bicarbonate-reversible formate inhibition at the donor side of Photosystem II. Biochim. Biophys. Acta **1273,** 1-3.

Winget, G.D., Izawa, S., and Good, N.E. (1965). Stoichiometry of photophosphorylation. Biochem. Biophys. Res. Commun. **21,** 438-441.

Wydrzynski, T., Baumgart, F., MacMillan, F., and Renger, G. (1990). Is there a direct chloride cofactor requirement in the oxygen evolving reactions of photosystem II? Photosynth. Res. **25,** 59-72.

Xiong, J., and Bauer, C.E. (2002). Complex evolution of photosynthesis. Annu. Rev. Plant Biol. **53,** 503-521.

Yachandra, V.K. (2005). The catalytic manganese cluster: organisation of the metal ions. In Photosystem II. The Light-Driven Water:Plastoquinone Oxidoreductase, T. Wydrzynski and K. Satoh, eds (Dordrecht: Springer), pp. 235-260.

Yachandra, V.K., DeRose, V.J., Latimer, M.J., Mukerji, I., Sauer, K., and Klein, M.P. (1993). Where plants make oxygen: a structural model for the photosynthetic oxygen evolving manganese cluster. Science **260,** 675-679.

Yano, J., Pushkar, Y., Glatzel, P., Lewis, A., Sauer, K., Messinger, J., Bergmann, U., and Yachandra, V.K. (2005). High-resolution Mn EXAFS of the oxygen-evolving complex in photosystem II: structural implications for the Mn_4Ca cluster. J. Am. Chem. Soc. **127,** 14974-14975.

Yano, J., Kern, J., Sauer, K., Latimer, M.J., Pushkar, Y., Biesiadka, J., Loll, B., Saenger, W., Messinger, J., Zouni, A., and Yachandra, V.K. (2006). Where water is oxidized to dioxygen: structure of the photosynthetic Mn_4Ca cluster. Science **314,** 821-825.

Zouni, A., Witt, H.T., Kern, J., Fromme, P., Krauß, N., Saenger, W., and Orth, P. (2001). Crystal structure of photosystem II from *Synechococcus elongatus* at 3.8 Å resolution. Nature **409,** 739-743.